UNIVERSITY OF NEBR.
LIBRARY
SEP 22 1948

JOURNAL OF THE AERONAUTICAL SCIENCES

VOLUME 15 SEPTEMBER, 1948 NUMBER 9

CONTENTS

Experimental Study of Cooling by Injection of a Fluid Through a Porous Material ..... POL DUWEZ AND H. L. WHEELER, JR. 509

Hyperbolic Column Formulas for Magnesium-Alloy Extrusions ..... E. H. SCHUETTE 523

Deep Ring Analysis ..... KUANG-SHENG CHING 531

Application of the Performance Operator to Aircraft Automatic Control ..... ROBERT C. SEAMANS, JR., BENJAMIN G. BROMBERG, AND L. E. PAYNE 535

Aerothermodynamic Design of Turbines for Aircraft Power Plants ..... JOHN E. TALBERT AND J. C. SMITH 556

The Aerodynamic Forces on an Oscillating Flap at Supersonic Speeds ..... JOHN W. MILES 565

Letters to the Editor 521, 529

Published by the
INSTITUTE OF THE AERONAUTICAL SCIENCES, INC.

JOURNAL OF THE AERONAUTICAL SCIENCES

Editor: HUGH L. DRYDEN, *Director of Aeronautical Research, N.A.C.A.*

Associate Editor: ROBERT R. DEXTER *Associate Editor:* BERNEICE H. JARCK

The Institute of the Aeronautical Sciences publishes monthly the JOURNAL OF THE AERONAUTICAL SCIENCES and the AERONAUTICAL ENGINEERING REVIEW.

The JOURNAL OF THE AERONAUTICAL SCIENCES prints papers of scientific and technical interest to Institute members and subscribers. In general, it provides an opportunity for specialists to publish articles disclosing new knowledge and new applications in the field of the aeronautical sciences. The JOURNAL restricts itself to the aeronautical aspects of advances in science and engineering, and papers printed have either been submitted directly to the JOURNAL or have been previously presented at a meeting of the Institute.

The AERONAUTICAL ENGINEERING REVIEW keeps members and subscribers informed regarding the contents of new books and current periodicals in the field of aeronautics. It reviews new developments in the aircraft industry and reports on progress from house organs and catalogs published by aircraft and engine manufacturers and other companies engaged in aeronautical activities. It publishes papers on applied engineering and aircraft production. News of Institute activities is published in the REVIEW.

Statements and opinions expressed in the JOURNAL are to be understood as individual expressions of the authors and not those of the Institute.

SUBSCRIPTION RATES

Journal of the Aeronautical Sciences
Published Monthly

United States and Possessions		Foreign Countries Including Canada (American Currency Rates)	
1 Year	$12.00	1 Year	$13.00
Single Copies	1.50	Single Copies	1.50

Aeronautical Engineering Review
Published Monthly

United States and Possessions		Foreign Countries Including Canada (American Currency Rates)	
1 Year	$3.00	1 Year	$3.50
Single Copies	0.50	Single Copies	0.50

Notices of change of address should be sent to the Institute at least 30 days prior to actual change of address.

Manuscripts for publication, proofs, and all correspondence should be addressed to the Editorial Office of the JOURNAL.

Correspondence regarding subscriptions may be addressed to Publication Office, 20th and Northampton Sts., Easton, Pa., or to the Editorial Office of the JOURNAL OF THE AERONAUTICAL SCIENCES, 2 East 64th Street, New York 21, New York.

Copyright, 1948, by the Institute of the Aeronautical Sciences, Inc.

Entered as Second Class Matter at the Post Office, Easton, Pa., May 1, 1937. Acceptance for mailing at a special rate of Postage provided for in the Act of August 24, 1912. Authorized April 29, 1937.

INSTITUTE of the AERONAUTICAL SCIENCES

President
JOHN K. NORTHROP

Vice-Presidents
SMITH J. DE FRANCE
C. L. JOHNSON
R. P. LANSING
EARL D. OSBORN

Director
S. PAUL JOHNSTON

Executive Vice-President
BENNETT H. HORCHLER

Past-Presidents
J. C. HUNSAKER
CHARLES L. LAWRANCE
DONALD W. DOUGLAS
GLENN L. MARTIN
CLARK B. MILLIKAN
T. P. WRIGHT
GEORGE W. LEWIS (Deceased)
JAMES H. DOOLITTLE
FRANK W. CALDWELL
HALL L. HIBBARD
HUGH L. DRYDEN
R. H. FLEET
CHARLES H. COLVIN
ARTHUR E. RAYMOND
P. R. BASSETT

Secretary
ROBERT R. DEXTER

Treasurer
SHERMAN M. FAIRCHILD

Controller
JOSEPH J. MAITAN

Counsel
ALLAN D. EMIL

COUNCIL

E. E. ALDRIN
REX B. BEISEL
LAWRENCE D. BELL
WILLIAM BOLLAY
W. A. M. BURDEN
VICTOR E. CARBONARA
FRANK O. CARROLL
CHARLES H. COLVIN
JAMES H. DOOLITTLE
C. C. FURNAS
LEROY R. GRUMMAN
J. A. HERLIHY
JEROME LEDERER
JOHN C. LESLIE
JACK MASON
C. KENNETH RAZAK
L. B. RICHARDSON
RUSSELL G. ROBINSON
GEORGE S. SCHAIRER
ERNEST G. STOUT
A. J. THIEBLOT

ADVISORY COMMITTEE

WALTER BEECH
FRANK W. CALDWELL
RALPH S. DAMON
KENNETH S. M. DAVIDSON
R. H. FLEET
R. PAUL HARRINGTON
R. M. HAZEN
HALL L. HIBBARD
J. C. HUNSAKER
TH. VON KÁRMÁN
THOMAS A. KNOWLES
I. M. LADDON
GROVER LOENING
GLENN L. MARTIN
CLARK B. MILLIKAN
THOMAS A. MORGAN
ARTHUR E. RAYMOND
F. W. REICHELDERFER
LAURANCE S. ROCKEFELLER
T. CLAUDE RYAN
ELMER A. SPERRY, JR.
EDWARD P. WARNER
BURDETTE S. WRIGHT
T. P. WRIGHT

HONORARY MEMBERS

JOHN R. ALISON
JOHN N. BROWN
FRANK O. CARROLL
E. U. CONDON
L. C. CRAIGIE
DONALD B. DUNCAN
HARRY F. GUGGENHEIM
GEORGE C. KENNEY
THEODORE LONNQUEST
JOSEPH J. O'CONNELL, JR.
HOWARD T. ORVILLE
GEORGE B. PEGRAM
E. M. POWERS
ALFRED M. PRIDE
J. LAURENCE PRITCHARD
F. W. REICHELDERFER
DELOS W. RENTZEL
CARL SPAATZ
W. STUART SYMINGTON
J. W. TICE
HOYT S. VANDENBERG

HONORARY FELLOWS

H. H. ARNOLD
FRANK W. CALDWELL
SIR GEOFFREY DE HAVILLAND
JAMES H. DOOLITTLE
DONALD W. DOUGLAS
HUGH L. DRYDEN
W. F. DURAND
SIR RICHARD FAIREY
SIR ROY FEDDEN
J. C. HUNSAKER
SIR MELVILL JONES
GLENN L. MARTIN
GEORGE J. MEAD
SIR FREDERICK HANDLEY PAGE
D. R. PYE
IGOR I. SIKORSKY
SIR GEOFFREY TAYLOR
TH. VON KÁRMÁN
EDWARD P. WARNER
T. P. WRIGHT

BENEFACTORS

E. E. ALDRIN
HART O. BERG (Deceased)
W. A. M. BURDEN
E. L. CORD
DONALD W. DOUGLAS
SHERMAN M. FAIRCHILD
SIR RICHARD FAIREY
R. H. FLEET
FLORENCE GUGGENHEIM (Deceased)
C. D. HANSCOM
JOHN P. V. HEINMULLER
ALEXANDER KLEMIN
PAUL KOLLSMAN
BELLA C. LANDAUER
WILLIAM LANDAUER
GROVER LOENING
EDMUND C. LYNCH (Deceased)
F. W. MAGIN
GLENN L. MARTIN
GEORGE J. MEAD
S. A. REED (Deceased)
LAURANCE S. ROCKEFELLER
EDWARD P. WARNER

AMERICAN FELLOWS

IRA H. ABBOTT
JOHN D. AKERMAN
E. E. ALDRIN
HARRY G. ARMSTRONG
KARL ARNSTEIN
J. L. ATWOOD
PAUL S. BAKER
RALPH S. BARNABY
P. R. BASSETT
WELLWOOD E. BEALL
REX B. BEISEL
G. M. BELLANCA
DON R. BERLIN
HENRY A. BERLINER
WILLIAM BOLLAY
GEORGE W. BRADY
LYMAN J. BRIGGS
W. G. BROMBACHER
WILLIAM G. BROWN
CHARLES P. BURGESS
KENNETH CAMPBELL
CHARLES H. CHATFIELD
ALLAN CHILTON
FRANKLIN R. COLLBOHM
CHARLES H. COLVIN
KARL T. COMPTON
EMERSON W. CONLON
JOHN W. CROWLEY, JR.
RALPH S. DAMON
LUIS DE FLOREZ
SMITH J. DE FRANCE
J. P. DEN HARTOG
WALTER S. DIEHL
C. S. DRAPER
IVAN H. DRIGGS
WILLIAM K. EBEL
C. L. EGTVEDT
FREDERIC FLADER
CHARLES FROESCH
JACK FRYE
GARLAND FULTON
LESTER D. GARDNER
RICHARD C. GAZLEY
MICHAEL E. GLUHAREFF
MELVIN N. GOUGH
LEROY R. GRUMMAN
HAROLD R. HARRIS
R. M. HAZEN
EDWARD H. HEINEMANN
S. D. HERON
HALL L. HIBBARD
L. S. HOBBS
PAUL E. HOVGAARD
WILLIAM HOVGAARD
ROBERT INSLEY
EASTMAN N. JACOBS
C. L. JOHNSON
S. PAUL JOHNSTON
ALEXANDER KARTVELI
PAUL H. KEMMER
CARLETON KEMPER
J. H. KINDELBERGER
OTTO E. KIRCHNER
ARTHUR L. KLEIN
ALEXANDER KLEMIN
W. B. KLEMPERER
PAUL KOLLSMAN
OTTO C. KOPPEN
B. V. KORVIN-KROUKOVSKY
S. M. KRAUS
ARNOLD M. KUETHE
I. M. LADDON
E. S. LAND
CHARLES L. LAWRANCE
JEROME LEDERER
JOHN G. LEE
JOHN C. LESLIE
CHARLES A. LINDBERGH
WILLIAM LITTLEWOOD
GROVER LOENING
ALBERT E. LOMBARD
F. A. LOUDEN
W. RANDOLPH LOVELACE, II
EUGENE E. LUNDQUIST
R. D. MACCART
JOHN R. MARKHAM
ERLE MARTIN
WM. H. MCAVOY
C. J. MCCARTHY
J. S. MCDONNELL
CLARK B. MILLIKAN
ROBERT J. MINSHALL
JOSEPH S. NEWELL
ALFRED S. NILES
JOHN K. NORTHROP
ARTHUR NUTT
SHATSWELL OBER
ROBERT R. OSBORN
W. BAILEY OSWALD
GEORGE A. PAGE, JR.
F. W. PAWLOWSKI
F. W. PENNOYER, JR.
A. A. PRIESTER
ARTHUR E. RAYMOND
F. W. REICHELDERFER
ELLIOTT G. REID
H. J. E. REID
H. C. RICHARDSON
L. B. RICHARDSON
RUSSELL G. ROBINSON
LEONARD E. ROOT
C. E. ROSENDAHL
ADDISON M. ROTHROCK
W. R. SEARS
WILLIAM T. SCHWENDLER
FRANCIS R. SHANLEY
JAMES M. SHOEMAKER
MAC SHORT
IGOR ALEXIS SIKORSKY
ABE SILVERSTEIN
SELDEN B. SPANGLER
ELMER A. SPERRY, JR.
JOHN STACK
ROBERT M. STANLEY
WILLIAM B. STOUT
HARRY A. SUTTON
C. FAYETTE TAYLOR
EDWARD S. TAYLOR
PHILIP B. TAYLOR
TH. THEODORSEN
T. E. TILLINGHAST
S. TIMOSHENKO
L. B. TUCKERMAN
RALPH H. UPSON
J. PARKER VAN ZANDT
J. G. VINCENT
RICHARD VON MISES
FRANK L. WATTENDORF
P. V. H. WEEMS
FRED E. WEICK
R. D. WEYERBACHER
JOHN B. WHEATLEY
ANDREW V. WILLGOOS
DONALD H. WOOD
ROBERT J. WOODS
JOHN E. YOUNGER
ALBERT F. ZAHM
STEPHEN J. ZAND

Corporate Members

of the

Institute of the Aeronautical Sciences

Academy of Aeronautics, Inc.
Casey Jones School of Aeronautics

Aerojet Engineering Corporation

Aeroproducts Division, General Motors Corporation

Aeroquip Corporation

Agawam Aircraft Products, Inc.

Airborne Instruments Laboratory, Inc.

Airchox Company Division, Joyce Aviation, Inc.

Aircraft Radio Corporation

AiResearch Manufacturing Company, Division of The Garrett Corporation

Allis-Chalmers Manufacturing Company

Allison Division, General Motors Corporation

Aluminum Company of America

American Airlines System

American Bosch Corporation

American Overseas Airlines, Inc.
Iceland Airport Corporation (Subsidiary)

American Phenolic Corporation

Associated Aviation Underwriters

Atlas Supply Company

Beech Aircraft Corporation

Bell Aircraft Corporation

Bendix Aviation Corporation
Bendix International Division
Bendix Products Division
Bendix Radio Corporation
Eclipse-Pioneer Division
Friez Instrument Division
Pacific Division
Scintilla Magneto Company

The BG Corporation

Boeing Airplane Company
Seattle Division
Wichita Division

Breeze Corporations, Inc.
Aircraft Standard Parts Company, Inc.
Aldrich Company
Anderson Stove Company, Inc.
Federal Laboratories, Inc.
Foundry Service, Inc.

Cal-Aero Technical Institute, A Division of Grand Central Airport Company

Cessna Aircraft Company

Chandler-Evans Division, Niles-Bement-Pond Company

Chase Aircraft Company, Inc.

Chase National Bank of the City of New York

The Cleveland Graphite Bronze Company

The Cleveland Pneumatic Tool Company
Automotive-Aircraft Division

Clifford Manufacturing Company, Division of Standard-Thomson Corporation

Consolidated Vultee Aircraft Corporation
Fort Worth Division
Stinson Aircraft Division

Continental Motors Corporation

Curtiss-Wright Corporation
Airplane Division
Propeller Division
Wright Aeronautical Corporation Division

Doak Aircraft Company, Inc.

Douglas Aircraft Company, Inc.
El Segundo Plant
Long Beach Plant
Santa Monica Plant

The Dow Chemical Company

Dzus Fastener Company, Inc.

Eastern Air Lines, Inc.

Eaton Manufacturing Company
Dynamatic Corporation (Subsidiary)
Eaton-Wilcox-Rich Ltd. (Subsidiary)

Thomas A. Edison, Incorporated, Instrument Division

Edo Corporation

Elastic Stop Nut
Corporation of America

Electrol Incorporated

Ethyl Corporation

Fairchild Camera & Instrument Corporation
Fairchild Aerial Surveys, Inc.

Fairchild Engine and Airplane Corporation
Al-Fin Division
Fairchild Aircraft Division
Fairchild Personal Planes Division
Fairchild Pilotless Plane Division
NEPA Division
Ranger Aircraft Engines Division
Stratos Corporation (Subsidiary)

Federal Telephone and Radio Corporation
Federal Electric Manufacturing Company, Ltd.
Federal Telecommunication Laboratories, Inc. (Partial Subsidiary)

General Electric Company
Aircraft Gas Turbine Division
Aviation Divisions

General Tire and Rubber Company of California, Research and Development Division

The B. F. Goodrich Company

The Goodyear Tire & Rubber Company
Goodyear Aircraft Corporation

Grumman Aircraft Engineering Corporation

W. &. L. E. Gurley

The International Nickel Company, Inc.

Irving Air Chute Company, Inc.

Jack & Heintz Precision Industries, Inc.

Johns-Manville Sales Corporation

Walter Kidde & Company, Inc.

Kollsman Instrument Division, Square D Company

Lavelle Aircraft Corporation

Lear Incorporated

Link Aviation, Inc.

The Liquidometer Corporation

Lockheed Aircraft Corporation
Airquipment Company (Subsidiary)
Lockheed Air Terminal (Subsidiary)
Lockheed Aircraft Overseas Corporation (Subsidiary)
Lockheed Aircraft Service, Inc. (Subsidiary)

Longines-Wittnauer Watch Company, Inc.

The Glenn L. Martin Company
GLM Chemical Division
Rotawings Division

Warren McArthur Corporation

McDonnell Aircraft Corporation

Minneapolis-Honeywell Regulator Company
Brown Instrument Company (Subsidiary)

Moore Drop Forging Company

National City Bank of New York

National Credit Office, Inc.

North American Aviation, Inc.
North American Aviation, Inc., of Texas

Northrop Aircraft, Inc.

Northwest Airlines, Inc.

Owens-Corning Fiberglas Corporation

Pan American World Airways System

The Parker Appliance Company

Pesco Products Division, Borg-Warner Corporation

Phillips Petroleum Company

Pure Oil Company

Radioplane Company

Republic Aviation Corporation

A. V. Roe Canada Limited

John A. Roebling's Sons Company

Rohr Aircraft Corporation

Ryan Aeronautical Company

Shell Oil Company, Inc.

Simmonds Aerocessories, Inc.

Socony-Vacuum Oil Company, Inc.

Solar Aircraft Company

Sperry Gyroscope Company Division of The Sperry Corporation

Square D Company

Standard Oil Company of California

Standard Oil Company (Indiana)

Standard Oil Company of New Jersey

The Texas Company

Thompson Products, Inc.

Tinnerman Products, Inc.

Union Carbide and Carbon Corporation
Bakelite Corporation
Electro Metallurgical Company
Haynes Stellite Company
The Linde Air Products Company
National Carbon Company, Inc.

United Air Lines, Inc.

United Aircraft Corporation
Chance Vought Aircraft Division
Hamilton Standard Propellers Division
Pratt & Whitney Aircraft Division
Sikorsky Aircraft Division
United Aircraft Export Corporation
United Aircraft Service Corporation

United States Aviation Underwriters, Inc.

United States Rubber Company
Dominion Rubber Company, Ltd.

Vickers, Inc.

Warner Aircraft Corporation

The Weatherhead Company
Angola, Indiana Division
Columbia Products Division
Houma Division
The Weatherhead Company of Canada (Subsidiary)

Westinghouse Electric Corporation
Aviation Gas Turbine Division
Industrial Electronics Division
Marine & Aviation Sales Department
Small Motor Division, Aviation Sales

Weston Electrical Instrument Corporation

Wyman-Gordon Company

Young Radiator Company

EDITORIAL COMMITTEE

HUGH L. DRYDEN, *Chairman*

Aerodynamics

Francis Clauser
Howard Emmons
R. Paul Harrington
R. T. Jones
W. B. Klemperer
Otto C. Koppen
John G. Lee
H. P. Liepmann
C. C. Lin
H. F. Ludloff
John R. Markham
Clark B. Millikan
Shatswell Ober
W. Bailey Oswald
Allen E. Puckett
Elliott G. Reid
H. J. E. Reid
Russell Robinson
L. E. Root
G. B. Schubauer
W. R. Sears
John Stack
Th. von Kármán
Richard von Mises

Air Transport

A. W. Dallas
Charles Froesch
J. A. Herlihy
Otto E. Kirchner
John C. Leslie

Aircraft Design

W. E. Beall
Rex B. Beisel
W. K. Ebel
Hall L. Hibbard
C. L. Johnson
I. M. Laddon
C. J. McCarthy
Fred E. Weick
Robert J. Woods

Physiologic Problems

H. G. Armstrong
Louis H. Bauer
Eugene Du Bois
W. Randolph Lovelace, II
Ross A. McFarland
A. D. Tuttle

Aircraft Propulsion

George W. Brady
Frank W. Caldwell
L. S. Hobbs
E. E. Johnson
Joseph Keenan
R. P. Kroon
Arthur Nutt
Hans Reissner
Abe Silverstein
C. Fayette Taylor
E. S. Taylor
P. Taylor

Structures and Materials

W. B. Bleakney
E. W. Conlon
J. P. Den Hartog
L. H. Donnell
E. C. Hartmann
N. J. Hoff
E. E. Lundquist
C. F. Nagel, Jr.
J. S. Newell
Alfred S. Niles
W. Ramberg
E. Reissner
F. R. Shanley
H. W. Sibert
C. R. Strang
S. Timoshenko
H. S. Tsien
Chi-Teh Wang

Meteorology

C. F. Brooks
D. M. Little
E. J. Minser
F. W. Reichelderfer
H. C. Willett

Fuels and Oils

A. L. Beall
J. H. Doolittle
Graham Edgar
R. T. Goodwin
S. D. Heron
A. M. Rothrock

Instruments

Allan G. Binnie
W. G. Brombacher
J. Callahan
Charles H. Colvin
C. S. Draper
O. E. Esval
David W. Moore
W. A. Reichel
C. F. Savage
O. Hugo Schuck
R. Sylvander

Rotating Wing Aircraft

Robert Coleman
K. H. Hohenemser
G. Horvay
Alexander Klemin
Ralph McClarren
R. H. Miller
R. H. Prewitt
Igor I. Sikorsky
Robert A. Wolf

Vibration and Flutter

Lee Arnold
M. A. Biot
William Bollay
Chieh-Chien Chang
J. P. Den Hartog
Manfred Rauscher

Flight Testing

W. K. Ebel
R. R. Gilruth
Melvin N. Gough
Robert Stanley
E. G. Stout

I.A.S. REPRESENTATIVES TO OTHER ORGANIZATIONS

Aircraft Industries Association of America, Inc.—CHARLES MARCUS

American Association for the Advancement of Science—J. C. HUNSAKER

American Society of Mechanical Engineers—CHARLES H. COLVIN

American Standards Association—P. R. BASSETT

Engineering Society of Detroit—DONALD C. HUNT, GEORGE TWENEY

Greater New York Safety Council—WILLIAM LITTLEWOOD

Daniel Guggenheim Medal Board of Award—CHARLES H. COLVIN, GROVER LOENING, S. PAUL JOHNSTON

Institute of Radio Engineers—L. M. HULL

Manufacturers Aircraft Association—ARTHUR E. RAYMOND

National Aeronautic Association—WILLIAM R. ENYART

National Fire Protection Association—E. E. ALDRIN

National Research Council Engineering Division—HUGH L. DRYDEN

National Safety Council—JEROME LEDERER

New York Museum of Science and Industry—LESTER D. GARDNER

Society of Automotive Engineers—STEPHEN J. ZAND

JOURNAL OF THE AERONAUTICAL SCIENCES

VOLUME 15 SEPTEMBER, 1948 NUMBER 9

Experimental Study of Cooling by Injection of a Fluid Through a Porous Material*

POL DUWEZ† AND H. L. WHEELER, JR.‡

California Institute of Technology

SUMMARY

A method of coping with the high rates of heat transfer encountered in the field of jet propulsion consists of making the parts to be cooled of a porous material and forcing the cooling fluid through the pores in a direction opposite to that of the heat flow. This method is referred to as "sweat-cooling." The study of sweat-cooling heat transfer discussed in this paper has the limited objective of defining the variables involved in the problem and of establishing the experimental techniques. A full description of these techniques is given. Extensive tables and graphs of the data obtained are also included. This experimental study of sweat-cooling has shown that either a liquid or a gas may be used efficiently as a cooling fluid. A theoretical expression is derived relating the surface temperature of the porous material, the weight flow rate of the coolant, and the temperature and weight flow rate of the main stream of hot gas. The validity of this expression is discussed on the basis of the experimental data that have been obtained.

NOMENCLATURE

β = u_w/U
c_p = specific heat of coolant
δ = laminar-layer thickness
D = diameter of sweat-cooled tube
g = acceleration of gravity
k = effective conductivity coefficient for coolant
λ = friction factor for circular pipes
M = mass flow for turbulent core per unit cross-sectional area
m = mass flow of coolant per unit area of surface
μ = viscosity coefficient in turbulent core
μ_c = viscosity coefficient of coolant
Pr_c = $\mu_c c_p/k$ = Prandtl Number of coolant
Q = weight rate of flow of coolant per unit area
q = heat transfer across unit area of protective layer
Re = Reynolds Number of main stream computed from W and kinematic viscosity
ρ_c = density of coolant
ρ_s = mass density of turbulent core
τ = shear stress per unit area within the laminar layer
τ_0 = shear stress at wall, determined by bulk characteristics
T = average temperature of turbulent core
T_0 = temperature of gas entering coolant manifold
T_1 = temperature of sweat-cooled wall
T_2 = temperature of outside surface of porous specimen
θ = $(T - T_1)/(T_1 - T_0)$
U = bulk or average velocity of main stream
u_w = wall velocity
V = maximum velocity of main stream measured in center of turbulent core
v = velocity of coolant leaving porous wall
W = weight rate of flow per unit area in main stream computed from V, T, and the density of the gas (considered to be air)
ψ = velocity distortion factor
ξ = temperature distortion factor

(I) INTRODUCTION

THE HIGH TEMPERATURES encountered in the operation of jet engines have imposed drastic requirements upon the materials used in their construction. To meet these requirements, research may be directed toward finding alloys and ceramic materials that are inherently refractory or toward materials capable of being efficiently cooled.

Besides the conventional method of cooling by means of a liquid in contact with a material exposed to a high rate of heat transfer, a less orthodox method consists of making the part to be cooled of a porous material and forcing a cooling fluid through the pores. In this scheme the temperature of the coolant, which moves in

Presented at the Third National Flight Propulsion Meeting, I.A.S., Cleveland, March 19, 1948.

* This work was done at the Jet Propulsion Laboratory, California Institute of Technology, under contracts with the Army Ordnance Department, Washington, D.C., and the Air Materiel Command, Army Air Force, Wright Field, Ohio. The authors wish to thank these agencies for the permission to publish the results of this investigation.

† Associate Professor of Mechanical Engineering and Chief of the Materials Section of Jet Propulsion Laboratory.

‡ Research Engineer, Jet Propulsion Laboratory.

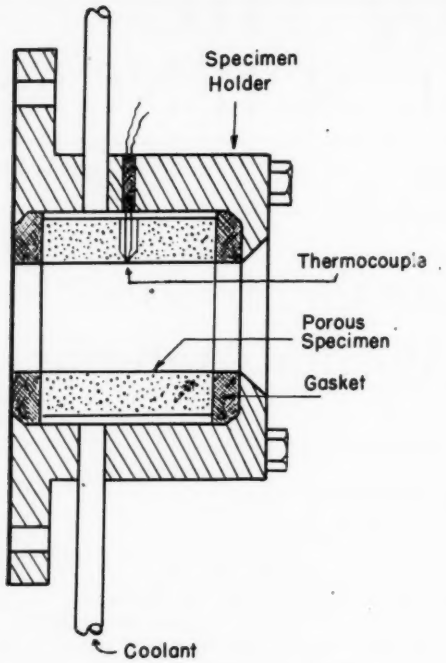

FIG. 1. Sweat-cooled test section.

a direction opposite to that of the heat flow, increases gradually while passing through the porous material. On emerging from the wall the coolant forms a protective layer on the surface exposed to heat transfer. This method, referred to as "sweat-cooling," was proposed by the senior author at the Jet Propulsion Laboratory in September, 1944, and experimental work on the preparation of porous metals was started early in 1945.

The sweat-cooling method opens new lines of research in the fields of heat transfer, flow of fluids through porous materials, and powder metallurgy. The study of the heat-transfer problem discussed in this paper has the limited objective of defining the different variables involved in the problem and establishing the proper experimental techniques.

(II) Description of Experimental Equipment

The present experimental investigation was limited to the case of a cylindrical duct made of a porous material through the walls of which coolant was injected. The test section, containing the porous duct 1 in. in diameter and $1^1/_2$ in. long, was designed so that it could be used with two different burners. In one burner an oxyhydrogen flame was used as the source of the stream of hot gas, the gas temperature being around 4,200° F. and the velocity about 300 ft. per sec. In the second burner a gasoline-air flame served as the source of hot gas. The gas temperature was only moderately high (around 2,000° F. maximum), but very high velocities corresponding to Mach Numbers approaching 1.0 could be obtained, with resulting Reynolds Numbers up to 140,000. While the oxyhydrogen unit simulates conditions of temperatures and velocities present in the combustion chamber of a rocket motor, the gasoline-air burner operates approximately in the range of a gas turbine.

(A) *The Sweat-Cooled Cylindrical Duct*

The test section with the sweat-cooled cylindrical duct is shown in Fig. 1. The porous cylindrical specimen is clamped between the two sections of a stainless-steel holder. Coolant is forced through the walls of the specimen from a small annular space between the holder and the specimen. The porous specimen is thermally insulated from the holder by transite gaskets.

For measuring the inside wall temperature of the specimen, a chromel-alumel thermocouple is installed in the following manner: A $^1/_8$-in. diameter hole is drilled approximately 80 per cent of the way through the specimen wall. The remaining 20 per cent is drilled with a $^1/_{16}$-in. drill. A conical-shaped bead, approximately $^1/_{10}$ in. long and with a maximum diameter slightly greater than $^1/_{16}$ in., is formed on the ends of the chromel and alumel wires. This bead is generally cast in a carbon mold using silver solder. The bead is driven into the small hole in the porous wall until its tip is just flush with the inner wall. The wires coming from the back of the bead are separated and centered in the large hole. The hole is then filled in with a cement composed of magnesium oxide and sodium silicate. After the cement has been baked it is virtually impossible to remove the thermocouple installation from the wall. This type of installation allows for a maximum of strength and thermal contact with the hot surface of the wall, while affording a minimum of leakage around the bead and a minimum of interference to the normal pattern of coolant flow through the specimen.

The outside wall temperature was measured by a chromel-alumel thermocouple peened into the outer surface of the specimen. All thermocouple leads were brought out through the gasket between the two sections of the specimen holder. The rate of flow of coolant was metered by means of a 60-cm. scale Fisher Porter Flowrator operated at a pressure of 60 lbs. per sq.in. A series of floats was designed so that a wide range of flows could be covered.

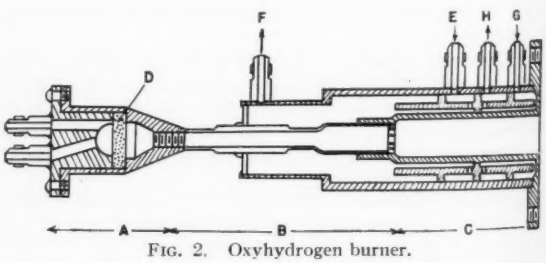

FIG. 2. Oxyhydrogen burner.

(B) *The Oxygen-Hydrogen Burner*

The oxygen-hydrogen burner, shown in Fig. 2, consists essentially of a mixing chamber A, an injector B, and a combustion chamber C. The gases are mixed by passing them through a porous disc D. This arrangement produces a considerably hotter flame than the commercially available mixers. The injector B is the burner tip of a standard No. 15 Victor welding torch. The combustion chamber C, 4 in. long and 1 in. in diameter, is water-cooled. The water entering through the nipple E cools a portion of the combustion chamber and the burner; this water is then discarded through nipple F. The water entering the forward portion of the chamber and circulating from G to H is metered, and its temperature rise is recorded. Hence, the heat transfer between the flame and a section of the combustion chamber preceding the sweat-cooled specimen may be evaluated. This quantity is taken as an index of the conditions of combustion and is referred to as the potential heat transfer. The test section is bolted to the end of the combustion chamber.

The rate of flow of hydrogen and oxygen through the burner was measured by calibrated orifice flowmeter. For all of the tests, the total gas flow rate amounted to approximately 6×10^{-3} lbs. per sec. at stoichiometric mixture ratio. The flame temperature was estimated by inserting various refractory materials of known melting point into the combustion chamber. By this rather crude means, the temperature of the gas stream was established as being between 4,000° and 4,500°F.

(C) *The Gasoline-Air Burner*

The experimental burner for the production of high-speed and moderately high-temperature gas is shown in Fig. 3. It consists of an injection chamber, a combustion chamber, a ceramic nozzle with a throat section 1 in. in diameter, and a straightening tube 1 in. in diameter and 20 in. long. The axis of the chamber is inclined 30° from the horizontal to avoid accumulation of fuel.

The injection chamber contains four tangential air-fuel inlets, arranged in pairs. It serves to initiate and control combustion and can also be considered as a pilot burner. The major portion of the air-fuel mixture is supplied, during normal operation, through the front inlets of the injector section. Oxidation patterns on the interior walls indicate that the gas in the upper end of the injection chamber is relatively stagnant, and combustion is reinitiated from this area if the flame in the combustion chamber is extinguished.

The combustion chamber, which is flanged and bolted to the injection chamber, is primarily intended to furnish sufficient volume to complete combustion. Two air-fuel inlets are provided at the midpoint of the chamber. These inlets were seldom used for the injection of fuel, because it was found that a supply of air-fuel mixture in this region tended to render the combustion unstable. They have been found of some value, however, when used simply as air injectors to cool the combustion gases.

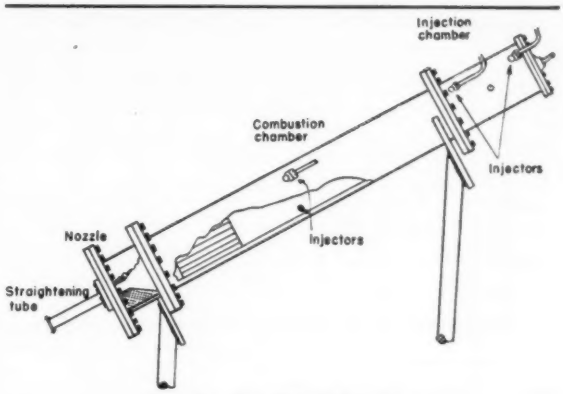

FIG. 3. Gasoline-air burner.

The lower end of the combustion chamber is filled with a nest of mild steel tubes 1 in. in diameter and approximately 10 in. long. These tubes transform the spiral path of the flame into a more or less axial flow.

At the exhaust end of the combustion chamber the gases are expanded through a fused silica nozzle with a throat section 1 in. in diameter. Between the nozzle and the specimen holder is a heavily lagged steel tube 20 in. long. The purpose of this tube is to stabilize the velocity profile of the hot gas before the gas flows through the sweat-cooled section.

Gasoline is supplied to the burner from a pressurized 40-gal. tank, controlled by means of needle valves and metered through a Fisher Porter Flowrater. Air is supplied from two 25-hp. two-stage compressors, metered through an orifice and controlled by means of gate valves.

Accurate determination of both the temperature and velocity of the gas stream flowing through the 1-in. diameter test section was extremely difficult. In view of the preliminary character of the present study, it was not felt justified to sacrifice simplicity and ruggedness of the metering apparatus to the accurate determination of temperature and velocity. The velocity was measured only in the center of the stream by means of a water-cooled total head tube placed at the outlet of the test section. Temperature measurements were accomplished with an unshielded chromel-alumel thermocouple introduced radially into the stream through the wall of the straightening tube about 1 in. above the test section. A thermocouple recovery factor, obtained by comparison with the more delicate Pratt and Whitney type of probe described in reference 1, was introduced into the temperature reduction equation, but no attempt was made to introduce theoretical corrections for radiation losses. The quantities measured by thermocouple and total head tube was transformed into gas temperature and gas velocity (or Mach Number) by means of standard adiabatic equations.

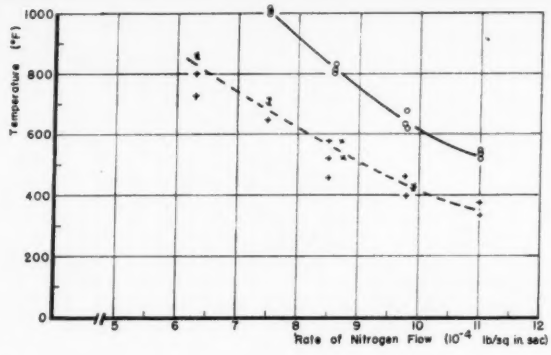

FIG. 4. Surface temperature vs. rate of nitrogen flow in experiments with the oxyhydrogen burner.

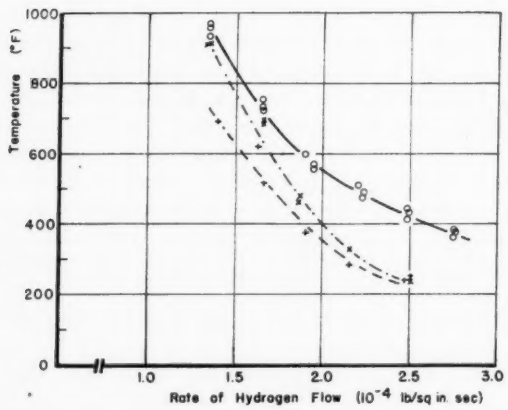

FIG. 5. Surface temperature vs. rate of hydrogen flow in experiments with the oxyhydrogen burner

(III) RESULTS OF EXPERIMENTS WITH THE OXYGEN-HYDROGEN BURNER

All of the experiments with the oxygen-hydrogen burner were performed with a gas temperature of approximately 4,200°F., a velocity of 300 ft. per sec., and a Reynolds Number of the order of 1,500, as previously mentioned. These conditions resulted in a potential heat transfer of approximately 0.85 B.t.u. per sq.in. sec. to the conventionally cooled chamber upstream of the porous section. The experimental procedure consisted of recording the surface temperature of the specimen as a function of the weight rate of flow of coolant.

The results of a preliminary experiment on the technique of cooling by water injected through a porous material exposed to a flow of gas at high temperature have shown (cf. reference 2) that there is a critical value in the amount of coolant, above which the surface temperature of the porous material remains near or below the boiling point of water and below which the surface temperature increases rapidly with decreasing flow. On the other hand, when a gas is used as a coolant, the curve of surface temperature vs. amount of gas coolant is continuous, since the coolant does not undergo any change of phase.

The results of measurements with copper, nickel, and stainless-steel specimens are summarized in the curves of Figs. 4 and 5. In these graphs the surface temperature is plotted against the flow of coolant. The measurements of surface temperature vs. rate of coolant flow for approximately the same value of potential heat transfer were not always consistent. This is understandable, since the same heat transfer to the cooling coil may be obtained for more than one set of values of gas temperature and gas velocity, whereas it is probable that each of these variables taken independently

TABLE 1

Results of Experiments with the Oxygen-Hydrogen Burner

Flow of Coolant (10^{-4} Lbs. per Sq.In. Sec.)	Surface Temperature T_1 (°F.)			Heat Transferred to Coolant (B.t.u. per Sq.In. Sec.)			Exit Velocity of Coolant (Ft. per Sec.)		
	Copper	Nickel	Stainless steel	Copper	Nickel	Stainless steel	Copper	Nickel	Stainless steel
Nitrogen Cooling									
6	..	900	970	...	0.122	0.132	...	2.79	2.94
7	1,150	700	760	0.185	0.108	0.118	3.86	2.78	2.92
8	910	570	620	0.165	0.097	0.107	3.75	2.82	2.96
9	740	480	500	0.147	0.089	0.094	3.63	2.89	2.96
10	630	420	430	0.136	0.084	0.087	3.66	3.01	3.05
11	550	370	370	0.128	0.079	0.079	3.80	3.12	3.12
12	480	...	...	0.119	...	...	3.86	..	..
Hydrogen Cooling									
1.2	1,100	...	...	0.415	...	...	8.91	..	..
1.4	900	740	910	0.389	0.313	0.393	9.07	8.00	9.07
1.6	750	560	670	0.363	0.260	0.320	9.22	7.77	8.61
1.8	630	440	510	0.336	0.220	0.261	9.34	7.71	8.23
2.0	550	360	400	0.319	0.190	0.217	9.62	7.81	8.19
2.2	490	300	320	0.306	0.164	0.179	9.95	7.96	8.17
2.4	440	260	260	0.293	0.146	0.146	10.29	8.23	8.23
2.6	400	230	225	0.282	0.132	0.126	10.65	8.54	8.42
2.8	370	...	...	0.275	...	...	11.10	..	..

has an effect on the conditions of heat transfer in the sweat-cooled section. As a consequence, there was considerable disagreement in the measurements performed in various tests with the same sweat-cooled section.

In spite of this uncertainty in the conditions of heat transfer prevailing in the sweat-cooled section, the measurements brought out several interesting facts. As could be expected, the quantity of gas required for a given cooling effect is dependent upon the nature of the gas used as a coolant. The curves of Figs. 4 and 5 show that, for a given wall temperature, the required weight rate of flow of nitrogen is approximately five times greater than that of hydrogen.

This ratio of 5 between the hydrogen and nitrogen flows is not yet theoretically explained. Some pertinent facts that may serve as a guide in establishing a theory explaining the difference between hydrogen and nitrogen cooling might be derived from this data. If it is assumed that the temperature of the coolant at the inside surface of the sweat-cooled tube is equal to that of the porous material (cf. reference 3), the quantity of heat q absorbed by the coolant before entering the main stream of gas is simply

$$q = Qc_p(T_1 - T_0)$$

The velocity with which the coolant leaves the porous wall will be $v = Q/\rho$. This relation is based on the assumption that the pores are so close together that the individual streams of coolant coalesce shortly after leaving the porous wall. The values of q and v are given in Table 1. From this data, it can be seen that for a given surface temperature, the heat transferred to the coolant hydrogen is higher than for the coolant nitrogen. The reason for this behavior is probably related to the thermal conductivity of the two gases and the thickness of the boundary layer.

A comparison of the results obtained with the three different metals indicates that heat transfer in sweat-cooling depends somewhat on the nature of the porous metal. For a given hot-gas stream and for a given amount of coolant, the wall temperature of the copper specimen was several hundred degrees higher than that of the nickel or stainless-steel specimens. This influence of the nature of the porous material on the heat transfer in sweat-cooling has been evidenced also with the tests made with the gasoline-air burner. A quantitative explanation of this effect is still lacking.

(IV) Results of Experiments with the Gasoline-Air Burner

The purpose of the measurements made with the gasoline-air burner was to establish a relation between the surface temperature of the porous material and the weight rate of coolant flow for different conditions of temperature and velocity in the main stream of hot gas.

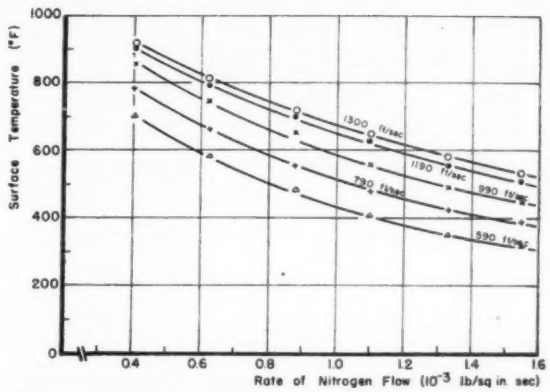

FIG. 6. Surface temperature vs. rate of nitrogen flow for a gas temperature of 1,300°F. in experiments with the gasoline-air burner.

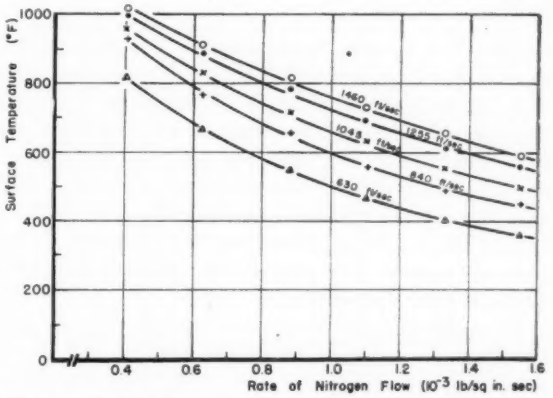

FIG. 7. Surface temperature vs. rate of nitrogen flow for a gas temperature of 1,500°F. in experiments with the gasoline-air burner.

The four significant variables involved in this problem are (1) the temperature T of the stream of gas flowing through the sweat-cooled tube; (2) the velocity V of the same gas; (3) the weight rate of coolant flow Q; and (4) the surface temperature T_1 of the sweat-cooled specimen. The procedure consisted in measuring the variation of the surface temperature T_1 of the sweat-cooled specimen as a function of the rate of coolant flow Q for a series of values of velocity V and temperature T of the stream of hot gas. The standard values of T were 1,100°, 1,300°, 1,500°, 1,700°, and 1,900°F. At each temperature from two to five different velocities were used. The velocity range was more or less dictated by the conditions of operation of the combustion chamber. At 1,300°F., for example, the velocities were between 650 and 1,400 ft. per sec., whereas at 1,900°F. the range was from 1,300 to about 1,800 ft. per sec. The outside surface temperature T_2 of the sweat-cooled specimen in contact with the incoming coolant gas was also measured in all tests.

A complete description of the results obtained with the four different porous materials is beyond the scope of this paper. Hence, only the experiments on stain-

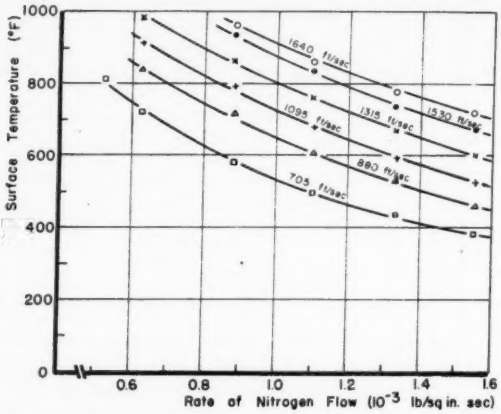

FIG. 8. Surface temperature vs. rate of nitrogen flow for a gas temperature of 1,700°F. in experiments with the gasoline-air burner.

less steel will be presented at length. The fundamental graphs expressing the results of these measurements show the dependence of surface temperature T_1 of the specimen on the rate of coolant flow G for given gas temperatures and gas velocities (cf. Figs. 6 to 9, inclusive). Curves have also been traced for the variation of the temperature T_2 as a function of the rate of coolant flow. These curves are not included in the present paper because they have essentially the same shape as those shown in Figs. 6 to 9.

By comparing all the results obtained with one porous material, it can be shown that the curves of T_1 vs. Q fall in a logical sequence, the curves being shifted toward a higher temperature when either the temperature or the velocity of the gas is increased. It is also interesting to note that the curves tend to be extremely flat and approach a horizontal asymptote when the rate of coolant flow is increased.

A comparison of the curves of T_1 vs. Q obtained for the same conditions of gas temperature and gas velocity, but for the four different porous materials, indicates again that the T_1 vs. Q relation depends on the nature of the porous sample.

The results of the measurements, as given in the preceding section, were reduced to obtain a more systematic tabulation in which the gas temperature, gas velocity, and the rate of coolant flow would have the same sets of values for all the tests. The method employed was as follows: From the curves of T_1 vs. Q, presented in Figs. 6 to 9, inclusive, values of temperature T_1 were read corresponding to the rates of coolant flow of 0.4, 0.6, 0.8, 1.0, 1.2, 1.4, and 1.6×10^{-3} lbs. per sq.in. sec. These temperatures were plotted against the gas velocity V. By replotting the data in the form of T_1 vs. V diagrams, accidental errors could be detected, since, if one of the original T_1 vs. Q curves was slightly out of place, none of the points corresponding to that curve would fall on the continuous curves of the T_1 vs. V diagrams. Using the T_1 vs. V diagrams, new values of T_1 were then obtained for gas velocities of 600, 800, 1,000, 1,200, 1,400, 1,600, and 1,800 ft. per sec. A typical set of reduced data thus obtained is presented in Tables 2 to 5, inclusive, for porous stainless-steel specimens.

(V) Interpretation of Results

Several investigators have recently attempted to formulate a theory of heat transfer between a stream of gas and a porous wall through which a cooling gas is injected. Besides the theoretical treatments of Yuan[4] and Rannie,[5] the junior author has also proposed a semiempirical but simple method of correlating the experimental results. In the following, the different theoretical treatments are briefly summarized and their application to the available experimental results is discussed.

In establishing an empirical equation for heat transfer, the following simplifying assumptions were made by H. L. Wheeler: (1) The flow within the tube consists of a turbulent core and a laminar protective layer; (2) the protective layer has reached steady-state conditions over the length of the tube; (3) values of specific heat, thermal conductivity, etc., are average values; and (4) radiation heat transfer to the wall is negligible.

If δ is the thickness of the laminar boundary layer in a conventional pipe, the two following equations can be written (cf. p. 46, reference 6):

$$\left.\begin{aligned} \tau &= \mu(u_w/\delta) \\ \tau_0 &= (\lambda/8)\rho_s U^2 \end{aligned}\right\} \qquad (1)$$

If it is assumed that the shear force on the turbulent side of a line dividing the laminar and turbulent regions is equal to the viscous force on the other side, then $\tau = \tau_0$ and

$$\delta = 8\mu(u_w/\lambda\rho U^2)$$

Denoting the ratio u_w/U by β and replacing $\rho_s U$ by the mass flow M, the expression for δ becomes

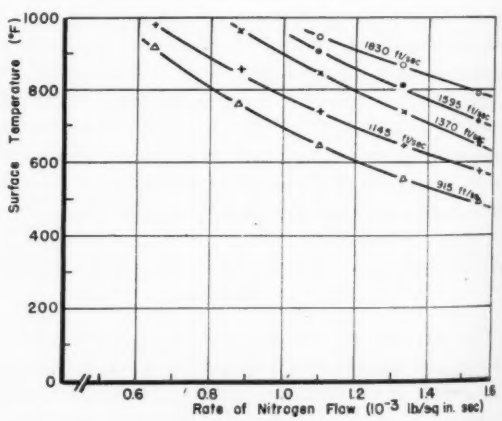

FIG. 9. Surface temperature vs. rate of nitrogen flow for a gas temperature of 1,900°F. in experiments with the gasoline-air burner.

TABLE 2
Reduced Data for a Porous Stainless-Steel Specimen and a Gas Temperature of 1,300°F.

Q (10^{-3} Lbs. per Sq.In. Sec.)	T_1 (°F.)	T_2 (°F.)	q (B.t.u. per Sq.In. Sec.)	$\frac{T-T_1}{T_1-T_0}$	$\frac{T-T_1}{T-T_0}$	$\frac{v}{V}$ (10^{-3})	$\frac{Q}{W}$ (10^{-3})
V = 600 ft. per sec.			R_e = 41,000			W = 0.095 lb. per sq.in. sec.	
1.6	308	180	0.090	4.35	0.81	7.0	16.8
1.4	334	200	0.088	3.80	0.79	6.3	14.7
1.2	382	230	0.090	3.04	0.75	5.8	12.6
1.0	434	270	0.088	2.45	0.71	5.1	10.5
0.8	506	330	0.085	1.86	0.65	4.4	8.4
0.6	594	410	0.075	1.37	0.58	3.6	6.3
0.4	707	530	0.062	0.95	0.48	2.7	4.2
V = 800 ft. per sec.			R_e = 55,000			W = 0.126 lb. per sq.in. sec.	
1.6	387	210	0.122	2.97	0.75	5.8	12.7
1.4	418	230	0.117	2.61	0.72	5.3	11.1
1.2	467	265	0.109	2.27	0.68	4.8	9.5
1.0	524	310	0.110	1.75	0.64	4.2	7.9
0.8	593	380	0.102	1.38	0.58	3.6	6.3
0.6	679	470	0.088	1.04	0.51	2.9	4.8
0.4	788	585	0.070	0.72	0.42	2.1	3.2
V = 1,000 ft. per sec.			R_e = 69,000			W = 0.158 lb. per sq.in. sec.	
1.6	451	230	0.147	2.29	0.70	5.0	10.1
1.4	483	260	0.140	2.03	0.67	4.5	8.9
1.2	535	300	0.135	1.68	0.63	4.1	7.6
1.0	595	350	0.127	1.37	0.57	3.6	6.3
0.8	664	430	0.116	1.09	0.52	3.1	5.1
0.6	748	520	0.088	0.83	0.45	2.5	3.8
0.4	853	630	0.077	0.59	0.37	1.8	2.5
V = 1,200 ft. per sec.			R_e = 82,000			W = 0.189 lb. per sq.in. sec.	
1.6	504	255	0.168	1.88	0.65	4.4	8.5
1.4	539	285	0.159	1.66	0.62	4.0	7.4
1.2	590	330	0.152	1.39	0.58	3.6	6.4
1.0	650	390	0.141	1.14	0.53	3.2	5.3
0.8	726	470	0.128	0.89	0.47	2.7	4.2
0.6	808	560	0.107	0.68	0.40	2.2	3.2
0.4	907	665	0.082	0.48	0.32	1.6	2.1
V = 1,400 ft. per sec.			R_e = 96,000			W = 0.221 lb. per sq.in. sec.	
1.6	550	270	0.186	1.60	0.61	4.0	7.2
1.4	590	310	0.177	1.39	0.58	3.6	6.3
1.2	640	365	0.167	1.18	0.54	3.2	5.4
1.0	700	425	0.154	0.97	0.49	2.8	4.5
0.8	780	500	0.139	0.74	0.43	2.4	3.6
0.6	860	585	0.116	0.56	0.36	1.9	2.7
0.4	955	695	0.087	0.39	0.28	1.4	1.8

$$\delta = \mu/(\lambda/8\beta)M \qquad (2)$$

Consider an element of fluid of unit area and thickness dy (y being the direction perpendicular to the wall of the tube). The viscous shear across dy will be $\mu du/dy$. If a fluid is injected through the porous wall, there will be superimposed on this factor a further stress $\rho_c v_y(du/dy)$ representing the rate at which momentum is gained across dy by a mass of coolant $\rho_c v$ flowing outward from the wall. The total shear stress then in the laminar layer will be

$$\tau = \mu(du/dy) + \rho_c v_y(du/dy)$$

If du/dy may be represented by $\psi(u_w/\delta)$, where ψ is a distortion factor which relates the velocity gradient at the wall to the average velocity gradient and is assumed to be a function of the ratio m/M, then τ at a point $y = \delta$ will be

$$\tau = \mu\psi(u_w/\delta) + \rho_c v u_w$$

Taking this new value of shear in place of that given by Eq. (1), the thickness of the boundary layer δ will be

$$\delta = \mu_c/[(\lambda/8\beta\psi)M - (m/\psi)] \qquad (3)$$

Eq. (3) is similar to Eq. (2), except for an additional term representing the mass flow of coolant and a correction for nonlinearity of the velocity profile.

It is probable that values of λ and β do not have the same significance in a sweat-cooled tube as in a conventional pipe. In order to evaluate δ on the basis of Eq. (3), experimental values of β, ψ, and λ should be obtained for a sweat-cooled tube in which no heat transfer is occurring.

The case of a sweat-cooled tube in which heat is transferred from the protective layer to the metal wall will be considered next. For a thermally conservative system, the heat transferred through the protective layer to the wall is equal to the increase in enthalpy of the gas passing through the porous wall, or

$$q = \xi(k/\delta)(T - T_1) = mc_p(T_1 - T_0) \qquad (4)$$

where ξ is a distortion factor relating the temperature gradient in the protective layer close to the wall to the average temperature gradient in the layer. The factor

TABLE 3

Reduced Data for a Porous Stainless-Steel Specimen and a Gas Temperature of 1,500°F.

$\frac{Q}{}$ (10^{-2} Lbs. per Sq.In. Sec.)	T_1 (°F.)	T_2 (°F.)	$\frac{q}{}$ (B.t.u. per Sq.In. Sec.)	$\frac{T-T_1}{T_1-T_0}$	$\frac{T-T_1}{T-T_0}$	$\frac{v}{V}$ (10^{-3})	$\frac{Q}{W}$ (10^{-3})
V = 600 ft. per sec.			R_e = 35,000			W = 0.085 lb. per sq.in. sec.	
1.6	338	185	0.102	4.50	0.82	7.3	18.9
1.4	371	205	0.101	3.88	0.79	6.6	16.5
1.2	428	235	0.104	3.08	0.75	6.1	14.2
1.0	487	285	0.101	2.49	0.71	5.4	11.8
0.8	565	350	0.096	1.86	0.66	4.7	9.5
0.6	670	450	0.087	1.41	0.58	3.9	7.1
0.4	813	590	0.073	0.94	0.49	2.9	4.7
V = 800 ft. per sec.			R_e = 47,000			W = 0.113 lb. per sq.in. sec.	
1.6	414	220	0.132	3.25	0.77	6.0	14.2
1.4	455	240	0.130	2.79	0.73	5.5	12.4
1.2	513	275	0.129	2.28	0.70	5.0	10.6
1.0	574	330	0.122	1.87	0.65	4.4	8.9
0.8	660	410	0.115	1.45	0.59	3.8	7.5
0.6	760	520	0.101	1.09	0.52	3.2	5.3
0.4	886	660	0.080	0.76	0.43	2.3	3.5
V = 1,000 ft. per sec.			R_e = 58,000			W = 0.142 lb. per sq.in. sec.	
1.6	476	240	0.157	2.59	0.72	5.1	11.3
1.4	524	270	0.154	2.20	0.69	4.7	9.9
1.2	583	310	0.150	1.82	0.65	4.3	8.5
1.0	643	370	0.140	1.52	0.61	3.8	7.1
0.8	731	455	0.128	1.18	0.54	3.3	5.7
0.6	828	565	0.110	0.90	0.47	2.6	4.3
0.4	945	700	0.086	0.64	0.39	1.9	2.8
V = 1,200 ft. per sec.			R_e = 70,000			W = 0.170 lb. per sq.in. sec.	
1.6	525	255	0.177	2.19	0.69	4.5	9.4
1.4	580	290	0.174	1.84	0.65	4.2	8.2
1.2	638	335	0.166	1.54	0.61	3.8	7.1
1.0	700	400	0.154	1.29	0.56	3.3	6.0
0.8	784	490	0.140	1.02	0.51	2.8	4.7
0.6	878	600	0.117	0.78	0.44	2.3	3.5
0.4	990	730	0.090	0.56	0.36	1.7	2.4
V = 1,400 ft. per sec.			R_e = 81,000			W = 0.198 lb. per sq.in. sec.	
1.6	568	265	0.194	1.91	0.65	4.0	8.1
1.4	627	305	0.190	1.60	0.61	3.7	7.1
1.2	685	360	0.180	1.35	0.58	3.4	6.1
1.0	750	430	0.166	1.12	0.53	3.0	5.1
0.8	827	520	0.148	0.90	0.47	2.5	4.0
0.6	914	620	0.124	0.70	0.41	2.0	3.0
0.4	1,020	750	0.093	0.51	0.34	1.5	2.0
V = 1,600 ft. per sec.			R_e = 93,000			W = 0.227 lb. per sq.in. sec.	
1.6	600	275	0.206	1.76	0.63	3.6	7.1
1.4	665	320	0.203	1.43	0.59	3.4	6.2
1.2	725	385	0.192	1.20	0.55	3.0	5.3
1.0	790	455	0.176	1.00	0.51	2.7	4.4
0.8	860	540	0.155	0.82	0.45	2.3	3.5
0.6	940	640	0.128	0.65	0.39	1.8	2.6
0.4	1,040	765	0.095	0.48	0.32	1.3	1.8

ξ, like ψ, is assumed to depend on the ratio m/M. Eq. (4) is correct, provided the coolant reaches the wall temperature. A justification for this assumption has been given in reference 3.

From Eq. (4) it follows that the thickness of the boundary layer will be given by

$$\delta = (\xi k/mc_p)[(T - T_1)/(T_1 - T_0)]$$

Substituting this relation in Eq. (3) and denoting the ratio of constants $(\mu_c c_p)/k$ by Pr_c,

$$\left(\frac{T - T_1}{T_1 - T_0}\right)\frac{1}{Pr_c} = 1\Big/\left(\frac{\xi\lambda}{8\beta\psi}\frac{M}{m} - \frac{\xi}{\psi}\right)$$

Replacing the ratio of mass flows by the ratio of weight flows and the temperature ratio by θ, a more convenient form is obtained:

$$\theta = Pr_c/\{[(\lambda\xi/8\beta\psi)(w/Q)] - (\delta/\psi)\} \qquad (5)$$

Since the terms on the right-hand side of Eq. (5) have been assumed to be functions of Q/W, Eq. (5) may be written

$$\theta/Pr_c = f(Q/W) \qquad (6)$$

The validity of Eq. (6) can be discussed on the basis of experimental results.

Values of θ/Pr_c and Q/W, given in Tables 2 through 5, have been plotted on the graph of Fig. 10. As evidenced by this graph, all the experimental results obtained for a given porous material fall more or less on a single curve. The empirical relation (6) seems, therefore, to have some value and is useful in reducing the ex-

TABLE 4
Reduced Data for a Porous Stainless-Steel Specimen and a Gas Temperature of 1,700 °F.

Q (10^{-3} Lbs. per Sq.In. Sec.)	T_1 (°F.)	T_2 (°F.)	q (B.t.u. per Sq.In. Sec.)	$\frac{T-T_1}{T_1-T_0}$	$\frac{T-T_1}{T-T_0}$	$\frac{v}{V}$ (10^{-3})	$\frac{Q}{W}$ (10^{-3})
V = 600 ft. per sec.			R_c = 30,000			W = 0.077 lb. per sq.in. sec.	
1.6	322	180	0.096	5.69	0.85	7.1	20.8
1.4	358	205	0.096	4.83	0.83	6.5	18.2
1.2	417	240	0.100	3.81	0.79	6.0	15.6
1.0	487	290	0.101	2.98	0.75	5.4	13.0
0.8	570	360	0.097	2.31	0.70	4.7	10.4
0.6	688	470	0.089	1.66	0.62	3.9	7.8
0.4	850	...	0.076	1.10	0.52	3.0	5.2
V = 800 ft. per sec.			R_c = 40,000			W = 0.103 lb. per sq.in. sec.	
1.6	415	205	0.133	3.84	0.79	6.0	15.5
1.4	462	235	0.133	3.24	0.76	5.5	13.6
1.2	525	275	0.132	2.64	0.72	5.0	11.6
1.0	597	330	0.128	2.13	0.68	4.5	9.7
0.8	691	410	0.121	1.65	0.62	3.9	7.8
0.6	810	525	0.107	1.22	0.55	3.3	5.8
0.4	949	...	0.186	0.86	0.46	2.4	3.9
V = 1,000 ft. per sec.			R_c = 49,000			W = 0.128 lb. per sq.in. sec.	
1.6	493	235	0.164	2.92	0.75	5.2	12.5
1.4	546	265	0.162	2.48	0.71	4.8	10.9
1.2	613	310	0.159	2.04	0.67	4.4	9.4
1.0	684	375	0.150	1.68	0.63	3.9	7.8
0.8	788	460	0.140	1.29	0.56	3.4	6.2
0.6	904	580	0.121	0.97	0.49	2.8	4.7
0.4	1,028	...	0.094	0.72	0.42	2.0	3.1
V = 1,200 ft. per sec.			R_c = 59,000			W = 0.154 lb. per sq.in. sec.	
1.6	563	260	0.192	2.35	0.70	4.7	10.4
1.4	618	295	0.187	2.01	0.67	4.3	9.1
1.2	688	345	0.181	1.66	0.62	3.9	7.8
1.0	761	420	0.169	1.38	0.58	3.5	6.5
0.8	866	510	0.156	1.06	0.52	3.0	5.2
0.6	979	630	0.132	0.80	0.44	2.5	3.9
0.4	1,095	...	0.101	0.60	0.37	1.8	2.6
V = 1,400 ft. per sec.			R_c = 69,000			W = 0.180 lb. per sq.in. sec.	
1.6	628	285	0.217	1.96	0.66	4.3	8.9
1.4	683	325	0.209	1.69	0.63	3.9	7.8
1.2	753	380	0.200	1.41	0.59	3.3	6.7
1.0	831	460	0.186	1.16	0.54	3.1	5.6
0.8	934	560	0.169	0.90	0.48	2.7	4.4
0.6	1,042	685	0.141	0.68	0.41	2.2	3.3
0.4	1,156	...	0.107	0.51	0.33	1.6	2.2
V = 1,600 ft. per sec.			R_c = 79,000			W = 0.206 lb. per sq.in. sec.	
1.6	689	310	0.242	1.66	0.62	3.9	7.8
1.4	744	360	0.230	1.44	0.59	3.6	6.8
1.2	815	420	0.219	1.20	0.54	3.3	5.8
1.0	896	505	0.202	0.99	0.49	2.9	4.9
0.8	996	610	0.182	0.77	0.43	2.5	3.9
0.6	1,096	740	0.149	0.59	0.37	2.0	2.9
0.4	1,216	...	0.113	0.43	0.30	1.4	1.9

perimental data to a single curve involving only two dimensionless parameters.

A second theoretical study of the heat transfer in a sweat-cooled duct has been reported by Rannie.[5] This second study gives the temperature and velocity profiles in the laminar protective layer and leads to a solution of the heat transfer through the laminar protective layer [cf. Eq. (20), reference 5]. In this solution, however, the thickness of the protective layer is a variable and is left undetermined. In order to obtain a comparison with the experimental results, it was assumed in reference 5 that the boundary-layer thickness was the same as that for the flow through an ordinary pipe. This hypothesis may be acceptable if the velocity of the coolant normal to the wall is small in comparison with that of the main stream. For the experiments reported here, the ratio of these two velocities is smaller than 0.01 (cf. Tables 2 through 5). Thus, the final results given in reference 5 can be written

$$\frac{T-T_1}{T_1-T_0} = 1 - \frac{e^{-Pr_c \frac{Q}{W}\sqrt{\frac{2}{C_f}}\,y^*}}{1+\left(\frac{2}{\sqrt{C_f}}\frac{1}{y^*}-1\right)\left(1-e^{-\frac{Q}{W}\sqrt{\frac{2}{C_f}}\,y^*}\right)}$$

This expression is Eq. (20) of reference 5, written in the nomenclature of the present paper. If it is assumed that $y^* = 5.6$ and $C = 0.046/Re^{0.2}$, then the quantity $(T - T_1)/(T - T_0)$ can be computed as a function of Q/W for different values of the Reynolds Number. The experimental values of $(T - T_1)/$-

TABLE 5

Reduced Data for a Porous Stainless-Steel Specimen and a Gas Temperature of 1,900°F.

Q (10^{-3} Lbs. per Sq.In. Sec.)	T_1 (°F.)	T_2 (°F.)	q (B.t.u. per Sq.In. Sec.)	$\frac{T-T_1}{T_1-T_0}$	$\frac{T-T_1}{T-T_0}$	$\frac{v}{V}$ (10^{-3})	$\frac{Q}{W}$ (10^{-3})
V = 800 ft. per sec.			R_e = 34,000			W = 0.094 lb. per sq.in. sec.	
1.6	404	225	0.129	4.62	0.82	6.0	17.0
1.4	470	260	0.135	3.67	0.78	5.6	14.9
1.2	560	305	0.143	2.79	0.74	5.2	12.8
1.0	650	370	0.141	2.19	0.69	4.8	10.6
0.8	748	460	0.132	1.72	0.63	4.1	8.5
0.6	900	600	0.120	1.22	0.55	3.5	6.4
0.4	1,048	...	0.096	0.88	0.40	2.6	4.3
V = 1,000 ft. per sec.			R_e = 43,000			W = 0.117 lb. per sq.in. sec.	
1.6	507	250	0.169	3.26	0.77	5.3	13.7
1.4	572	290	0.171	2.70	0.73	4.9	12.0
1.2	657	340	0.172	2.15	0.68	4.6	10.3
1.0	751	410	0.166	1.71	0.63	4.1	8.5
0.8	851	515	0.153	1.36	0.58	3.6	6.8
0.6	994	640	0.134	0.99	0.50	3.0	5.1
0.4	1,144	...	0.105	0.71	0.41	2.2	3.4
V = 1,200 ft. per sec.			R_e = 51,000			W = 0.141 lb. per sq.in. sec.	
1.6	588	270	0.202	2.58	0.72	4.8	11.4
1.4	654	320	0.199	2.17	0.69	4.4	9.9
1.2	735	380	0.195	1.78	0.64	4.1	8.5
1.0	832	455	0.186	1.42	0.59	3.7	7.1
0.8	933	575	0.169	1.13	0.53	3.4	5.7
0.6	1,070	690	0.145	0.84	0.45	2.6	4.3
0.4	1,226	...	0.113	0.60	0.37	1.9	2.8
V = 1,400 ft. per sec.			R_e = 60,000			W = 0.164 lb. per sq.in. sec.	
1.6	655	295	0.228	2.16	0.69	4.4	9.8
1.4	720	350	0.222	1.84	0.65	4.0	8.5
1.2	800	415	0.214	1.53	0.60	3.7	7.3
1.0	900	500	0.203	1.22	0.55	3.3	6.1
0.8	1,000	630	0.187	0.98	0.49	2.9	4.9
0.6	1,135	730	0.157	0.73	0.42	2.3	3.7
0.4	1,284	...	0.119	0.51	0.34	1.7	2.4
V = 1,600 ft. per sec.			R_e = 69,000			W = 0.188 lb. per sq.in. sec.	
1.6	714	320	0.252	1.87	0.65	4.0	8.5
1.4	775	375	0.241	1.62	0.62	3.8	7.4
1.2	858	450	0.231	1.34	0.57	3.4	6.4
1.0	958	445	0.218	1.07	0.52	3.0	5.3
0.8	1,060	690	0.194	0.86	0.46	2.6	4.3
0.6	1,187	780	0.162	0.64	0.39	2.1	3.2
V = 1,800 ft. per sec.			R_e = 77,000			W = 0.211 lb. per sq.in. sec.	
1.6	767	340	0.272	1.65	0.62	3.7	7.6
1.4	825	410	0.259	1.44	0.59	3.4	6.6
1.2	912	480	0.248	1.19	0.54	3.1	5.7
1.0	1,012	585	0.231	0.95	0.48	2.8	4.7
0.8	1,113	740	0.205	0.76	0.43	2.4	3.8
0.6	1,238	825	0.170	0.57	0.36	1.9	2.8

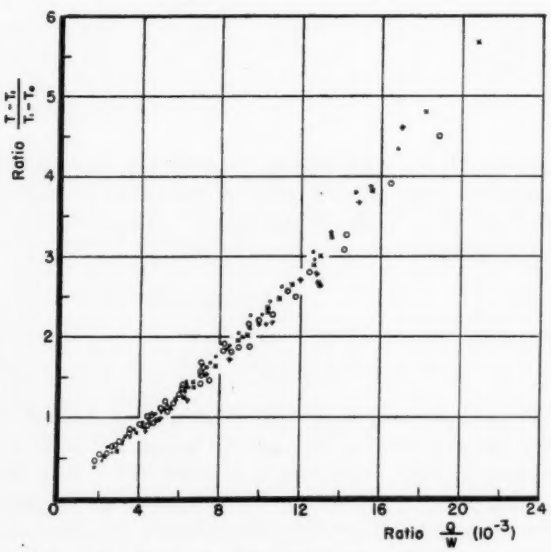

FIG. 10. Ratio $(T - T_1)/(T_1 - T_0)$ vs. ratio Q/W.

$(T - T_0)$, shown in Tables 2 through 5, have been plotted vs. the ratio Q/W in Fig. 11 for porous stainless steel. On this figure, two theoretical curves corresponding to a Reynolds Number of 30×10^3 and 100×10^3, respectively, have also been traced. The experimental results seem to fall on a single curve having the shape of the theoretical curves. The different symbols corresponding to different gas temperatures are too scattered to show the small dependency upon the Reynolds Number predicted by this theory. Moreover, the difference between experimental and theoretical values is, in general, appreciable.

Yuan[4] made a theoretical investigation of the flow of a hot fluid over a sweat-cooled porous plate. He assumed that (1) both the fluid passing over the plate and the fluid forced through the plate are incompressible; (2) the viscosities of both fluids are constant; and (3) no turbulent flow is involved in the problem. The momentum and energy equations for the boundary layer were set up with the velocity of the injection as-

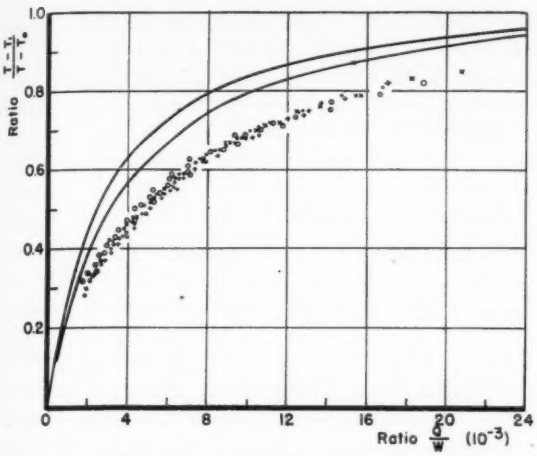

FIG. 11. Ratio $(T - T_1)/(T - T_0)$ vs. ratio Q/W.

sumed to be uniform over the entire plate. In solving the laminar boundary-layer equation, the momentum and energy equations were reduced to an integral form similar to the Kármán integral relation of the Prandtl equation. The solutions were obtained by assuming the velocity and temperature profiles in the boundary layer as either a polynomial of the fourth degree or an exponential function.

The solutions of the equations gave relationships between velocity and temperature layer thicknesses on the one hand, and the distance, in the direction of flow, from the leading edge of the sweat-cooled plate on the other. Calculations were carried out for the temperature profiles in the boundary layer at different Prandtl Numbers. These calculations were made possible by assuming a constant ratio of the thickness of the temperature layer to that of the velocity layer. This assumption was justified, since similar profiles were assumed for velocity and temperature distributions. The thicknesses of the temperature and velocity layers do not differ appreciably within the range of Reynolds Numbers encountered in this investigation.

Knowing that the quantity of heat removed from the plate by the coolant is equal to the quantity of heat that is transferred to the plate through the protective layer, a relation between the wall temperature and the rate of coolant flow was established. The final result is a linear relation between the temperature ratio θ and the square of the ratio of coolant velocity v to average main stream velocity U.

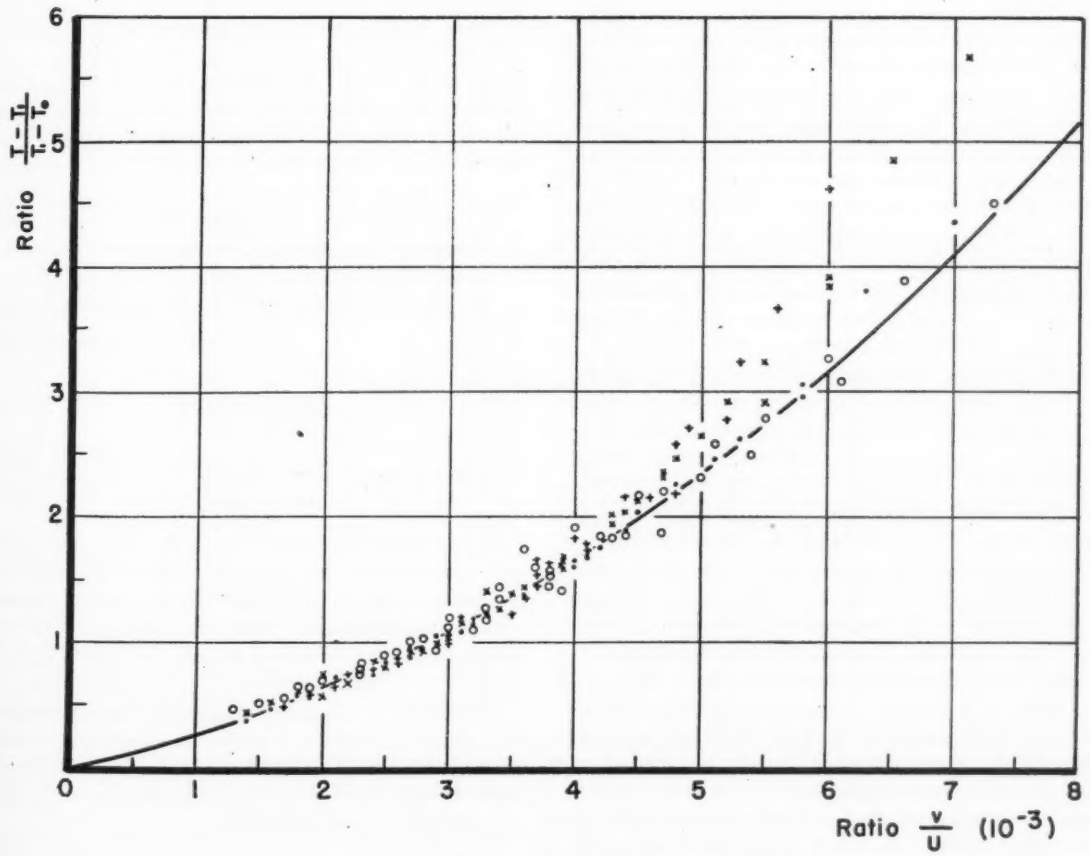

FIG. 12. Ratio $(T - T_1)/(T_1 - T_0)$ vs. ratio v/U.

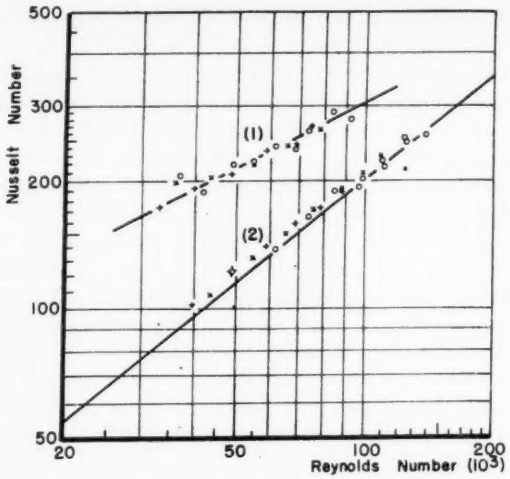

FIG. 13. Nusselt Number vs. Reynolds Number for a $1^1/_2$-in. long duct and an 8-in. long duct.

Although the theoretical study of Yuan is not exactly applicable to the conditions under which the experiments were carried out, it is interesting to compare the theoretical curve of θ vs. v/U with the experimental results. As shown in Fig. 12, the measurements obtained with a stainless-steel specimen are in excellent agreement with the theoretical curve computed for a Reynolds Number of 30,000. This agreement may be just a coincidence, since, as indicated in reference 4, the relation between the temperature ratio θ and v/U is dependent on the Reynolds Number, whereas the experiments seem to indicate that the Reynolds Number effect is of secondary importance. In addition, as mentioned previously, the results of tests made with porous copper, porous nickel, and a porous ceramic material did not duplicate the results obtained with porous stainless steel and, if plotted on the graph of Fig. 12, would not fall on the theoretical curve.

Normally, one would not expect the physical properties of the porous material to influence the boundary-layer conditions. One possible explanation for the effect of the material on the conditions of heat transfer is the existence of a longitudinal temperature gradient along the sweat-cooled wall. It is probable that the mixing of the cooling gas with the turbulent core produces a progressive decrease in the rate of heat transfer along the sweat-cooled section. The result is a temperature gradient in the longitudinal direction. It therefore seems probable that the thermal conductivity of the sweat-cooled material enters into the problem. On this basis, it is possible to explain that, while the theories predict the same coolant flow to obtain a given wall temperature, more coolant is actually required to cool copper than a ceramic material.

In trying to correlate the experimental results with theoretical studies, the exact conditions in which tests were performed should be borne in mind. The relatively short length of the sweat-cooled section, for example, is an important factor. If a longer tube has been used, the surface temperature of the specimen would probably have shown a decrease in the downstream direction. Because only one thermocouple was used on the inside surface of the $1^1/_2$-in. long specimen, this gradient was not observed. Additional experiments with a longer sweat-cooled section will probably throw some light on this aspect of the problem.

(VI) Summary and Conclusions

The experimental study of heat transfer in a sweat-cooled duct has shown that:

(1) The surface temperature of the porous material is a decreasing function of the coolant flow when both temperature and velocity of the main gas stream are constant. The surface temperature decreases slowly when the rate of coolant flow is increased beyond a certain value.

(2) The relation of surface temperature to rate of coolant flow is influenced by both the temperature and the velocity of the main gas stream.

(3) A correlation of all the results measured with any porous material and cooling gas may be obtained by using either one of the ratios $(T - T_1)/(T_1 - T_0)$ or $(T - T_1)/(T - T_0)$ and relating it to a function Q/W or to v/U.

(4) Only a fair agreement is obtained between the available theoretical studies and the experimental results. It seems, however, that most of the difference may be due to the fact that the experimental conditions do not correspond to those assumed in the theories.

(5) The experimental results indicate that under the conditions present in this investigation, the nature of the porous material has a marked effect on the average heat transfer to the wall of the sweat-cooled specimen.

Appendix

Measurement of Heat Transfer to a Cylindrical Water-Cooled Duct

The measurements of heat transfer to a conventionally water-cooled duct were made with the purpose of obtaining a basis of comparison for the results obtained with the sweat-cooled section. Experiments were made with two ducts of different length, $1^1/_2$ and 8 in. long, respectively. Both ducts were 1 in. in diameter.

The results of the heat transfer tests are summarized in a graph of Nusselt Number vs. Reynolds Number, presented in Fig. 13. The measurements obtained with the 8-in. duct show a satisfactory agreement with the generally accepted relation

$$(h/k)D = 0.02R_e^{0.8} \qquad \text{(A-1)}$$

corresponding to the straight line shown in Fig. 13. The measurement obtained with a tube $1^1/_2$ in. long gave a Nusselt Number higher than predicted by Eq. (A-1). The results seem to be on a straight line, which would correspond to the relation

$$(h/k)D = 0.95R_e^{0.8} \qquad \text{(A-2)}$$

An important result of the heat-transfer measurements with water-cooled ducts is that the conventional relation (A-1) does not apply to a tube $1^1/_2$ in. long and 1 in. in diameter. Hence, the experimentally determined relation between Nusselt Number and Reynolds Number (curve 1 of Fig. 13) should be taken as a basis of comparison for the sweat-cooling results.

The fact that the measurements of heat transfer made with a water-cooled section 8 in. long agree closely with the generally accepted Eq. A-1) is an indirect proof that the measurements of velocity and temperature of the main gas stream were reliable.

References

[1] Hottel, H. C., and Kalitinsky, A., *Temperature Measurements in High Velocity Air Streams*, Journal of Applied Mechanics, p. A-25, March, 1945.

[2] Duwez, Pol, *Experimental Study of Cooling by Infiltration of a Fluid Through a Porous Material*, Sixth International Congress for Applied Mechanics, Paris, September, 1946.

[3] Weinbaum, S., and Wheeler, H. L., Jr., *Heat Transfer in Sweat-Cooled Porous Metals* (in preparation).

[4] Yuan, S. W., *A Theoretical Investigation of the Temperature Field in the Laminar Boundary Layer on a Porous Flat Plate with Fluid Injection*, U.S.N. Project SQUID Technical Report No. 4, September 5, 1947 (Polytechnic Institute of Brooklyn).

[5] Rannie, W. D., *A Simplified Theory of Porous Wall Cooling* (to be published).

[6] Bakhmeteff, Boris A., *The Mechanics of Turbulent Flow*, Princeton University Press, 1936.

Letters to the Editor

Dear Sir:

In the May issue of the JOURNAL, F. A. Cleveland presented an excellent paper on "Afterburners for Turbojet Engines".

He analysed afterburning in ducts with constant cross-sectional area and said that the fuel flow in this case can be selected in any arbitrary manner up to a maximum value being limited by the airflow available for the combustion [Eq. (16) in his paper].

This assertion may be correct in certain practical cases but does not apply to general conditions, since there exist other limits that sometimes can present themselves prior to the above-mentioned one. I should like to point out these limits here.

If we disregard pressure losses due to friction and diffusion losses along the combustion chamber, static pressure decrease arises according to the energy equation

$$-v\,dp = V\,dV/g \qquad (1)$$

where v is the specific volume and V is the gas velocity. This results in corresponding total pressure decrease. Considering the basic premise A = const. (between stations 6 and 9) we can write Eq. (1), after a few transformations and integration, as follows:

$$p_9/p_6^* = \Lambda - \gamma_6 M_6[V_9/V_6 - \Lambda] \qquad (2)$$

where the term

$$\gamma_6 M_6 = V_6^2/gRt_6 \qquad (3)$$

characterizes the original condition of afterburning (at station 6) and where the velocity ratio V_9/V_6 is a function of heat input Q (fuel flow) and of original condition. The relation $V_9/V_6 = f(Q)$ can be derived by simple means, but it has no practical significance, because a computation using a total heat-entropy diagram is more convenient.

Eq. (2) shows that the pressure ratio p_9/p_6 can considerably decrease if the term (3) reaches high values. This can happen especially at take-off and in flight at sea level. Important decrease in static pressure p_9 with increasing heat input can possibly check the latter by the following two limits: (a) the static pressure p_9 approaches the critical pressure; (b) the static pressure p_9 approaches the ambient static pressure p_0.

The second case will occur instead of the first if the pressure difference $p_6 - p_0$ is comparatively small. If the fuel flow is selected higher than is compatible with one of the above-mentioned limits, a decrease in airflow will result.

As is to be seen from Eq. (2), the Mach Number M_6 influences to a high degree the static pressure decrease, while the velocity V_6, which must be low enough to avoid flame blowout, is not the only criterion for static pressure decrease (disregarding here friction losses, etc), since the value of the static temperature t_6 according to Eq. (3) must be also considered. In practical computations, of course, losses due to friction and diffusion must be added to the aforesaid theoretical pressure decrease, and they will cause limit (a) or (b) to be reached even sooner. However, it seems worth while to compute p_9/p_6 according to Eq. (2) in order to estimate real pressure p_9.

The Mach Number M_6 can be kept low by suitable diffuser design. But first investigation should be made, considering the turbojet regulation proceeding, to find out those turbojet operating conditions for which the turbine exit Mach Number M_6 reaches its highest value.

When making up exact computations, there must also be taken in account the alteration of the original condition of afterburning (station 6) by the additional afterburning fuel flow.

GÜNTHER HELMECKE
Cité Voisin, Bât.A
Rue de Faulquières
Decize/Nièvre, France

Dear Sir:

The article on "Buckling of Curved Sheets in Compression and Its Relation to the Secant Modulus," by E. H. Schuette, JOURNAL OF THE AERONAUTICAL SCIENCES, Vol. 15, No. 1, January, 1948, is extremely interesting and worth while. Certain tests upon flat plate elements which were analyzed by the writer showed strengthening of such plates through curvature induced during the application of load, the certainty and degree of such strengthening being related to the stiffening effect of the edge stiffeners. As such curvature did not exist initially transversely of the flat

plate elements, curved plate behavior had to be determined from the variation of curvature with load, failure occurring when the load became large enough to permit buckling but only when the induced radius of curvature failed to keep pace with the requirements for curved plate behavior at the stress existing.

In view of the above observations, correlation of data obtained by Mr. Schuette might be improved, I believe, by measuring curvature close to the failure load and noting the relation of such variations from initial curvature to the R/T ratio of the specimen. At least the relatively wide range of plotted points requires narrowing through definite allowance for such effects, if any. The important data is the final, not the initial, curvature.

To emphasize the point, it seems well to consider somewhat briefly the nature of the tests upon flat plate elements which led to such observations.

Twenty-eight test sections were available. Nominal dimensions of these U-shaped, roof-deck type of beam sections were the same except for two flat plate widths (and several thicknesses), the tests being parted into those involving 5.5-in. wide flat plates and those 10.5 in. wide. Each group was divisible in turn into two groups, one of which had the flanges held in fixed spacing laterally at several points spanwise, the other in which there was no such lateral restraint and flanges tended to spread laterally through a rotation of the flanges about the lines of junction of flanges and webs. Suppose R and U define restrained and unrestrained groups, respectively, and N and W define the narrower and the wider web plates (in compression), respectively, so that there might be a trend from most edge restrained to least edge restrained represented by RN, RW, UN, and UW.

The above tests, be it noted, were part of a program carried out by Dr. George Winter at Cornell University for the American Iron and Steel Institute.

It was found that the failure load might be calculated by means of the formula $M_c = f_y S_e$ to yield a value P_c calculated for the failure load. M_c is the calculated failure moment, f_y is the yield point of the material, and S_e the section modulus of the reduced section. Reduction in all cases was based on the formula $(b/t) = 10{,}320/\sqrt{f_y}$ or (w/t), whichever is less, where w is the clear web width between flanges and b is the equivalent web width, t being the thickness. This (b/t) formula corresponds to that for *supported edge plates*. In the case of R sections, this formula gave substantially the lower limit of strength (two minor exceptions), while the upper limit was substantially given by the formula for *clamped edge plates* using 13,630 for the coefficient, there being four cases of exceeding the upper limit. The balance of cases were scattered in between. In the case of the U sections, all of the N and two of the W behaved as though the (b/t) formula in 10,320 yielded *average values*, while the remaining two W sections behaved as though *unreduced*.

Now the basis for comparison will be the value of the ratio (P_u/P_c) of the ultimate test value to the calculated value.

Out of 15 R sections, seven were RN.

RN.—With P_c based on *clamped* edges, two had (p_u/P_c) of 1.004 and 1.030. The latter value was in the range of $(w/t) = 175$. Below $(w/t) = 100$ (the stiffer sections), the ratio closely approached 1.000. At least one section stiffened somewhat by curvature.

RW.—Of these eight sections, three were strengthened by curvature, the ratios being 1.068, 0.992 (where 0.85 was expected), and 1.045. These sections were less stiff than RN.

UN.—Four sections with P_c calculated as *supported*. One section, with $(p_u/p_c) = 1.042$, was definitely strengthened by curvature.

UW.—Four sections, all of which were effectively strengthened by curvature, with (P_u/P_c) (P_c based on *supported edges*) taking the values 1.048, 1.017, 1.173, and 1.374. The last two, or 50 per cent of this most flexible group, behaved substantially as unreduced. *Basing P_c on solid sections*, the last two have (P_u/P_c) ratios of 0.966 and 1.176.

To recapitulate, the number of sections strengthened by induced curvature were one, three, one, four, the last including two that were substantially solid. The numbers are about on the basis of relative flexibility, the more flexible, the more numerous. More exactly, 1/7, 3/8, 1/4, and 4/4 are the ratios of number strengthened to number in the group.

These analyses were made by the writer because of the unsatisfactory character of the Sechler type of plot for the setting of allowable effective widths of flat plate elements as used by Dr. Winter. The points on the Sechler plot showed an excessive scatter, the range of which strongly indicated differences of behavior of flat plates with character of edge stiffening. Further details may be found in *Proc. A.S.C.E.* about February, 1946. The conclusion derived from the analyses was that there were marked differences in behavior with edge stiffening and that close estimates of the average failure load (most U group elements) or of the minimum ultimate strength (all R group elements) were possible with the simplest of effective width formulas derivable from buckling theory. (Further tests covered short columns with unstiffened flanges which behaved well when P_c column values were based on an effective flange width of (b/t) $3{,}672/\sqrt{f_y}$).

In view of the above analyses, I feel that it would be well worth while reporting radii of curvature of curved sheets close to failure and evaluating them with due regard to edge stiffening and (R/t) ratios in order to narrow the range of scatter. I feel sure that trends may develop which can be eliminated by closer analysis.

The utility of these observations and analyses resides in the ability to derive simpler formulas; to calculate more exactly minimum strength values; to evaluate edge conditions; and last, but probably not least, the concept of a slight imposed initial curvature in flat elements to direct and ensure behavior as solid elements without any reduced effective width.

EDWARD ADAMS RICHARDSON
Bethlehem Steel Company

Changes of Address

Since the Post Office Department does not as a rule forward magazines to forwarding addresses, it is important that the Institute be notified of changes in address 30 days in advance of publishing date to ensure receipt of every issue of the *Journal* and *Review*.

Notices should be sent directly to the Institute of the Aeronautical Sciences, 2 East 64th Street, New York 21, N.Y.

Hyperbolic Column Formulas for Magnesium-Alloy Extrusions

E. H. SCHUETTE*
The Dow Chemical Company

SUMMARY

Results are presented for tests of 89 Z-section columns of M, FS-1, J-1, O-1, and O-1HTA alloys. The tests were conducted in an effort to arrive at suitable column formulas for use in design. In addition to prescribing such formulas, the following supplementary conclusions were reached:

(1) The tangent modulus column curve does not give consistently good fits to test data for magnesium-alloy extrusions.

(2) The end fixity achieved by a column tested flat-ended is probably influenced by the cross-sectional shape of the column.

(3) Rounds and shapes follow qualitatively different column curves.

INTRODUCTION

THE BEHAVIOR OF SIMPLE COLUMNS within the elastic range is well understood. For predicting column strength beyond the elastic range, a number of methods, both empirical and theoretical, have been proposed. For magnesium alloys, the problem of arriving at a suitable method has been complicated by a lack of adequate test data. A brief survey of column data for magnesium alloy extrusions gave indication not only that the data were insufficient for obtaining conclusive results but that curves based on tests of rounds (comprising a large portion of the total data) would not be satisfactory for the design of shapes. As a consequence of that survey, a new test program, comprising 89 specimens and covering M, FS-1, J-1, O-1, and O-1HTA alloys was undertaken. The results of that program are the subject of this report.

SYMBOLS

A = area of column cross section, sq.in.
E = modulus of elasticity, ksi
E_t = tangent modulus of elasticity, ksi
F_{cy} = compressive yield stress, ksi
K = empirical constant
L = column length, in.
L' = column effective pin-ended length, in.
P = load, kips
R = minimum radius of gyration of column cross section, in.
c = fixity coefficient in the Euler column formula when given in the form, $P/A = c\pi^2E/(L/R)^2$
n = empirical constant
ksi = kips (thousands of pounds) per sq.in.

Received February 12, 1948.
* Division of Tests, Magnesium Laboratories.

EXPERIMENTAL WORK

Specimens and Method of Testing

To avoid introducing an excessive number of variables, a single Z-section shape, Dow die No. 4, was selected for all the alloys. The pieces chosen for test showed the following average dimensions:

Flange width (overall):	1.50 in.
Web width (overall):	1.75 in.
Flange thickness:	0.182 in.
Web thickness:	0.184 in.

Specimen lengths and areas are given in Tables 1–5. The ends of the specimens were milled flat, square, and parallel. The accuracy obtained by this procedure has not been evaluated, but the fact that it is generally as accurate as is warranted by the probable straightness of the columns is attested to by the consistent results and smooth curves obtained. In only two cases, numbers 16 and 32, did it appear, upon placing the columns in the machine, that the ends were not properly squared with the column axis. Since the columns were milled in pairs, clamped together, this probably means that numbers 15 and 31 were also below the desired level of accuracy. All four gave low points on the final plots. Moreover, the two specimens specifically noted (16 and 32) in each case accounted for the low point of the pair.

The specimens were tested flat-ended on the 30,000-lb. range of a 300,000-lb. capacity testing machine. The ram elevation was maintained essentially constant for all tests, and, for the ram setting, loads, and range used, the machine is believed to have given an accuracy of better than 1 per cent.

The lower end of each specimen was located with the aid of concentric rings on the testing machine head. Checking of the vertical alignment was facilitated by the fact that a thin oil film on the upper head was squeezed out by the pressure of the specimen, leaving a clear mark and making it easy to determine whether subsequent specimens were bearing in the same place as the first. Testing was begun on the shortest specimen, so that a minimum of misalignment was present when the mark was first produced.

The testing machine was run at a rate of 0.3 in. per min. until near the maximum load, when the rate was reduced to 0.05 in. per min. up to failure. Only the

TABLE 1
Column Test Results for M Alloy Z-Section

Column No.	F_{cy}, Ksi	L, In.	A, Sq.In.	P, Kips	P/A, Ksi	$(P/A)/F_{cy}$	L'/R, $1.691 \times L$	$\sqrt{F_{cy}}(L'/R)$, $(\text{Ksi})^{1/2}$	$F_{cy}(L'/R)^2$, Ksi
1	9.7	26.40	0.806	6.47	8.03	0.828	44.7	139.2	19,400
2	9.7	26.40	0.804	7.09	8.81	0.909	44.7	139.2	19,400
3	9.7	33.92	0.806	7.14	8.85	0.912	57.4	178.8	31,960
4	9.7	33.93	0.806	6.99	8.67	0.894	57.4	178.8	31,960
5	9.7	39.46	0.806	6.96	8.64	0.890	66.7	207.8	43,100
6	9.7	39.46	0.806	6.95	8.62	0.889	66.7	207.8	43,100
7	9.7	44.80	0.806	6.89	7.31	0.754	75.7	236.0	55,700
8	9.7	44.81	0.804	6.23	7.75	0.799	75.7	236.0	55,700
9	9.7	53.32	0.806	5.07	6.29	0.649	90.1	280.6	78,700
10	9.7	53.31	0.804	4.83	6.01	0.620	90.1	280.6	78,700
11	9.7	63.32	0.806	4.20	5.21	0.537	107.0	333.2	110,900
12	9.8	63.30	0.807	4.14	5.13	0.524	107.0	335.0	112,200
13	9.8	73.20	0.807	3.39	4.20	0.429	123.9	388.0	150,400
14	9.8	73.21	0.807	3.41	4.23	0.432	123.9	388.0	150,400
15	9.7	86.72	0.806	2.03	2.52	0.260	146.7	457	208,800
16	9.7	86.72	0.804	1.81	2.25	0.232	146.7	457	208,800
17	9.5	106.93	0.809	1.57	1.94	0.204	180.9	557	310,000
18	9.5	106.91	0.809	1.50	1.85	0.195	180.9	557	310,000

TABLE 2
Column Test Results for FS-1 Alloy Z-Section

Column No.	F_{cy}, Ksi	L, In.	A, Sq.In.	P, Kips	P/A, Ksi	$(P/A)/F_{cy}$	L'/R, $1.691 \times L$	$\sqrt{F_{cy}}(L'/R)$, $(\text{Ksi})^{1/2}$	$F_{cy}(L'/R)^2$, Ksi
19	13.6	22.19	0.819	11.79	14.41	1.061	37.5	138.3	19,140
20	13.6	22.20	0.816	11.92	14.63	1.078	37.5	138.3	19,140
21	13.7	28.49	0.819	11.80	14.42	1.053	48.2	178.3	31,800
22	13.5	28.49	0.817	11.19	13.70	1.015	48.2	177.1	31,400
23	13.6	33.33	0.819	10.26	12.53	0.921	56.3	207.4	43,000
24	13.6	33.32	0.816	11.16	13.69	1.007	56.3	207.4	43,000
25	13.6	37.87	0.819	9.19	11.22	0.825	64.0	236.0	55,700
26	13.6	37.85	0.816	9.25	11.33	0.834	64.0	236.0	55,700
27	13.7	44.94	0.819	7.38	9.01	0.658	75.9	280.8	78,800
28	13.6	44.93	0.819	7.06	8.62	0.634	75.9	279.8	78,100
29	13.6	53.67	0.819	5.43	6.64	0.489	90.7	334.6	112,000
30	13.6	53.67	0.819	5.33	6.51	0.479	90.7	334.6	112,000
31	13.6	61.97	0.819	4.16	5.08	0.374	104.8	386.2	149,100
32	13.7	61.97	0.819	3.93	4.80	0.350	104.8	388.0	150,400
33	13.6	73.08	0.819	3.55	4.34	0.320	123.6	456	207,600
34	13.7	73.08	0.819	3.27	4.00	0.292	123.6	457	208,800
35	13.5	89.69	0.817	2.35	2.88	0.214	151.8	557	310,000
36	13.5	89.67	0.817	2.19	2.68	0.199	151.8	557	310,000

TABLE 3
Column Test Results for J-1 Alloy Z-Section

Column No.	F_{cy}, Ksi	L, In.	A, Sq.In.	P, Kips	P/A, Ksi	$(P/A)/F_{cy}$	L'/R, $1.691 \times L$	$\sqrt{F_{cy}}(L'/R)$, $(\text{Ksi})^{1/2}$	$F_{cy}(L'/R)^2$, Ksi
37	19.1	18.71	0.788	15.37	19.52	1.022	31.7	138.5	19,190
38	19.1	18.71	0.787	15.38	19.56	1.024	31.7	138.5	19,190
39	19.1	24.11	0.787	14.51	18.46	0.966	40.8	178.1	31,740
40	19.1	24.11	0.787	15.33	19.50	1.021	40.8	178.1	31,740
41	19.2	28.07	0.792	13.89	17.54	0.914	47.5	208.6	43,500
42	19.1	28.06	0.787	14.20	18.07	0.945	47.5	207.4	43,000
43	19.1	31.84	0.788	12.24	15.57	0.815	53.9	235.4	55,400
44	19.2	31.84	0.792	11.95	15.10	0.786	53.9	236.0	55,700
45	19.1	37.99	0.787	9.44	11.99	0.628	64.2	280.4	78,600
46	19.1	37.99	0.787	9.51	12.09	0.633	64.2	280.4	78,600
47	19.1	45.27	0.788	7.43	9.44	0.494	76.5	334.2	111,700
48	19.1	45.26	0.787	6.99	8.88	0.465	76.5	334.2	111,700
49	19.1	52.23	0.788	6.09	7.73	0.405	88.4	386.0	149,000
50	19.1	52.22	0.787	5.87	7.46	0.391	88.4	386.0	149,000
51	19.1	61.61	0.788	4.52	5.74	0.300	104.2	456	207,600
52	19.1	61.60	0.787	4.59	5.84	0.306	104.2	456	207,600
53	19.2	75.16	0.792	3.21	4.06	0.212	127.2	557	310,000

TABLE 4
Column Test Results for O-1 Alloy Z Section

Column No.	F_{cy}, Ksi	L, In.	A, Sq.In.	P, Kips	P/A, Ksi	$(P/A)/F_{cy}$	L'/R, 1.691 × L	$\sqrt{F_{cy}}(L'/R)$, (Ksi)$^{1/2}$	$F_{cy}(L'/R)^2$, Ksi
55	24.1	16.59	0.821	20.65	25.18	1.043	28.06	137.9	19,000
56	24.1	16.59	0.821	20.67	25.20	1.045	28.06	137.9	19,000
57	24.1	21.58	0.821	20.52	25.02	1.038	36.5	179.2	32,120
58	24.1	21.57	0.821	19.60	23.90	0.991	36.5	179.2	32,120
59	24.1	25.22	0.818	18.05	22.08	0.916	42.7	209.8	44,000
60	24.1	25.22	0.811	18.32	22.62	0.939	42.7	209.8	44,000
61	24.1	28.45	0.821	15.62	19.05	0.790	48.1	236.2	55,800
62	24.1	28.45	0.821	15.90	19.39	0.804	48.1	236.2	55,800
63	24.1	33.75	0.821	12.37	15.08	0.626	57.1	280.4	78,600
64	24.1	33.76	0.821	12.64	15.41	0.640	57.1	280.4	78,600
65	24.1	40.24	0.811	9.26	10.42	0.432	68.0	334.0	111,400
66	24.1	40.24	0.811	9.23	11.38	0.472	68.0	334.0	111,400
67	24.1	46.68	0.818	7.32	8.95	0.371	79.0	388.0	150,400
68	24.1	46.69	0.811	7.27	8.96	0.372	79.0	388.0	150,400
69	24.1	54.98	0.818	5.66	6.92	0.287	92.9	456	207,600
70	24.1	54.97	0.811	5.66	6.98	0.295	92.9	456	207,600
71	24.1	66.94	0.818	3.94	4.82	0.200	113.2	556	309,000
72	24.2	66.94	0.813	4.07	5.01	0.207	113.2	557	310,000

TABLE 5
Column Test Results for O-1HTA Alloy Z-Section

Column No.	F_{cy}, Ksi	L, In.	A, Sq.In.	P, Kips	P/A, Ksi	$(P/A)/F_{cy}$	L'/R, 1.691 × L	$\sqrt{F_{cy}}(L'/R)$, (Ksi)$^{1/2}$	$F_{cy}(L'/R)^2$, Ksi
73	37.5	13.28	0.796	28.66	36.04	0.961	22.46	137.5	18,900
74	37.5	13.29	0.796	28.42	35.74	0.953	22.46	137.5	18,900
75	37.5	17.17	0.789	29.05	36.84	0.983	29.02	177.9	31,620
76	37.5	17.16	0.789	27.75	35.20	0.939	29.02	177.9	31,620
77	37.5	20.02	0.789	28.21	35.80	0.955	33.8	207.0	42,800
78	37.5	20.02	0.789	28.75	36.44	0.972	33.8	207.0	42,800
79	37.5	22.74	0.789	26.60	33.74	0.900	38.4	235.2	55,300
80	37.5	22.74	0.789	27.58	34.98	0.932	38.4	235.2	55,300
81	37.5	27.06	0.790	21.51	27.26	0.727	45.7	280.0	78,300
82	37.5	27.05	0.796	20.92	26.30	0.701	45.7	280.0	78,300
83	37.5	32.29	0.796	15.98	20.08	0.536	54.6	334.2	111,700
84	37.5	32.38	0.796	15.73	19.79	0.528	54.6	334.2	111,700
85	37.5	37.45	0.790	12.50	15.83	0.423	63.3	387.8	150,300
86	37.5	37.45	0.790	12.33	15.62	0.417	63.3	387.8	150,300
87	37.5	44.06	0.796	9.75	12.25	0.327	74.5	456	207,600
88	37.5	44.06	0.796	9.69	12.17	0.325	74.5	456	207,600
89	37.5	53.61	0.790	6.45	8.17	0.218	90.6	555	308,000
90	37.5	53.63	0.790	6.14	7.77	0.207	90.6	555	308,000

maximum load was recorded; no additional deflection or other data were taken.

Method of Reducing Data

The area of each length of extrusion used was determined from a single specimen as

$$\frac{\text{Weight (lbs.)}}{\text{Length (in.)} \times \text{Density (lbs. per cu.in.)}}$$

Since, for a given material, the areas determined in this way showed less than 2 per cent variation, it was not thought necessary to make a separate check of area for each individual specimen. The densities used in the calculation were as follows:

M:	0.0635 lbs. per cu.in.
FS-1:	0.0645
J-1:	0.0649
O-1 or O-1HTA:	0.0658

The actual radius of gyration R was not calculated. Calculations for a simplified three-piece section, without radii, and combining the extreme values of recorded dimensions, gave the following values:

Smallest flanges, smallest web:	R = 0.3028 in.
Smallest flanges, largest web:	0.3018
Largest flanges, smallest web:	0.3060
Largest flanges, largest web:	0.3074

These values show a variation of less than 2 per cent. Since these maximum and minimum combinations were not all actually realized, the true variation was undoubtedly even less than indicated. Consequently, the radius of gyration was assumed constant, and its actual value not determined.

The correction for end fixity was obtained from the specimens in the elastic range, excluding numbers 15 and 16, known to be inaccurate. The calculations are indicated in Table 6. The average value of $(L'/R)/L$ obtained from these specimens was used in reducing all the data. With R assumed constant, an intermediate calculation for L/R is unnecessary. In order to check for any large error, however, the degree of fixity was

TABLE 6
Calculation of $(L'/R)/L$

Column No.	P/A, Ksi	L, In.	$(L'/R)_{cal.} = \sqrt{\pi^2 E/(P/A)}$	$(L'/R)/L$, 1/In.
13	4.20	73.20	123.7	1.690
14	4.23	73.20	123.2	1.682
17	1.94	106.93	181.9	1.701
18	1.85	106.91	186.2	1.742
35	2.88	89.69	149.2	1.663
36	2.68	89.67	154.8	1.725
53	4.06	75.16	125.8	1.673
71	4.82	66.94	115.4	1.726
72	5.01	66.94	113.2	1.692
85	12.50	37.45	63.6	1.699
86	12.33	37.45	64.0	1.710
87	9.75	44.06	72.4	1.645
88	9.69	44.06	72.6	1.650
89	6.45	53.61	88.6	1.654
90	6.14	53.63	90.8	1.693

Average value of $(L'/R)/L = 1.691$

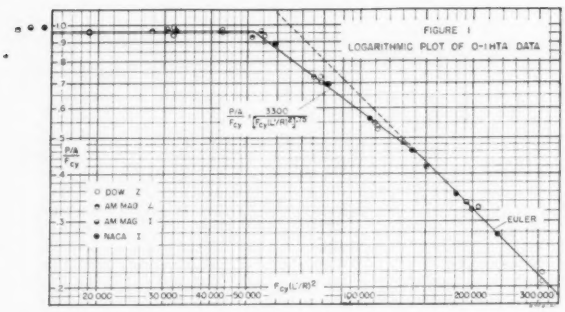

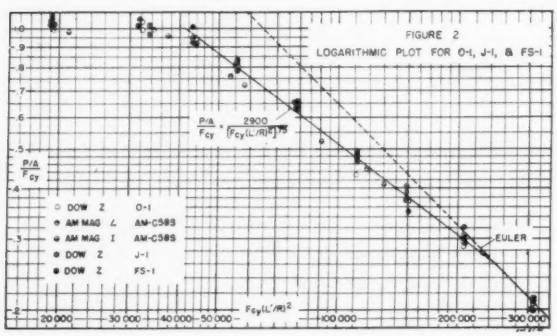

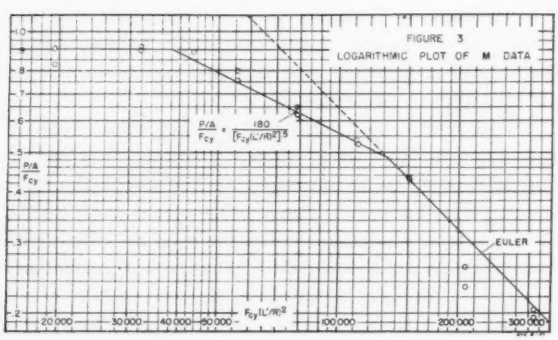

calculated using an average of the previously listed approximate values of R. The value obtained was $c = 3.77$, an entirely reasonable value for this type of testing.

Method of Obtaining Column Formulas

In order to include in the analysis data from other sources, and also to aid in obtaining general column formulas, a set of generalized parameters was adopted. The failing stress was given in terms of the compressive yield stress—that is, as $(P/A)/F_{cy}$. By dividing both sides of the Euler formula by F_{cy},

$$(P/A)/F_{cy} = \pi^2 E/F_{cy}(L'/R)^2$$

the second parameter, $F_{cy}(L'/R)^2$ or $\sqrt{F_{cy}}(L'/R)$, is obtained.

For possible help in arriving at suitable short-column formulas, the plots of $(P/A)/F_{cy}$ vs. $F_{cy}(L'/R)^2$ were made on log-log paper (Figs. 1 to 3), and it was found that excellent fits could be obtained on such plots with straight lines, indicating formulas of the type

$$(P/A)/F_{cy} = K[F_{cy}(L'/R)^2]^{-n}$$

Included in Figs. 1 to 3 are some additional column data on American Magnesium Corporation angle and I-beam sections, and an N.A.C.A. I-beam section, obtained from references 1 and 2. As given in the references, these data were reduced on the assumption of full fixity. Based on the author's experience, however, even though a very nearly uniform contact may be obtained between specimen and bearing plate, column imperfections and flexibility of the testing machine make a fixity coefficient of four unlikely of attainment. Consequently, for plotting in this report, the test data were adjusted for the following values of fixity coefficient c, calculated from points in the elastic range:

Am. Mag.	L	3.97
Am. Mag.	I	3.65
N.A.C.A.	I	3.79

The N.A.C.A. tests were on Dowmetal O-1HTA. The American Magnesium Corporation tests were on alloy AM-C58S, equivalent to O-1, and AM-C58S-T5, essentially equivalent to O-1HTA.

Probably the straight lines shown in Figs. 1 to 3 are not the best fits that could be made to each individual set of data. They were selected with a view to obtaining formulas as much alike as possible for the several alloys and with exponents readily handled in slide-rule calculations. On the whole, little adjustment was necessary to achieve these ends; the extreme consistency of the several test series plotted in Figs. 1 to 3 is, in fact, surprising.

Because log-log plots are often misleading as to accuracy of curve fitting, the test data and curves are replotted on rectangular coordinates in Figs. 4 to 7. Here the abscissa has been changed to $\sqrt{F_{cy}}(L'/R)$ to

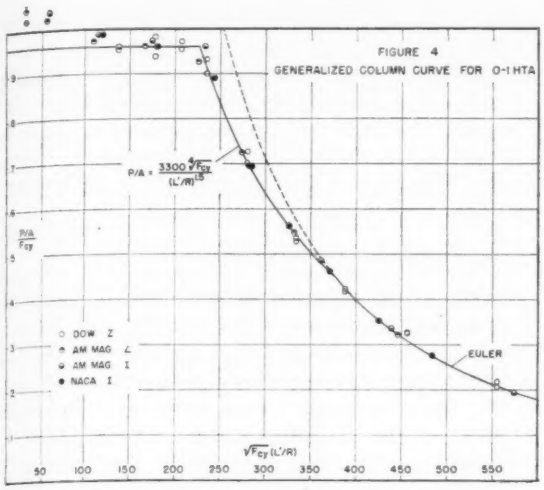

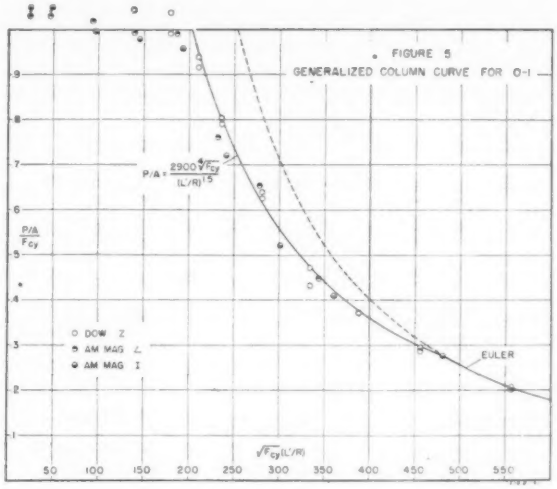

give a better distribution of the test points on the graph and to produce curves more nearly corresponding to the conventional P/A vs. L'/R plot.

The good agreement obtained between curves and test data is clearly shown by these plots. It should be emphasized at this point that Fig. 4 includes data for material whose compressive yield stresses vary from 30.2 ksi (Am. Mag. L) to 37.5 ksi (Dow Z). In Fig. 5, the corresponding spread is from 21.2 ksi (Am. Mag. I) to 24.1 ksi (Dow Z), and in Fig. 6, from 13.6 ksi (FS-1) to 19.1 ksi (J-1). The curves in Figs. 5 and 6, moreover, are identical.

The recommended column formulas, obtained from the plots just presented, are as follows:

M alloy:

$$P/A = \frac{180\sqrt{F_{cy}}}{L'/R} \text{ (Max. } P/A = 0.90F_{cy})$$

FS-1, J-1, and O-1 alloys:

$$P/A = \frac{2{,}900\sqrt[4]{F_{cy}}}{(L'/R)^{1.5}} \text{ (Max. } P/A = F_{cy})$$

O-1HTA alloy:

$$P/A = \frac{3{,}300\sqrt[4]{F_{cy}}}{(L'/R)^{1.5}} \text{ (Max. } P/A = 0.96F_{cy})$$

All stresses are used in kips per sq.in.

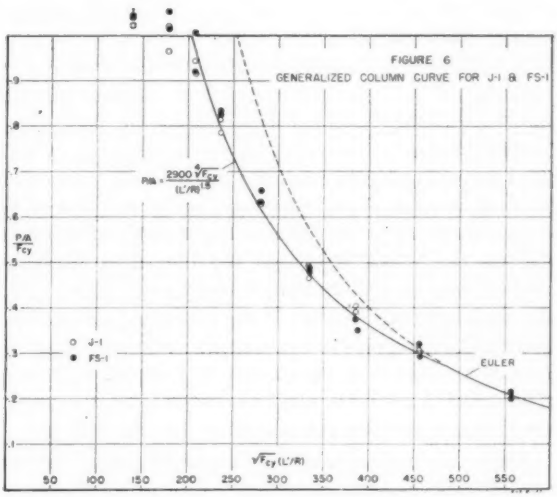

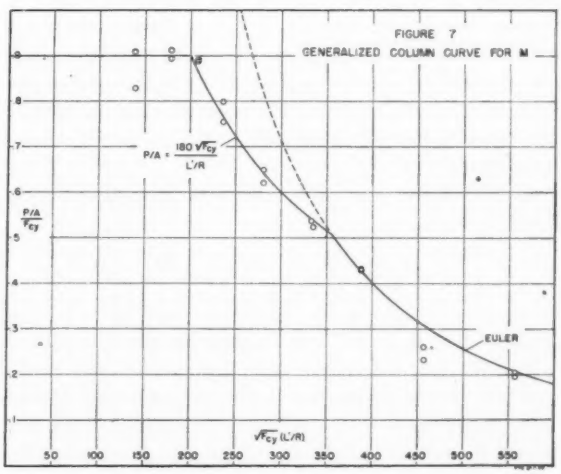

Fits Obtained by Other Methods

A column curve that could be obtained directly from the stress-strain curve would possess the distinct advantage that, once the method had been proved, a column curve for a new material could be prescribed without the need for any column tests. For this reason, the use of the tangent modulus to replace the initial modulus in the Euler formula,

$$P/A = \pi^2 E_t/(L'/R)^2$$

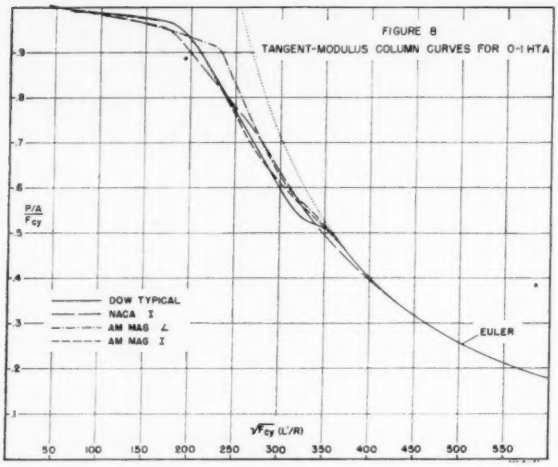

has been proposed as a method for predicting short-column strength. In a number of instances, this method has given good results for aluminum alloys. A brief study was therefore made to determine its possible applicability to extruded magnesium alloys.

In Fig. 8 are shown four tangent-modulus column curves for O-1HTA—a curve obtained from the typical O-1HTA stress-strain curve given in reference 3 and three curves obtained from the stress-strain curves for the column material of references 1 and 2. Complete stress-strain curves for the material tested in this investigation were not available for obtaining tangent-modulus values. It is immediately noted that, while the data plotted in Fig. 4 are extremely consistent, there is considerable scatter in the curves of Fig. 8. Detailed comparison shows also that in only one case (Am. Mag. L) is there satisfactory agreement between the tangent-modulus column curve and the test data.

There are two possibilities to consider here. Either the differences in Fig. 8 are due to difficulties in obtaining accurate tangent-modulus values from stress-strain curves, or materials possessing different tangent moduli are capable of giving column test results of the consistency evidenced by Fig. 4. It is, however, immaterial which explanation is the more nearly correct one; in either case, it appears that the tangent-modulus method must be considered unsatisfactory because of the much better fit obtained by the proposed hyperbolic formulas.

Consideration was also given to formulas of the Rankine type:

$$P/A = F_{cy}/[1 + k(L'/R)^n]$$

If such a formula is to produce a good fit, a plot of $[F_{cy}/(P/A)] - 1$ vs. L'/R on log-log paper should show a straight line. A few trials of such a plot were made, and they definitely did not show straight lines. Consequently, because of the relative simplicity of the proposed hyperbolic formulas, which did give good fits, study of the Rankine-type formula was not pursued further.

With regard to such empirical curves as the straight line and the Johnson parabola, a brief study of the Figs. 4 to 7 will show that the general shape of the curve is such that it could not be well represented by either a straight line with a horizontal cutoff or an inverted parabola.

Minimum Property Column Curves

Because of the general interest in curves for material of minimum properties, it is desirable to construct graphs based on the proposed hyperbolic formulas, incorporating minimum values of compressive yield stress. Such minimum values have been prescribed for three of the materials tested—namely, O-1HTA, O-1, and J-1. The column curves for these materials, with minimum properties, are given in Fig. 9 in the conventional form of P/A vs. L'/R.

Discussion

Effect of Shape on Column Fixity

In the section on "Method of Obtaining Column Formulas," different values were ascribed to the fixity coefficient for the two different sections tested by the American Magnesium Corporation. This procedure might well cause the reader some concern, in view of the fact that for the present investigation, a constant value was taken for all five materials. However, in this case, it is felt that the end justifies the means. The procedure gave considerably better fits than would have been obtained if an average value of c had been used for both sections. It would appear, moreover, that the proposed hyperbolic curves could still be justified if the American Magnesium data were left out of consideration. If, then, the use of fairly reasonable assumptions makes these latter data agree closely with the rest, it is well to proceed on the basis of those assumptions.

From the above reasoning, one may conclude that the fixity obtained in a flat-end column test is very likely influenced by the shape of the section tested.

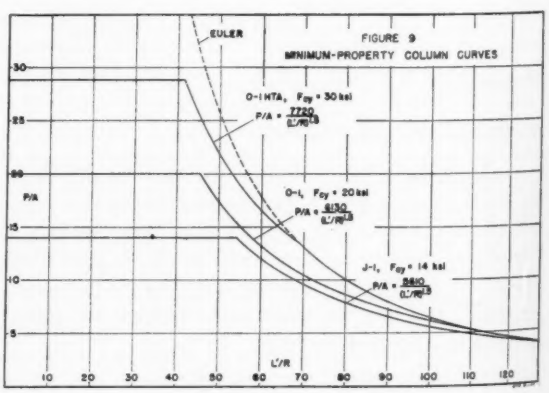

Comparison with Column Data on Rounds

In the "Introduction," it was stated that a survey of previously obtained data gave indication that column data on rounds would be unsatisfactory for the design of shapes. The present data now enable a further check of that situation. In Fig. 10, therefore, the curves obtained herein for shapes are plotted along with applicable test data on rounds taken from reference 4. It is evident, even though the data on rounds are insufficient for accurately prescribing the curves, that these data show lower slopes than were obtained for shapes; the curves leave the horizontal cutoff at lower values of $F_{cy}(L'/R)^2$ and intersect the Euler curve at higher values of $(P/A)/F_{cy}$.

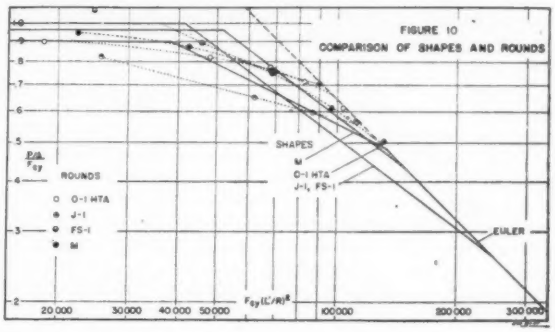

Conclusions

(1) The following formulas give excellent fits to the test data in the short-column range:

M alloy:

$$P/A = \frac{180\sqrt{F_{cy}}}{L'/R} \text{ (Max. } P/A = 0.90F_{cy})$$

FS-1, J-1, and O-1 alloys:

$$P/A = \frac{2{,}900\sqrt[4]{F_{cy}}}{(L'/R)^{1.5}} \text{ (Max. } P/A = F_{cy})$$

O-1HTA alloy:

$$P/A = \frac{3{,}300\sqrt[4]{F_{cy}}}{(L'/R)^{1.5}} \text{ (Max. } P/A = 0.96F_{cy})$$

All stresses are used in kips per sq. in. These formulas are recommended for design.

(2) The tangent-modulus column curve does not give consistently good fits to test data for magnesium-alloy extrusions.

(3) The end fixity achieved by a column tested flat-ended is probably influenced by the cross-sectional shape of the column.

(4) Rounds and shapes follow qualitatively different column curves.

References

[1] Leary, J. R., and Holt, M., *Column Strength of Extruded Magnesium Alloys AM-C58S and AM-C58S-T5*, N.A.C.A. T.N. No. 994, December, 1945.

[2] Heimerl, G. J., and Niles, D. E., *Column and Plate Compressive Strengths of Aircraft Structural Materials-Extruded O-1HTA Magnesium Alloy*, N.A.C.A. T.N. No. 1156, January, 1947.

[3] Eastman, E. J., McDonald, J. C., and Moore, A. A., *The Relation of Stress to Strain in Magnesium Base Alloys*, Journal of the Aeronautical Sciences, Vol. 12, No. 3, July, 1945.

[4] Rappleyea, F. A., *Strength of Magnesium Alloy Columns*, Journal of the Aeronautical Sciences, Vol. 12, No. 3, July, 1945.

Letters to the Editor

Dear Sir:

I wish to congratulate J. F. McBrearty for his interesting paper "A Critical Study of Aircraft Landing Gears," which appeared in May, 1948, issue of the JOURNAL OF THE AERONAUTICAL SCIENCES.

During World War II, I have had the opportunity of working as test engineer with Olaer Comp. in France, maker of hydraulic installations for aircraft. I was attached to the drop-test department of that company, and the machine in use was similar to one shown in the picture in the McBrearty paper, but of smaller size. Test results were recorded on moving film. The assembly of landing gear and shock absorber was dropped onto a platform with piezoquartz unit connected to the recording apparatus. Already at that time some of the aspects mentioned and summarized in Mr. McBrearty's paper were observed.

Shock absorbers in use were of the hydropneumatic type patented by Olaer Comp. The amount of oil air pressure, and valve settings were adjusted independently to suit different types of aircraft, their load, landing speed, etc. Of course, each specific group of shock absorbers had a maximum and minimum value of permissible static load (gross weight of the airplane).

Some of the results are of particular interest to the investigators of drag failures in the main landing gear initiated by compression forces in elements designed for tension stresses, as in the example mentioned by Mr. McBrearty on page 269 under No. (1). Drop tests of the landing gears produce a graph of oscillatory character mainly dependent on the damping characteristics of the shock absorber itself; however, the elastic properties of the whole structure and of the tires have a considerable influence upon the final result. For each particular gear assembly with a particular shock absorber there were differences in the character of the resonance vibrations for different loads and heights of free drop.

To be sure, these vertical vibrations do not correspond exactly to forces and accelerations present during a normal airplane landing. It was suggested that a moving platform be constructed under the drop-test machine in order to provide the conditions similar to those that would occur in real landings. Of course, there are many difficulties, but none of them is of insurmountable

character at the present time. Electronic devices can be easily used for proper recording of the resulting forces, deflections, and accelerations in any plane (mainly vertical and horizontal).

These vertical oscillations in some peculiar landing conditions may result in resonance-actuated horizontal oscillations in the drag plane, causing the total instantaneous forces to exceed the permissible values. From my past experience as a pilot and test-flight engineer I know cases where normal landing with great forward velocity and without much sinking caused greater drag forces on the landing gear than landing with the same airplane and the same load with a high sinking speed. The only explanation of this is the combination of the vertical and horizontal forces together with oscillations from the vertical shock absorber which excite critical response at the natural frequency of the gear assembly, increasing the oscillatory and spin-up drag forces.

JERZY ILLASZEWICZ, P. ENG.
Victoriaville, P.Q., Canada

Dear Sir:

Certain calculations and conclusions presented by Alan Pope in his paper "On Airfoil Theory and Experiment" (JOURNAL OF AERONAUTICAL SCIENCES, vol. 15, No 7, pp. 407–410, July, 1948) concerning the theoretical aerodynamic centers of airfoils with thickness, are in error.

The formula for M_c, the moment about the center of the airfoil's "parent" circle is stated correctly (page 407), but this center is *not* the midpoint of the airfoil, as the author seems to believe. In fact, the center is located at a distance $(2 + \epsilon)c$ forward of the trailing edge, while the mid-chord point is at a distance $t/2 = 2c\,(1 + \epsilon^2)$ forward of the trailing edge.

Thus, the correct formula for calculating A.C., is as follows:

$$M_{ac} = M_c - L[t - (2 + \epsilon)c - (\text{a.c.})t]$$

etc., where L denotes the lift and t the chord.

The result, which can easily be confirmed by subtracting $[(2 + \epsilon)c - t/2]/t$ from Professor Pope's result, is

$$\text{a.c.} = 1 - \frac{1}{4(1 + \epsilon^2)}\left(2 + \epsilon + \frac{1}{1 + \epsilon}\right)$$

or, retaining only $O(\epsilon^2)$,

$$\text{a.c.} = (1/4) + (\epsilon^2/2)$$

Thus, von Kármán and Burgers[1] are correct in stating that the aerodynamic center lies at the quarter-chord, to the order of approximation represented by $O(\epsilon)$. Incidentally, it seems advisable to retain, at most, ϵ^2 terms, since the expression used by Professor Pope for t[i.e., $t = 4c(1 + \epsilon^2)$] is an approximation and is correct only to this order.

The numerical values of a.c. according to the corrected formula are considerably different from those given by the author; for example,

$$d/t = 0.09, \quad \epsilon = 0.069, \quad \text{a.c.} = 0.252$$
$$d/t = 0.15, \quad \epsilon = 0.115, \quad \text{a.c.} = 0.256$$

Obviously, Fig. 2 of the paper requires correction.

Thus, it is seen that the location of the theoretical aerodynamic center (inviscid-fluid approximation) at the quarter-chord is not, as Professor Pope has stated, a "thin-airfoil approximation" and is not in the same category as the rough value 2π for the lift-curve slope.

REFERENCE

[1] von Kármán, Th., and Burgers, J. M., *Aerodynamic Theory*, Vol. 2, p. 71; W. F. Durand, Editor, Springer, Berlin, 1935.

W. R. SEARS
Cornell University

Announcing a New Department . . . Readers' Forum

It has been suggested by several members of the I.A.S. Editorial Committee that the *Journal* open a special department to fill the need for the more immediate communication of essential results of research in the greatly expanded and accelerated fields of the aeronautical sciences. Therefore, it has been decided to establish a new department, the "Readers' Forum," which will include letters to the editor for the quick publication of (1) brief reports of important findings in aeronautical sciences and (2) discussions of papers published in the *Journal*.

Specifications for Submission of Material

(1) All letters should be accompanied by a suggested short title, giving some indication to the reader of the subject under discussion.

(2) These letters should not exceed 800 words in length.

(3) Publication will be completed 6 to 8 weeks after receipt of the material.

(4) The Editorial Committee will not hold itself responsible for the opinions expressed by the correspondents, and no proofs will be sent to the authors.

(5) All letters should be double-spaced.

It is hoped that the new department may be started with the January, 1949, issue of the *Journal*. Contributions should be sent to:

Editor, Journal of the Aeronautical Sciences
2 East 64th street
New York 21, New York

Deep Ring Analysis

KUANG-SHENG CHING*

Bureau of Aircraft Industry, China

SUMMARY

A paper with the title of "Calculation of the Stresses in Annular Frames" by H. Fahlbusch and W. Wegner[1] was published in the November, 1941, issue of the *Journal of the Royal Aeronautical Society*. It deals with the depth effect insofar as the neutral axis of the ring is offset from the skin line, but no consideration is given to curvature (the distribution of stress due to bending being as for a straight beam) or to the deformation due to direct load and shear force.

In the present paper the curved-beam theory and also the direct and shear deformations have been taken into consideration. The result obtained agrees with the above-mentioned paper in the region of small ratio of depth to outside radius but differs considerably when the depth-radius ratio is large.

INTRODUCTION

THE INSTALLATION of a jet engine in the fuselage usually requires the introduction of a deep ring structure that clears the jet pipe and acts as main support for the empennage structure.

Curves are available in the Royal Aeronautical Society Data Sheets on Stressed Skin Structures for the calculation of circular rings. However, as mentioned in those sheets, these curves are reasonably accurate provided the ratio of the depth of the ring to the outside radius is less than one-tenth. The curved-beam theory has to be used to calculate the bending stress.[2] Therefore it is obvious that we have to consider the depth effect on the stressing of a thick ring which forms important structural components in a single jet engine aircraft.

SYMBOLS

E = Young's modulus
G = shear modulus
R_0 = outside radius
R_c = radius to centroidal axis
A = cross-sectional area of the ring
A_s = cross-section area of the ring to take shear
e = distance between centroidal axis and neutral axis
q = shear flow in supporting skin
α = shear distribution factor across the section in the calculation of shear energy[2]
$K = \alpha(AE/A_sG)$, a constant
U = strain energy
M = bending moment, positive producing tension in concave side
V = shear, positive producing positive moment as θ increases
H = direct force positive producing tension
M, V, H = applied bending moment, shear, and direct loads
M_B, V_B, H_B = bending moment, shear, direct load at $\theta = 0°$

Received February 5, 1948.

* Captain.

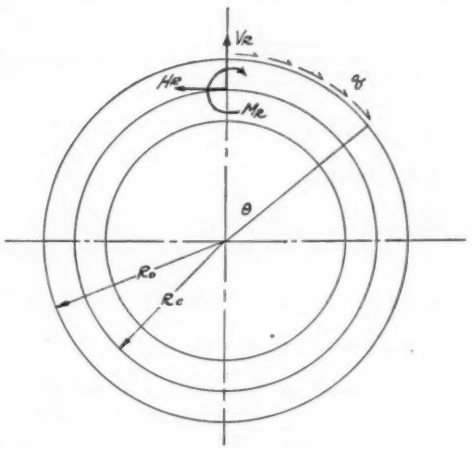

FIG. 1.

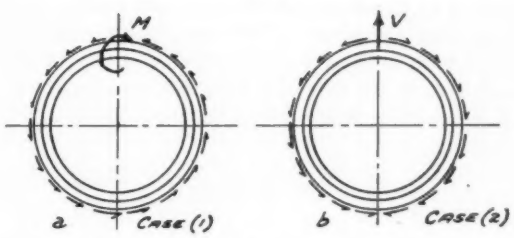

FIG. 2.

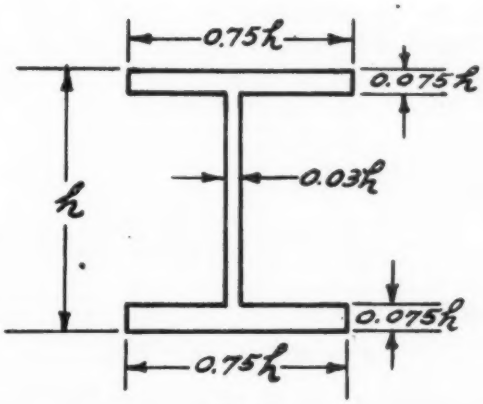

FIG. 3.

The strain energy of a curved beam under combined loading for a circular ring is

$$U = \int_0^{2\pi} \left(\frac{M_\theta^2}{2AEeR_c} + \frac{\alpha V_\theta^2}{2A_sG} + \frac{H_\theta^2}{2AE} - \frac{M_\theta H_\theta}{AER_c} \right) R_c d\theta \quad (1)$$

To find M_R, V_R, and H_R, we have

$$\partial U/\partial M_R = 0, \qquad \partial U/\partial V_R = 0, \qquad \partial U/\partial H_R = 0$$

i.e.,

$$\int_0^{2\pi}\left[\left(\frac{1}{e}\frac{\partial M_\theta}{\partial M_R} - \frac{\partial H_\theta}{\partial M_R}\right)\frac{M_\theta}{R_c} + \left(\frac{\partial H_\theta}{\partial M_R} - \frac{1}{R_c}\frac{\partial M_\theta}{\partial M_R}\right)H_\theta + K\frac{\partial V_\theta}{\partial M_R}V_\theta\right]d\theta = 0 \tag{2}$$

$$\int_0^{2\pi}\left[\left(\frac{1}{e}\frac{\partial M_\theta}{\partial V_R} - \frac{\partial H_\theta}{\partial V_R}\right)\frac{M_\theta}{R_c} + \left(\frac{\partial H_\theta}{\partial V_R} - \frac{1}{R_\theta}\frac{\partial M_\theta}{\partial V_R}\right)H_c + K\frac{\partial V_\theta}{\partial V_R}V_\theta\right]d\theta = 0 \tag{3}$$

$$\int_0^{2\pi}\left[\left(\frac{1}{e}\frac{\partial M_\theta}{\partial H_R} - \frac{\partial H_\theta}{\partial H_R}\right)\frac{M_\theta}{R_c} + \left(\frac{\partial H_\theta}{\partial H_R} - \frac{1}{R_c}\frac{\partial M_\theta}{\partial H_R}\right)H_\theta + K\frac{\partial V_\theta}{\partial H_R}V_\theta\right]d\theta \tag{4}$$

In Fig. 1, by statics,

$$M_\theta = M_R + V_R R_c \sin\theta - H_R R_c (1 - \cos\theta) + R_0\int_0^\theta q[R_0 - R_c\cos(\theta - \psi)]d\psi \tag{5}$$

$$V_\theta = V_R\cos\theta - H_R\sin\theta + R_0\int_0^\theta q\sin(\theta - \psi)d\psi \tag{6}$$

$$H_\theta = H_R\cos\theta + V_R\sin\theta - R_0\int_0^\theta q\cos(\theta - \psi)d\psi \tag{7}$$

Two basic cases of loading are considered here. Case 1 is a circular ring with an applied moment at $\theta = 0°$, and Case 2 is a ring with a vertical shear at $\theta = 0°$. Both of these applied load systems are assumed to be balanced by the shear from the supporting skin. In the second case the shear distribution in the skin is assumed to be in the form of flexural bending, which is nearly true in the case of a deep ring because the ring is so much more rigid than the supporting skin.

In case (1):

$$q = -M/2R_0^2\pi \tag{8}$$

In case (2):

$$q = (V/R_0\pi)\sin\psi \tag{9}$$

For case (1), substituting Eqs. (5), (6), (7), and (8) into Eqs. (2), (3), and (4), it can be found that

$$M_R = {}^1/_2 M$$
$$V_R = -(3M/2\pi R_c)f_1$$
$$H_R = 0$$

where

$$f_1 = \frac{1}{3W}\left(1 + 2W\frac{1 - WX}{1 + KWX - WX}\right) \tag{10}$$

In the above equation

$$W = R_0/R_c, \qquad X = e/R_0$$

Now considering case (2) we substitute Eqs. (5), (6), (7), and (9) into Eqs. (2), (3), and (4) and get

$$M_R = -(3VR_c/4\pi)f_2$$
$$V_R = {}^1/_2 V$$
$$H_R = (3V/4\pi)f_3$$

where

$$f_2 = -\frac{1}{3}\left(1 + 2\frac{3WX + KW^2X^2 - W^2X^2 - 2KW^2X - 2}{1 + KWX - WX}\right) \tag{11}$$

$$f_3 = -\frac{1}{3}\left(1 - 4W\frac{1 + KX - WX}{1 + KWX - WX}\right) \tag{12}$$

Substituting these results into Eqs. (5), (6), and (7) for case (1) we get:

$$\left.\begin{aligned}
\frac{M_\theta}{M} &= \left(\frac{M_\theta}{M}\right)_{\text{thin ring}} + \frac{1}{2\pi}\left(\frac{1}{W} - 3f_1 + 2\right)\sin\theta \\
\frac{V_\theta R_c}{M} &= \left(\frac{V_\theta R_0}{M}\right)_{\text{thin ring}} - \\
&\quad \frac{1}{2\pi}\left[\frac{1}{W} - 1 + \left(3f_1 - \frac{1}{W} - 2\right)\cos\theta\right] \\
\frac{H_\theta R_c}{M} &= \left(\frac{H_\theta R_0}{M}\right)_{\text{thin ring}} + \\
&\quad \frac{1}{2\pi}\left(\frac{1}{W} - 3f_1 + 2\right)\sin\theta
\end{aligned}\right\} \tag{13}$$

where

$$\left(\frac{M_\theta}{M}\right)_{\text{thin ring}} = \frac{1}{2\pi}[(\pi - \theta) - 2\sin\theta]$$

$$\left(\frac{V_\theta R_0}{M}\right)_{\text{thin ring}} = -\frac{1}{2\pi}[1 + 2\cos\theta]$$

$$\left(\frac{H_\theta R_0}{M}\right)_{\text{thin ring}} = -\frac{1}{2\pi}[2\sin\theta]$$

and for case (2)

$$\left.\begin{aligned}
\left(\frac{M_\theta}{VR_c}\right) &= \left(\frac{M_\theta}{VR_0}\right)_{\text{thin ring}} - \frac{1}{2\pi}\left[\frac{3}{2}(f_2 + f_3) - \right. \\
&\quad \left. 2W - 1 - \left(\frac{3}{2}f_3 - 2w + \frac{1}{2}\right)\cos\theta\right] \\
\left(\frac{V_\theta}{V}\right) &= \left(\frac{V_\theta}{V}\right)_{\text{thin ring}} + \frac{1}{2\pi}\left[\frac{3}{2}(1 - f_3)\sin\theta\right] \\
\left(\frac{H_\theta}{V}\right) &= \left(\frac{H_\theta}{V}\right)_{\text{thin ring}} + \frac{1}{2\pi}\left[\frac{3}{2}(f_3 - 1)\cos\theta\right]
\end{aligned}\right\} \tag{14}$$

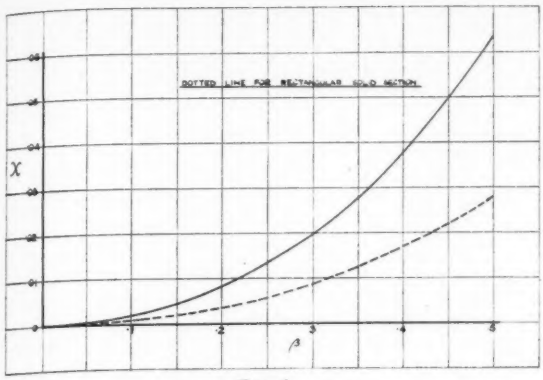

FIG. 4.

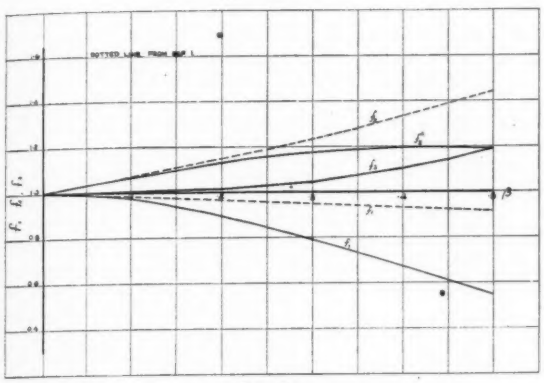

FIG. 5.

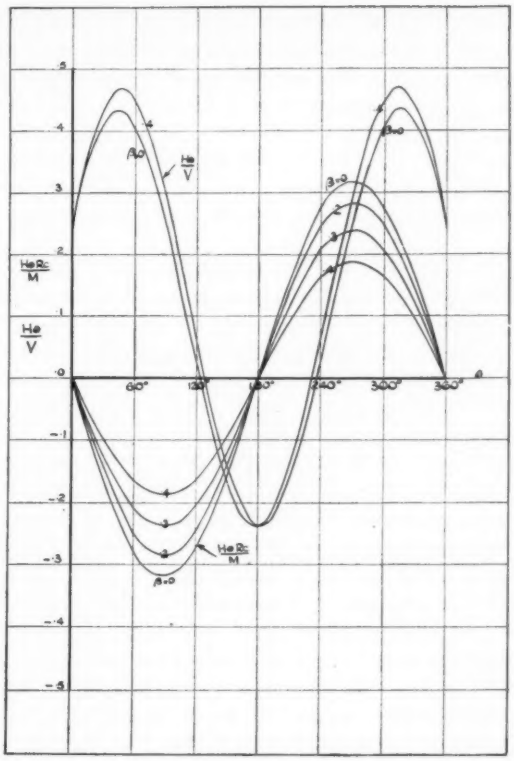

FIG. 6.

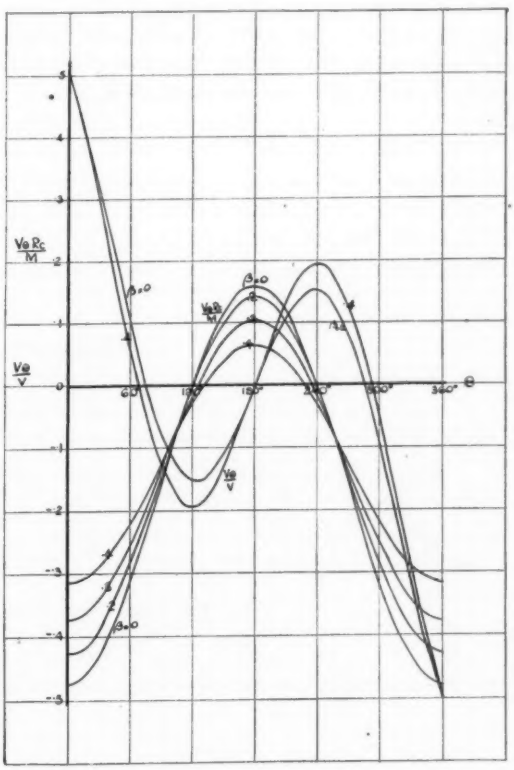

FIG. 7.

where

$$\left(\frac{M_\theta}{VR_0}\right)_{\text{thin ring}} = -\frac{1}{2\pi}\left[\frac{\cos\theta}{2} - (\pi-\theta)\sin\theta + 1\right]$$

$$\left(\frac{V_\theta}{V}\right)_{\text{thin ring}} = \frac{1}{2\pi}\left[(\pi-\theta)\cos\theta - \frac{1}{2}\sin\theta\right]$$

$$\left(\frac{H_\theta}{V}\right)_{\text{thin ring}} = \frac{1}{2\pi}\left[\frac{3}{2}\cos\theta + (\pi-\theta)\sin\theta\right]$$

If we put $X = 0$ and $K = 0$ in Eqs. (13) and (14), the results coincide exactly with those in the paper by Fahlbusch and Wegner.[1]

The variables in f_1, f_2, and f_3 are X, W, and K, and all of them depend on the section properties. For a typical I-beam (or box beam) section as shown in Fig. 3, which the author believes can represent an ordinary ring section for heavy load, we find

$$\left.\begin{aligned} X &= 1 - {}^1/_2\beta - \left\{0.138\beta/\left[0.75\log_e\frac{1-0.925\beta}{(1-\beta)(1-0.075\beta)} + 0.03\log_e\frac{1-0.075\beta}{1-0.925\beta}\right]\right\} \\ W &= 2/(2-\beta) \\ K &= \frac{\alpha AE}{A_sG} = \frac{1\times 0.118h^2}{0.0255h^2}\times 3 = 13.9 \end{aligned}\right\} \quad (15)$$

Here $\beta = h/R_0$, and we assume that the shear distribution factor is equal to one that is nearly true for a beam with thin web and that A_r is equal to the web area. E/G is assumed to be 3 for duralumin or steel sheet

The values of X, f_1, f_2, and f_3 have been calculated and plotted in Figs. 4 and 5. A curve of X for a solid rectangular section is also plotted in Fig. 4 for comparison.

The values of f_1, f_2, and f_3 deduced from Fahlbusch and Wegner[2] are also plotted in Fig. 5; we see that f_3 varies only slightly with a range of β for both results but f_1 varies considerably. All the values of f_1, f_2, and f_3 vary greatly with a large range of β—e.g., from 0.3 to 0.5. In this graph the x-axis represents the theory of thin ring as in ordinary textbooks.

The values of M_θ, V_θ, and H_θ have been calculated based on the sectional properties of Fig. 3. The results are plotted in Figs. 6, 7, and 8. It is interesting to compare these results with those of Fahlbusch and Wegner. The variation due to the depth effect in M_θ/VR_c, V_θ/V, and H_θ/V is comparatively small, but as in the case of M_θ/M, $V_\theta R_c/M$, and $H_\theta R_c/M$ which in the paper referred to, do not differ from the thin ring theory, however in the present paper, the variation is of considerable magnitude. It is obvious that this variation is to be attributed to the inclusion of the shear and direct load energy and the curved beam effect.

Therefore the author believes that, in the stressing of the deep ring at the end of the fuselage with a jet pipe passing through it, the depth effect should be considered, otherwise the variation due to depth effect might be considerable as demonstrated in Figs. 6, 7, and 8.

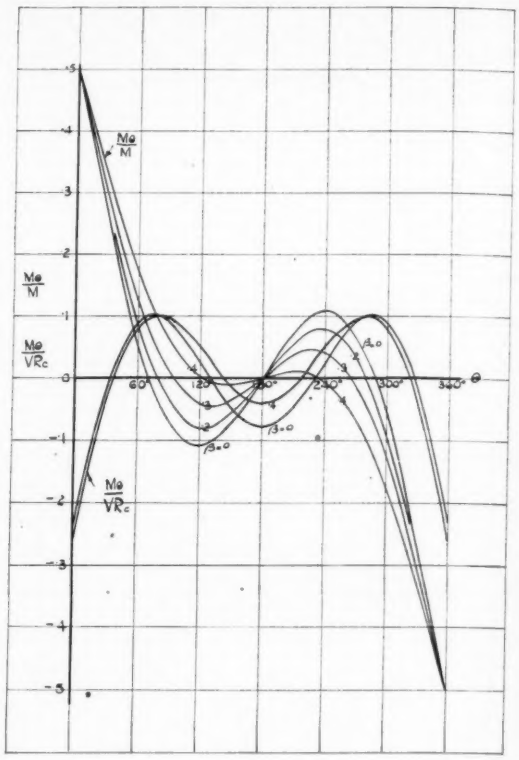

FIG. 8.

REFERENCES

[1] Fahlbusch, H., and Wegner, W., *Calculation of the Stresses in Annular Frames*, J.R.Ae.S., November, 1941.
[2] Timoshenko, S., *Strength of Material*, Vol. II.

Notice to Contributors

Manuscripts submitted for publication *must be* double- or triple-spaced originals. There should be wide margins on both sides of the sheets and triple spacing around formulas to allow for the marking of directions for the printer.

Original drawings (jet black India ink on white paper or tracing cloth) should accompany the manuscript. *(Blueprints are not acceptable.)* Photographs *must be* on glossy white paper.

Only the simplest formulas should be typewritten; all others should be carefully written in pen and ink. The difference between capital and lower-case letters and Greek symbols should be clearly distinguished.

See the Inside Back Cover of this issue for further details.

Application of the Performance Operator to Aircraft Automatic Control

ROBERT C. SEAMANS, JR.,* BENJAMIN G. BROMBERG,† AND L. E. PAYNE‡

Massachusetts Institute of Technology, McDonnell Aircraft Corporation, and Jackson & Moreland

SUMMARY

This paper contains a discussion of techniques that provide effective means for analyzing the performance of automatically controlled aircraft. These techniques are based on the performance operator—a concept developed by Dr. C. S. Draper and his associates in the Instrumentation Laboratory of Massachusetts Institute of Technology. The performance operator method has already been successfully applied in the complete analysis of complex Naval fire-control systems.

Until recently, the fundamental aeronautical design problems were largely concerned with fluid mechanics, structures, power plants, and static and dynamic stability as applied to aircraft controlled by human pilots. The increased emphasis on high-speed, automatically controlled flight has forced the designer out of these well-explored fields into comparatively uncharted realms of air-borne system dynamics. In these regions, the performance operator provides a straightforward procedure for understanding the necessary physical blending of the sensing and control equipment with the air frame in a manner to provide satisfactory flight maneuvers.

In this paper, the performance operator is described in general, and methods are introduced for determining specific performance operators for system components and for complete systems. The performance operator of an airplane can be determined experimentally from information obtained when sinusoidally oscillating the control surfaces in flight. It is shown that a simpler method, requiring considerably less flight time, involves the application of step displacements of the control surfaces. Flight-test data presented in the paper, obtained with the U.S. Air Force A-26 Medium Bomber, indicate good correlation between the two methods. Finally, it is shown that the performance operator makes it possible to design satisfactory longitudinal control equipment for the A-26 airplane.

INTRODUCTION

THE INSTRUMENTATION LABORATORY, of the Division of Industrial Cooperation of Massachusetts Institute of Technology, working under a contract initiated in May, 1946, by the Armament Laboratory of the Air Materiel Command, U.S. Air Force, is investigating the performance of air-borne tracking systems. Systems of this type include radar for directional sensing, computers for intelligence, servos or human pilots to actuate the controls, and aircraft to carry the useful load. Air-borne tracking systems are primarily military in nature, but, as shown in this paper, there are many commercial applications.

Presented at the Instruments Session, Sixteenth Annual Meeting, I.A.S., New York, January 26–29, 1948.

* Assistant Professor of Aeronautical Engineering and Director, Tracking Control Project, Instrument Laboratory.

† Chief, Guidance and Control Section, Guided Missile Department.

‡ Technical Publications Staff.

In designing a multiloop air-borne system, it is first necessary to determine the static and dynamic characteristics of each component. In order to test the servo control units for adaptability to military tracking systems, arrangements were made with the Minneapolis-Honeywell Regulator Company for the loan of an automatic pilot. These tests have been carried out both in flight and in the laboratory. A fixture was used in the laboratory to simulate the torques occurring about the hinge lines of the several control surfaces.

The Cornell Aeronautical Laboratory pioneered in dynamic flight tests and, hence, was logically equipped to assist in the flight program. During tests conducted by this group, the response of the aircraft was determined separately for applied displacements of the elevator, rudder, and ailerons. In each case, sinusoidal displacements and those of a step character were employed in order to ensure both steady-state and transient data. The Instrumentation Laboratory developed special instruments for the test, including a three-axis rate indicator, a three-axis accelerometer, and sensing elements for angle of attack and angle of yaw. Both longitudinal and lateral flight tests have been satisfactorily completed, and the aircraft has been transferred recently to the Instrumentation Laboratory for installation and test of necessary tracking equipment.

The method selected to present the longitudinal and lateral flight test results is important, since it must fulfill two necessary functions. The method must give the engineer and the designer a clear mental picture of the physical phenomena associated with the airplane's static and dynamic performances. It is equally important that the method yield information that can be used readily and economically in establishing the stability and the response time of the overall system. For example, by techniques developed at Cornell Aeronautical Laboratory, it is possible to evaluate the important stability derivatives from flight tests. Until recently, the dynamic stability derivatives had never been experimentally determined for the complete aircraft; therefore, this result provides the aircraft designer with a new tool of inestimable significance. When these stability derivatives are inserted in the airplane equations of motion, the airplane output for any control displacement can be determined. However, the control displacements in a multiloop system are functions of quantities involving all the components in an automatically controlled aircraft. In order to obtain the

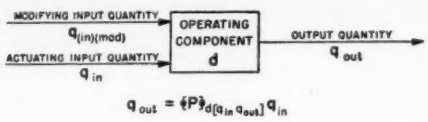

FIG. 1. Functional diagram of the operating component, *d*.

response of the complete system, it may be necessary to solve as many as 20 simultaneous differential equations. Without the aid of an adequate simulator, this "classical approach" entails a prohibitive outlay of effort.

A technique has been developed by the Instrumentation Laboratory that permits convenient determination of the response of compound systems. The technique is based on a mathematical concept, called the *performance operator*. This operator expresses the relationship between the output of a system and the actuating input, or forcing function, responsible for the output. In use, the performance operator employs conventional mathematical procedures in such a manner that complex functions involving derivatives, vectors, and nonlinearities can be segregated and divided into understandable effects.

(I) THE PERFORMANCE OPERATOR

The performance operator may be broadly defined as a concept designed to express in readily identifiable form the performance characteristics of an operating system or subsystem. "Performance characteristics" are understood to be those characteristics of a system which alter its output with respect to its input or inputs.

A simple operating component, designated *d*, is shown in the functional diagram of Fig. 1. Impressed on the system is a forcing function, or actuating input quantity, q_{in}. The action of the operating component on the actuating input gives rise to an output quantity, q_{out}. Depending upon the nature of the component, the output may differ from the actuating input in dimension, magnitude, phase, and integral or differential order. In this sense, the component can be said to *operate* on the actuating input to produce the output.

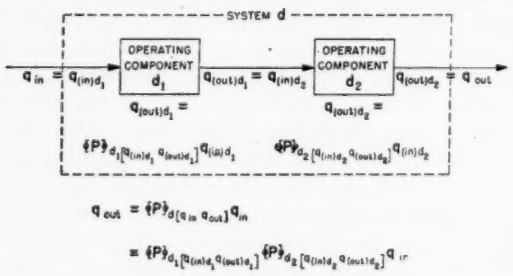

FIG. 2. Functional diagram of the system, *d*.

In terms of the performance operator this may be expressed:

$$q_{out} = \{P\}_{d[q_{in}q_{out}]} q_{in} \qquad (1)$$

The brackets $\{\ \}$ designate the term so enclosed as an operator; the form $\{P\}$ indicates that the term is a performance operator relating the magnitude of the output to the magnitude of the actuating input; the subscript *d* indicates the designated component; and the subscripts q_{in} and q_{out} indicate by their order and form the particular performance operator intended.

In the operating component of Fig. 1, an additional factor has been introduced in the form of a modifying input quantity, $q_{(in)(mod)}$. A modifying input is distinguished from an actuating input by noting that it can have no effect upon the output unless an actuating input is present; whereas, an actuating input can affect the output in the absence of a modifying input. The effect of a modifying input is to change the performance operator.

The location of the center of gravity of an airplane is an input that modifies the longitudinal response of the airplane to applied elevator displacements. In this example, the elevator displacement is the actuating input quantity. There are several output quantities that may be of interest—namely, rate of pitch, normal acceleration, and angle of attack. For this reason, at least three performance operators are needed in specifying the longitudinal characteristics of a particular aircraft. Each one of these performance operators is modified by the center-of-gravity position.

In practice, several operating components are usually found combined into a more complex system. The scheme of concepts, definitions, and notation chosen to describe the behavior of the system must be effective in permitting immediate, unambiguous specification of the performance characteristics of any selected operating component of the system. This makes it necessary for the notation associated with each performance operator to include complete information on the identity of the operating component involved, its output, and its actuating input. In each case, in addition to the performance operators, it is expected that a functional diagram (including a block for each operating component) is available for reference. From this diagram, it is possible to identify the modifying inputs that affect the performance operator associated with a given operating component.

The performance operator of a system comprising any number of operating components—whether connected in series, parallel, or with feedback returns—can be related to the component operators by carrying out the straightforward algebraic processes indicated on the pertinent functional diagram. Fig. 2 shows two operating components, d_1 and d_2, connected in series to form an open-end system, *d*. In this figure the performance operators for the individual components are specified, and the simple relationships between com-

ponent inputs and outputs are noted. However, reference to the functional diagram indicates that the input to operating component d_1 is also the input to system d, that the output from operating component d_1 is the input to operating component d_2, and that the output from operating component d_2 is the output from system d. It then becomes evident that

$$\{P\}_{d[q_{in}q_{out}]} = \{P\}_{d_1[q_{(in)d_1}q_{(out)d_1}]}\{P\}_{d_2[q_{(in)d_2}q_{(out)d_2}]} \quad (2)$$

It has already been stated that the performance characteristics of a system are understood to be those that alter its output with respect to its input. When the input and the output are scalar quantities, the operator is also scalar and serves only to account for changes in magnitude. However, when the input and the output are vector quantities having both magnitude and direction, the operator not only must relate the magnitude of the output to the magnitude of the input but must introduce a space orientation of the output vector with respect to the input vector. When this is the case, the vector nature of the performance operator is designated by the addition of a bar over the symbol—i.e.,

$$\bar{q}_{out} = \{\bar{P}\}_{()[q_{in}q_{out}]}\bar{q}_{in} \quad (3)$$

This equation is an extension of Eq. (1) in the sense that it permits a study of systems that experience derivative and integral effects and, in addition, are involved with space-dimensional geometry. The open-parentheses appearing as a subscript to the performance operator symbol in this equation signifies the designated component or system.

For the mathematical treatment of certain vectors, it is expedient to refer to the complex plane. This plane is familiar to most engineers as that defined by an axis of reals and an axis of imaginaries. All real numbers fall on the axis of reals, and numbers that are the product of real numbers and $\sqrt{-1}$ (which represents a unit vector along the axis of imaginaries and is usually represented by the symbol j) fall on the axis of imaginaries. The complex plane derives its title from this dual nature of numbers therein.

In general, a quantity in the complex plane is composed of both a real and an imaginary number, and its magnitude is a function of the size of each. Because its graphical representation may fall anywhere between the axis of reals and the axis of imaginaries, the quantity also has direction. From this point of view, a quantity occurring in the complex plane can be considered as a vector and is so classed in this paper. Since this type of vector is always contained within a plane, certain common vector operations—for example, the vector cross product—which involve three-dimensional space are never required. However, despite limitations of this kind, the vector remains an extremely useful concept to the aeronautical engineer in dealing with complex numbers.

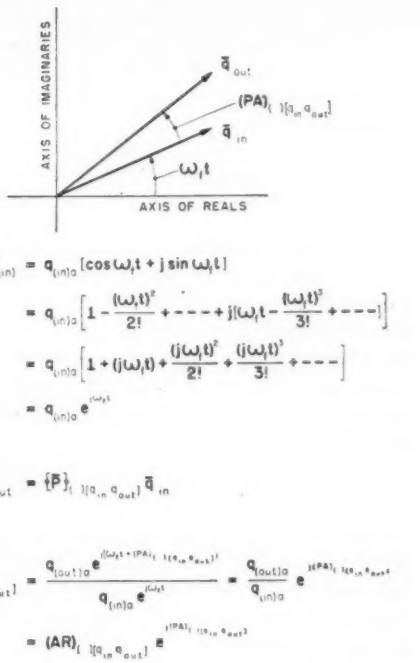
AXIS OF IMAGINARIES
AXIS OF REALS
$\bar{q}_{out}$
$(PA)_{()[q_{in}q_{out}]}$
$\bar{q}_{in}$
$\omega_f t$
$\bar{q}_{(in)} = q_{(in)a}[\cos\omega_f t + j\sin\omega_f t]$
$= q_{(in)a}\left[1 - \frac{(\omega_f t)^2}{2!} + - - - + j(\omega_f t - \frac{(\omega_f t)^3}{3!} + - - -\right]$
$= q_{(in)a}\left[1 + (j\omega_f t) + \frac{(j\omega_f t)^2}{2!} + \frac{(j\omega_f t)^3}{3!} + - - -\right]$
$= q_{(in)a}e^{(\omega_f t)}$
BY DEFINITION
$\bar{q}_{out} = \{\bar{P}\}_{()[q_{in}q_{out}]}\bar{q}_{in}$
THEREFORE
$\{\bar{P}\}_{()[q_{in}q_{out}]} = \frac{q_{(out)a}e^{(j\omega_f t + (PA)_{()[q_{in}q_{out}]})}}{q_{(in)a}e^{(j\omega_f t)}} = \frac{q_{(out)a}}{q_{(in)a}}e^{(PA)_{()[q_{in}q_{out}]}}$
$= (AR)_{()[q_{in}q_{out}]}e^{j(PA)_{()[q_{in}q_{out}]}}$

FIG. 3. Diagram showing the derivation of the vector performance operator.

(II) THE VECTOR PERFORMANCE OPERATOR

In developing the concept of a vector performance operator, it is necessary to expand the brief description of complex plane quantities contained in Part (I). In the complex plane a quantity is composed of both real and imaginary numbers and, hence, can be represented by a vector extending from the origin of the axis system to a particular coordinate in the plane. This quantity has magnitude with respect to the origin and direction as measured from the real axis, thus exhibiting its vector characteristics. An additional characteristic assigned to the vector quantities used in this paper is rotation about the origin at constant rates. The time for one complete revolution (2π rad.) of a vector about the origin is called the forcing period, T_f; the rate in revolutions per second is the reciprocal of the forcing period and is called the forcing frequency, n_f. At any instant, the angular position of a vector quantity of this character depends upon the forcing frequency and upon the elapsed time, t, for in this time it will have rotated through $n_f t$ parts of a complete revolution. It is more convenient to express the position of the vector quantity in radians, in order to avoid the continual use of the conversion factor, 2π. For this purpose, a new rate is defined called the angular forcing frequency, ω_f—that is,

$$\omega_f = 2\pi n_f = 2\pi/T_f \quad (4)$$

The generalized forcing function of concern in this paper is the input quantity, q_{in}. Vectorially, this quantity has the direction $\omega_f t$ and a magnitude, or amplitude, $q_{(in)a}$, as shown in Fig. 3. This vector input quantity is equal to the sum of its real and imaginary components, or

$$\begin{aligned}\bar{q}_{in} &= q_{(in)a}\cos\omega_f t + jq_{(in)a}\sin\omega_f t \\ &= q_{(in)a}[\cos\omega_f t + j\sin\omega_f t] \end{aligned} \tag{5}$$

The common practice, when projecting a vector onto X, Y, Z cartesian coordinates, is to make use of unit vectors that, by definition, have a magnitude of unity and are directed along the respective X, Y, Z axes. In this manner a vector can be expressed in terms of unit vectors and the projected magnitudes of the respective vectors along the axes in question. This is usually expressed as

$$\bar{A} = iA_X + jA_Y + kA_Z \tag{6}$$

The vector input quantity occurring in the complex plane is similarly expressed, as shown by Eq. (5). In this equation the unit vector along the imaginary axis is denoted by the symbol j; the unit vector along the real axis is implied, although for the sake of brevity it is not actually included.

The merit of the vector quantity is more fully understood when Eq. (5) is expanded by the use of a Maclaurin series, for then

$$\begin{aligned}\bar{q}_{in} &= q_{(in)a}\left\{\left[1 - \frac{(\omega_f t)^2}{2!} + \dots\right] + j\left[\omega_f t - \frac{(\omega_f t)^3}{3!} + \dots\right]\right\} \\ &= q_{(in)a}\left[1 + (j\omega_f t) + \frac{(j\omega_f t)^2}{2!} + \frac{(j\omega_f t)^3}{3!} + \dots\right] \\ &= q_{(in)a}e^{j\omega_f t} \end{aligned} \tag{7}$$

In this equation the vector input quantity is expressed concisely as the product of its amplitude, $q_{(in)a}$, and the exponential, $e^{j\omega_f t}$. The latter unit vector is rotated $\omega_f t$ rad. from the real axis. With this exponential form, the operations of differentiation and integration require only the multiplication or division of the vector quantity by $j\omega_f$. A comparison of Eqs. (5) and (7) shows that, when $\omega_f t$ equals $\pi/2$ rad.

$$\bar{q}_{in} = q_{(in)a}\,j = q_{(in)a}e^{j(\pi/2)} \tag{8}$$

From this, it can be seen that

$$j = e^{j(\pi/2)} \tag{9}$$

Hence, multiplication by $j\omega_f$ changes the magnitude of the vector function in direct proportion to the value of ω_f and advances the vector $\pi/2$ rad., or 90°, in a positive (counterclockwise) direction. Similarly, division by $j\omega_f$ changes the magnitude inversely with ω_f and retards the vector by 90°.

The response of a component or system to an applied vector input yields a vector output quantity that, for steady-state conditions, rotates at the same rate or frequency as the input. In general, however, the output is not in phase with the input but is advanced or retarded by a *phase angle*. The output vector quantity, with amplitude $q_{(out)a}$, is shown in Fig. 3 leading the input by the angle $(PA)_{O[q_{in}q_{out}]}$; therefore, it can be written

$$\bar{q}_{out} = q_{(out)a}e^{j[\omega_f t + (PA)_{O[q_{in}q_{out}]}]} \tag{10}$$

It is desirable to consider the operation on the vector input that is required to obtain the related output response. This operation, which affects both the magnitude and the phase of the output, is specified by the vector performance operator of Eq. (3). This equation can be combined with Eqs. (7) and (10) to give

$$\{\bar{P}\}_{O[q_{in}q_{out}]} = \frac{q_{(out)a}}{q_{(in)a}}e^{j(PA)_{O[q_{in}q_{out}]}} \tag{11}$$

Eq. (11) brings out a further advantage in the use of this type of vector function—that is, it yields a performance operator that is independent of time. However, the vector performance operator for a physically realizable component or system *is* a function of the forcing frequency.

The relationship between the amplitude of the output and the amplitude of the input is simply expressed by the amplitude ratio, $(AR)_{O[q_{in}q_{out}]}$, as

$$(AR)_{O[q_{in}q_{out}]} = q_{(out)a}/q_{(in)a} \tag{12}$$

It is convenient to consider the amplitude ratio as the product of two factors: (1) a reference amplitude ratio $(AR)_{O[q_{in}q_{out}](ref)}$, which is independent of the forcing frequency but which carries the dimensions of the amplitude ratio; (2) a dynamic amplitude ratio $(AR)_{O[q_{in}q_{out}](dyn)}$, which depends upon the forcing frequency but which is dimensionless. In equation form,

$$(AR)_{O[q_{in}q_{out}]} = (AR)_{O[q_{in}q_{out}](ref)}(AR)_{O[q_{in}q_{out}](dyn)} \tag{13}$$

The selection of the reference amplitude ratio depends upon the particular component or system undergoing specification. With some components and systems at zero frequency, when conditions are static, a given change in the level of the input yields a zero change in the output; with others, a proportional change is introduced; with the remaining, an infinite change is produced. An example of the latter is a servomotor that, when excited, continues rotating until it either reaches a limit stop or is de-energized. Another example is an airplane with the elevator displacement as the input quantity and the pitch angle as the output quantity. The limit in this case is a function of air speed and gravitational effects.

When considering a component or system exhibiting either zero or infinite response under static conditions, the choice of the reference amplitude ratio is arbitrary and should be selected for optimum convenience. However, when variations in the input produce proportional changes in the output, the component or system has a *sensitivity*, $S_{O[q_{in}q_{out}]}$, equal to the ratio of the static output to the input. Whenever it exists, this sensitivity serves as the reference amplitude ratio. In this circumstance and when the frequency is zero, the dynamic amplitude ratio is equal to unity. In summarizing the developments of this section, it can be generally stated that

$$\{\bar{P}\}_{O[q_{in}q_{out}]} = (AR)_{O[q_{in}q_{out}]} e^{j(PA)_{O[q_{in}q_{out}]}}$$
$$= (AR)_{O[q_{in}q_{out}](\text{ref})} \times (AR)_{O[q_{in}q_{out}](dyn)} e^{j(PA)_{O[q_{in}q_{out}]}} \quad (14)$$

and, when a finite response exists under static conditions,

$$\{\bar{P}\}_{O[q_{in}q_{out}]} = S_{O[q_{in}q_{out}]}(AR)_{O[q_{in}q_{out}](dyn)} e^{j(PA)_{O[q_{in}q_{out}]}} \quad (15)$$

The sensitivity carries an algebraic sign (plus or minus) so that for static conditions the phase angle of Eq. (15) is equal to zero. It should be noted that the reference amplitude ratio of Eq. (14) cannot always be defined in this same manner, because the phase angle at zero forcing frequency may be either 90° or 270°.

The vector quantities described in this paper are mathematical abstractions that help to establish a new approach to dynamic analysis. In addition, the vector performance operator can be used directly to obtain the response of a linear component or system to all periodic functions. A first step in obtaining this result is accomplished, as described in Part (III), by relating the periodic functions to vector quantities.

(III) Periodic Quantities

(a) General

A series of vector quantities can be used to represent any periodic real quantity, q_P. The series consists of one nonrotating vector along the axis of reals and an infinite number of paired vectors—the two vectors of each pair rotating in opposite directions at angular frequencies that are integral multiples of the fundamental forcing frequency ω_{f1}. Stated mathematically, the series is

$$q_P = \sum_{n=-\infty}^{n=\infty} q_n = \sum_{n=-\infty}^{n=\infty} \bar{K}_n e^{jn\omega_{f1}t} \quad (16)$$

For complete accuracy, all integral values of the number n, including zero, must be used in Eq. (16). The series usually converges rapidly, so that values of n greater than 20 are seldom necessary to obtain practical engineering accuracy. The coefficient $\bar{K}_n$ of the exponential time function in Eq. (16) has vector properties and can be evaluated by first multiplying each side of the equation by $e^{-jn\omega_{f1}t}$ and then integrating the resulting equation over a time interval of one fundamental forcing period, T_{f1}. This gives

$$\bar{K}_n = (1/T_{f1}) \int_{-T_{f1}/2}^{T_{f1}/2} q_P e^{-jn\omega_{f1}t} dt \quad (17)$$

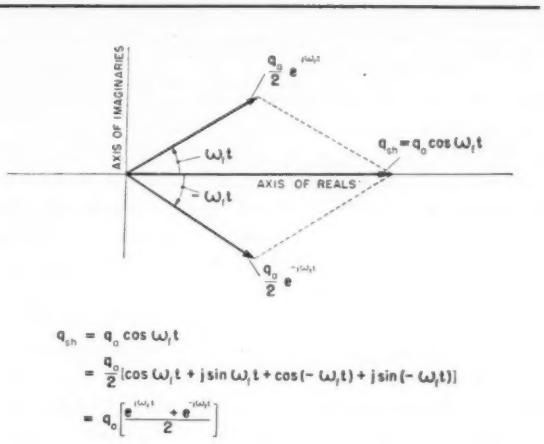
AXIS OF IMAGINARIES
AXIS OF REALS
$\omega_f t$
$-\omega_f t$
$q_{sh} = q_a \cos \omega_f t$
$\frac{q_a}{2} e^{j\omega_f t}$
$\frac{q_a}{2} e^{-j\omega_f t}$
$q_{sh} = q_a \cos \omega_f t$
$= \frac{q_a}{2}[\cos \omega_f t + j \sin \omega_f t + \cos(-\omega_f t) + j \sin(-\omega_f t)]$
$= q_a \left[\frac{e^{j\omega_f t} + e^{-j\omega_f t}}{2}\right]$

FIG. 4. Relationship between simple harmonic function and equivalent vector quantities.

Two types of periodic quantities, the simple harmonic and the square wave, are of particular interest. The first type is useful when analyzing the steady-state response; the second, when analyzing the transient response.

(b) Simple Harmonic Function

The simple harmonic function is useful because it lends itself conveniently both to experimental test and to mathematical analysis. There are many methods in the laboratory for producing harmonic motion. Ball-and-disc integrators, Scotch yokes, and bell cranks are a few of the mechanisms that can be employed to obtain this type of displacement. Harmonic voltages can be generated by means of alternators, tuning forks, or oscillators. By selecting the proper time reference, all of the resulting quantities can be written:

$$q_{sh} = q_a \cos \omega_f t \quad (18)$$

The amplitude of the quantity q_a is the maximum deviation of the quantity from its mean value, which in this case is zero. The harmonic quantity completes a full cycle every time the angle $\omega_f t$ is advanced 360° or 2π rad. It can be seen that the time for a complete cycle, called the *forcing* period T_f, is related to the angular forcing frequency ω_f by the same equation [Eq. (4)] that relates comparable parameters used to describe the vector input and output quantities.

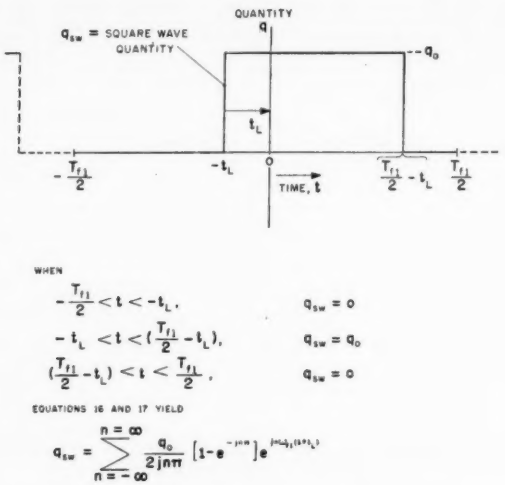

FIG. 5. Relationship between square wave function and infinite series of vector quantities.

The simple harmonic quantity q_{sh} can be expanded into the vector series of Eq. (16) by substituting Eq. (18) in Eq. (17) and solving for the coefficient $\bar{K}_n$. When the frequency of the fundamental vector quantity ω_{f1} in the series is set equal to the frequency of the harmonic motion ω_f.

$$\bar{K}_1 = \bar{K}_{(-1)} = q_a/2 \tag{19}$$

and

$$\bar{K}_0 = \bar{K}_2 = \bar{K}_3 = \ldots = \bar{K}_{(-2)} = \bar{K}_{(-3)} = \ldots = 0 \tag{20}$$

so that, by the use of Eq. (16),

$$q_{sh} = q_a\,[(e^{j\omega_f t} + e^{-j\omega_f t})/2]^* \tag{21}$$

Eq. (21) states that the simple harmonic function equals half the sum of two conjugate unit vectors, one rotating positively and the other negatively. These vectors are represented graphically, along with an alternate proof for the relationship of Eq. (21), in Fig. 4.

(c) *Square Wave Function*

The square wave has been used extensively by engineers for testing amplifiers and other electronic circuits. When the period of the square wave is long in comparison with the transient response time of the circuit, the square wave response during each half cycle is similar to that of a transient—in effect, giving the latter response in a repetitive form that can be observed on an oscilloscope.

* For certain functions, especially those that are nonsymmetrical with respect to the zero time axis, it is more convenient to use a sine function than a cosine function. The sine function lags the cosine function by $\pi/2$ rad., so that, when $q_{sh} = q_a \sin \omega_f t$, the use of Eqs. (9) and (21) shows that

$$q_{sh} = q_a[(e^{j\omega_f t} - e^{-j\omega_f t})/2j]$$

In Fig. 5, a generalized square wave function is shown pulsating between zero and a level designated as q_0 because the function usually has this value at zero time. The square wave function or quantity, q_{sw}, has a cyclic period, T_{f1}, and is symmetrical in the respect that half the period is devoted to the zero level and half to the level q_0. In Fig. 5, the square wave function is leading the zero reference time by an amount t_L or, stated mathematically,

$$-\frac{T_{f1}}{2} < t < -t_L \qquad : q_{sw} = 0$$

$$-t_L < t < \frac{T_{f1}}{2} - t_L \qquad : q_{sw} = q_0$$

$$\frac{T_{f1}}{2} - t_L < t < \frac{T_{f1}}{2} \qquad : q_{sw} = 0$$

The use of these conditions in Eq. (17) permits the evaluation of the nth square wave coefficient—i.e.,

$$\bar{K}_{n(sw)} = \frac{1}{T_{f1}}\int_{-t_L}^{(T_{f1}/2)\,-\,t_L} q_0 e^{-jn\omega_{f1}t}dt$$

$$= (q_0/2jn\pi)(1 - e^{-jn\pi})e^{jn\omega_{f1}t_L} \tag{22}$$

This equation, when combined with Eq. (16), gives the following expression for the square wave quantity:

$$q_{sw} = q_0 \sum_{n=-\infty}^{n=\infty} \frac{1}{2jn\pi}(1 - e^{-jn\pi})e^{jn\omega_{f1}(t+t_L)} \tag{23}$$

The square wave function is related in Eq. (23) to a series of vectors; consequently, when the input to a system can be represented by such a function, the output of the system can be obtained by application of the appropriate vector performance operator to each of the terms in the series. The amplitudes of the exponentials in Eq. (23) vary inversely with the order of the integer n and, in addition, depend upon whether n is zero, an odd integer, or an even integer; for when

$$n = 0, \qquad (1/2jn\pi)(1 - e^{-jn\pi}) = 1/2 \tag{24}$$

$$n = \text{odd integer}, \qquad \frac{1}{2jn\pi}(1 - e^{-jn\pi}) = \frac{1}{jn\pi} \tag{25}$$

$$n = \text{even integer}, \qquad \frac{1}{2jn\pi}(1 - e^{-jn\pi}) = 0 \tag{26}$$

With these three relationships, Eq. (23) can be converted to the form

$$q_{sw} = \frac{q_0}{2} + \frac{q_0}{\pi}\sum_{\substack{n=1,3,\ldots \\ -1,-3,\ldots}} \frac{1}{jn}\, e^{jn\omega_{f1}(t+t_L)} \tag{27}$$

A discussion of the response of a system to a square wave input is contained in Part (IV). In Part (V) techniques are presented for establishing the vector performance operator of a component or system by

either mathematical or experimental means. It is also shown in Part (V) that the simplest experimental method involves the application of long-period square waves, which become step functions in the limit. This method is based on the theoretical considerations of Eq. (27).

(IV) Response to a Square Wave Input

It may rightly be asked why stress is placed on the response of a system to a square wave input. In order to answer this question it is needful to consider what constitutes satisfactory performance under the actual operating conditions of typical automatically controlled aircraft. For example, in most multiengined aircraft used by the air lines, an automatic pilot relieves the human pilot during the more routine phases of a flight. The purpose of the automatic pilot is to hold the pitch and heading initiated by the pilot. When an airplane encounters a gust while in flight, the nose may be forced up or down; in either case the actual pitch of the airplane becomes altered from the pitch value set by the pilot. In a satisfactory system, the elevator is then actuated by the servo controls to restore the pitch angle to the pitch setting. A system that responds in this manner is *stable* as opposed to an unstable system, which augments an initial transient error. An unstable system, once displaced, never again reaches equilibrium but rather yields an error with progressively increasing magnitude.

Stability is a necessary criterion for dynamic performance, but equally important are the *degree of stability* and the *response time*. The degree of stability is a measure of the remoteness of a system from the condition of instability; it is associated with the number of oscillations required to damp out a given transient resulting from a step input. The response time is that required for the transient to become reduced to a stated fraction of its initial value.

The automatic pilot experiences step inputs not only when the airplane encounters a gust but also when the pilot switches from manual to automatic controls and when he retrims the aircraft, with the automatic equipment engaged. The degree of stability and the response time are important with each of these step inputs. The classical theoretical determination of the response to a step input is laborious and is seldom used. However, the degree of stability and the response time can readily be evaluated by the use of the square wave input, which, from Eq. (23) can be written

$$q_{\text{in}} = q_{(\text{in})0} \sum_{n=-\infty}^{n=\infty} \frac{1}{2jn\pi}(1 - e^{-jn\pi})e^{jn\omega_{f1}t} \tag{28}$$

The response of a component or system to a square wave input can be determined (1) by operating individually on each of the vectors in the series of Eq. (28) and (2) by superimposing the results, giving

$$q_{\text{out}} = q_{(\text{in})0} \sum_{n=-\infty}^{n=\infty} \frac{1}{2jn\pi}(1 - e^{-jn\pi})\{\bar{P}\}_{O[q_{\text{in}}q_{\text{out}}]}e^{jn\omega_{f1}t} \tag{29}$$

The ability to superimpose the vector responses to each of the terms in the series implies the existence of linear equations for the component or system. This same limitation is placed on most mathematical approaches, excepting step-by-step integration processes. To date, this technique has only been used for components and systems that have static sensitivities. In such cases, a vector performance operator can be replaced by the equivalent form of Eq. (15); therefore,

$$\frac{q_{\text{out}}}{q_{(\text{in})0}} = S_{O[q_{\text{in}}q_{\text{out}}]} \sum_{n=-\infty}^{n=\infty} \frac{(AR)_{O[q_{\text{in}}q_{\text{out}}](\text{dyn})}}{2jn\pi}(1 - e^{-jn\pi})e^{j[n\omega_{f1}t + (PA)_{O[q_{\text{in}}q_{\text{out}}]}]} \tag{30}$$

However, according to the definition of static sensitivity given in Part (II), the dynamic amplitude ratio is unity and the phase angle is zero at zero frequency. Therefore, when Eqs. (24), (25), and (26) are substituted in Eq. (30),

$$\frac{q_{\text{out}}}{q_{(\text{in})0}} = \frac{S_{O[q_{\text{in}}q_{\text{out}}]}}{2} + \frac{S_{O[q_{\text{in}}q_{\text{out}}]}}{\pi} \sum_{\substack{n=1,3,\ldots \\ -1,-3,\ldots}} \frac{(AR)_{O[q_{\text{in}}q_{\text{out}}](\text{dyn})}}{jn} e^{j[n\omega_{f1}t + (PA)_{O[q_{\text{in}}q_{\text{out}}]}]} \tag{31}$$

$$= \frac{S_{O[q_{\text{in}}q_{\text{out}}]}}{2} + \frac{2S_{O[q_{\text{in}}q_{\text{out}}]}}{\pi} \sum_{n=1,3,\ldots} \frac{(AR)_{O[q_{\text{in}}q_{\text{out}}](\text{dyn})}}{n} \sin\,[n\omega_{f1}t + (PA)_{O[q_{\text{in}}q_{\text{out}}]}] \tag{32}$$

The response of a component or system to a square wave forcing function can be obtained once the sensitivity, dynamic amplitude ratio, and phase angle have been determined by the summation of the Fourier series of Eq. (32). This series contains only odd harmonics, so that, when the dynamic amplitude ratio is equal to unity, the 19th harmonic, or tenth term, in the series is $^1/_{19}$th, or approximately 5 per cent, of the fun-

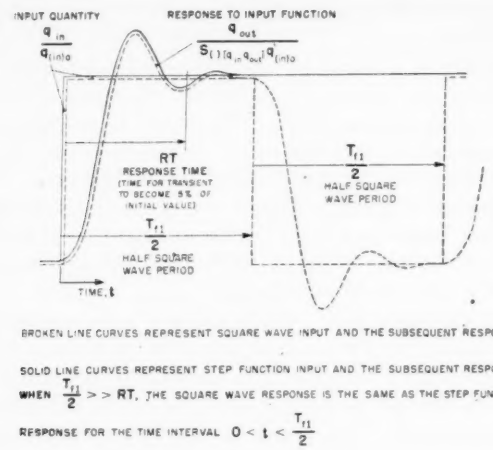
INPUT QUANTITY
$\frac{q_{in}}{q_{(in)0}}$
RESPONSE TO INPUT FUNCTION
$\frac{q_{out}}{S_{(\ )}(q_{in}, q_{out}, q_{(in)0}}$
RT
RESPONSE TIME
(TIME FOR TRANSIENT TO BECOME 5% OF INITIAL VALUE)
$\frac{T_{f1}}{2}$
HALF SQUARE WAVE PERIOD
$\frac{T_{f1}}{2}$
HALF SQUARE WAVE PERIOD
TIME, t
BROKEN LINE CURVES REPRESENT SQUARE WAVE INPUT AND THE SUBSEQUENT RESPONSE
SOLID LINE CURVES REPRESENT STEP FUNCTION INPUT AND THE SUBSEQUENT RESPONSE
WHEN $\frac{T_{f1}}{2} >> RT$, THE SQUARE WAVE RESPONSE IS THE SAME AS THE STEP FUNCTION
RESPONSE FOR THE TIME INTERVAL $0 < t < \frac{T_{f1}}{2}$

FIG. 6. Comparison of the response of a system to a square wave input with the response to a step function input.

damental. Usually, the amplitude ratio is considerably less than unity at the higher frequencies, so that the elimination of the 19th and higher harmonics incurs an inaccuracy of less than 2 per cent. Several methods for summing the Fourier series are discussed in Appendix B: These include a description of an electromechanical synthesizer that produces a graphical plot by oscillographic means, according to the relationship of Eq. (32). In this synthesizer the phase angle and the amplitude ratio of the first 17 harmonics (nine terms) can be introduced by the rotation of selsyn stators and the attenuation of the corresponding selsyn armature outputs.

In a stable component or system the transient inaccuracy resulting from an abrupt change in the input decreases and approaches zero asymptotically. Consequently, an infinite time is required to eliminate the inaccuracy for all idealized components or systems that do not have the limitations of Coulomb friction and electrical hash level common to all practical units. With an eye to such considerations, the response time of a component or system is arbitrarily defined as the time for the transient inaccuracy to fall below, never again to exceed, 5 per cent of its initial value.

In Fig. 6, the response to a step input is compared with the response to a square wave input. The half period of the square wave is selected enough greater than the response time so that at the termination of each half cycle the response is substantially quiescent. Therefore, at the beginning of each new half cycle, the response is nearly constant—a condition that also holds when time equals zero. For this reason, the component or system responds to the square wave input during the first half cycle as though a step input were applied, provided the half period is sufficiently longer than the response time. The validity of this heuristic reasoning is enhanced by the additional proof given in Appendix A and is corroborated by numerous examples successfully handled in this manner.

The fact that the square wave response is nearly equal to the step response during the first half cycle of the square wave permits its use when determining both the response time and the degree of stability. A low degree of stability in a system implies such nearness to the unstable region that a slight variation of system parameters might lead to instability. In comparison, a system with a high degree of stability can be constructed with low tolerances on the system parameters without danger of instability. A measure of the degree of stability is the number of oscillations required to damp an initial transient. More definitely, the ratio of a transient output peak, $q_{(out)(m+1)}$, to its preceding peak, $q_{(out)(m)}$, indicates the degree of stability, for, when this ratio equals unity, the system is on the borderline between instability and stability and, when it approaches zero, the degree of stability becomes large. The stability coefficient, *SC*, is a quantitative measure of the degree of stability and is related to the peak ratio by the expression

$$SC = 1 - [q_{(out)(m+1)}/q_{(out)(m)}]_{av} \qquad (33)$$

or, in percentage,

$$SC = \{1 - [q_{(out)(m+1)}/q_{(out)(m)}]_{av}\}\ 100 \qquad (34)$$

From Eq. (34), it can be seen that the stability coefficient is negative for unstable systems, is zero for borderline systems, and is 100 per cent for systems reaching a steady-state value "dead beat" with no overshoot. For best results in evaluating the stability coefficient, several peak ratios should be averaged, as is indicated in Eqs. (33) and (34).

Before obtaining the response of a system to a square wave input, it is necessary to obtain its vector performance operator. This entails a knowledge of the vector performance operators of each of the system components. Several methods for evaluating the component vector performance operators are discussed in Part (V).

(V) Methods for Determining Component Performance Operators

(*a*) *By Use of Performance Equations*

The performance operator of a component can be obtained either by computation or by direct measurement. The mathematical approach presupposes that the performance equations describing the characteristics of the component are available in accurate form. The performance equations offer the only method available when a component is in the design stage or when the effects of anticipated design changes of a completed unit are being studied.

The performance equations of a component are derived by summation of the pertinent physical quanti-

ties—e.g., forces, torques, currents, voltages. The resulting equations representing the physical phenomena can then be expressed in the following general form, plus an additional number of performance equations in direct proportion to the number of output quantities:

$$[\ldots + a_{\dot{q}_{(out)1}}\dot{q}_{(out)1} + a_{q_{(out)1}}q_{(out)1}] + [\ldots + a_{\dot{q}_{(out)2}}\dot{q}_{(out)2} + a_{q_{(out)2}}q_{(out)2}] + \ldots = [a_{q_{(in)1}}q_{(in)1} + a_{\dot{q}_{(in)1}}\dot{q}_{(in)1} + \ldots] + \ldots \quad (35)$$

and

$$[\ldots + b_{\dot{q}_{(out)1}}\dot{q}_{(out)1} + b_{q_{(out)1}}q_{(out)1}] + [\ldots + b_{\dot{q}_{(out)2}}\dot{q}_{(out)2} + b_{q_{(out)2}}q_{(out)2}] + \ldots = [b_{q_{(in)1}}q_{(in)1} + b_{\dot{q}_{(in)1}}\dot{q}_{(in)1} + \ldots] + \ldots \quad (36)$$

Although the number of performance equations depends in direct proportion upon the number of output quantities, which in this case are the dependent variables, there is no limit to the number of input quantities. However, only one input is shown in Eqs. (35) and (36) because, with linear equations, the effects of the various inputs can be superimposed and can be considered separately, according to Eq. (7), in the form

$$\bar{q}_{(in)1} = q_{(in)1a}e^{j\omega_f t} \quad (37)$$

The vector outputs are related to the vector input by the use of the vector performance operator defined in Eq. (3); therefore,

$$\bar{q}_{(out)1} = \{\bar{P}\}_{O[q_{(in)1}q_{(out)1}]}\bar{q}_{(in)1} = \{\bar{P}\}_{O[q_{(in)1}q_{(out)1}]}q_{(in)1a}e^{j\omega_f t} \quad (38)$$

and

$$\bar{q}_{(out)2} = \{\bar{P}\}_{O[q_{(in)1}q_{(out)2}]}\bar{q}_{(in)1} = \{\bar{P}\}_{O[q_{(in)1}q_{(out)2}]}q_{(in)1a}e^{j\omega_f t} \quad (39)$$

when expressions for the input and output quantities and their derivatives are substituted in the performance equations [Eqs. (35) and (36)], each term contains the kernel, $q_{(in)1a}e^{j\omega_f t}$. This kernel can be factored from the equations, leaving only the vector performance operators, the parameters of the component and the forcing frequency. It is possible to solve the equations simultaneously for the vector performance operators, one of which can be written as the quotient of determinants, or

$$\{\bar{P}\}_{O[q_{(in)1}q_{(out)1}]} = \frac{\begin{vmatrix} [\ldots a_{\dot{q}_{(in)1}}(j\omega_f) + a_{q_{(in)1}}][\ldots a_{\dot{q}_{(out)2}}(j\omega_f) + a_{q_{(out)2}}][\ldots \\ [\ldots b_{\dot{q}_{(in)1}}(j\omega_f) + b_{q_{(in)1}}][\ldots b_{\dot{q}_{(out)2}}(j\omega_f) + b_{q_{(out)2}}][\ldots \\ [\ldots \quad][\ldots \quad][\ldots \end{vmatrix}}{\begin{vmatrix} [\ldots a_{\dot{q}_{(out)1}}(j\omega_f) + a_{q_{(out)1}}][\ldots a_{\dot{q}_{(out)2}}(j\omega_f) + a_{q_{(out)2}}][\ldots \\ [\ldots b_{q_{(out)1}}(j\omega_f) + b_{q_{(out)1}}][\ldots b_{\dot{q}_{(out)2}}(j\omega_f) + b_{q_{(out)2}}][\ldots \\ [\ldots \quad][\ldots \quad][\ldots \end{vmatrix}} = (AR)_{O[q_{(in)1}q_{(out)1}]}e^{j(PA)_{O[q_{(in)1}q_{(out)1}]}} \quad (40)$$

Consequently, the amplitude and phase relationships of the vector performance operator are dependent upon the forcing frequency and the component parameters, according to Eq. (40).

The accuracy involved in computing the performance of a component is a function of the accuracy to which the values of the component parameters are known. The accuracy in the case of the airplane is admittedly approximate, because there is considerable latitude in the interpretation of certain of the stability derivatives. Several of these derivatives, such as $dC_L/d\alpha$, $dC_m/d\alpha$, and $dC_m/d\delta_E$, can be determined to a satisfactory degree of accuracy from wind-tunnel tests on large scale models, but other derivatives, such as the damping in pitch, dC_m/dq, require special tests and in most cases are not determined experimentally. Some of the derivatives are seriously affected by changes in the propeller thrust, but at present there is not available sufficient generalized data to compute with accuracy the effects of these power changes.

In contrast to the statements in the preceding paragraph, the techniques introduced in this paper do not require knowledge of the individual stability derivatives when the performance operator is obtained from flight test. Measurements for this purpose can be made at any desired altitude, attitude, and speed within the limits of the aircraft, and such effects as Mach Number and propeller normal force variation with pitch angle are automatically included. The effects of lag in the build-up of aerodynamic forces and torques caused by accelerations that require rapid changes in the flow pattern around the airplane are also included.

(*b*) *By Experimental Application of a Simple Harmonic*

The vector performance operator of a component can be evaluated experimentally by measuring the amplitude and phase of the response to a simple harmonic input of known amplitude and frequency. The input can be represented mathematically as

$$q_{in} = q_{(in)a}\cos\omega_f t \quad (41)$$

or, by Eq. (21),

$$q_{in} = [q_{(in)a}/2]e^{j\omega_f t} + [q_{(in)a}/2]e^{-j\omega_f t} \tag{42}$$

The response of the component can be determined by operating independently on the two conjugate vectors of Eq. (42), giving

$$\begin{aligned} q_{out} &= \{\bar{P}\}_{O[q_{in}q_{out}](\omega_f)} \frac{q_{(in)a}}{2} e^{j\omega_f t} + \{\bar{P}\}_{O[q_{in}q_{out}](-\omega_f)} \frac{q_{(in)a}}{2} e^{-j\omega_f t} \\ &= (AR)_{O[q_{in}q_{out}]} \frac{q_{(in)a}}{2} \left\{ e^{j[\omega_f t + (PA)_{O[q_{in}q_{out}]}]} + e^{-j[\omega_f t + (PA)_{O[q_{in}q_{out}]}]} \right\} \\ &= (AR)_{O[q_{in}q_{out}]} q_{(in)a} \cos \left\{ \omega_f t + (PA)_{O[q_{in}q_{out}]} \right\} \end{aligned} \tag{43}$$

As indicated by Eq. (43), the response to a simple harmonic input is itself a simple harmonic quantity, oscillating at the same frequency as the forcing frequency. However, the response (the output), is not in phase with the input, and its maximum deviation from zero, called the amplitude, equals the product of the amplitude ratio and the input amplitude, so that

$$q_{out} = q_{(out)a} \cos \left\{ \omega_f t + (PA)_{O[q_{in}q_{out}]} \right\} \tag{44}$$

The measurements that must be made to determine the amplitude ratio and the phase angle are shown in Fig. 7. A comparison of Eq. (43) with Eq. (44) indicates that

$$(AR)_{O[q_{in}q_{out}]} = q_{(out)a}/q_{(in)a} \tag{45}$$

Therefore, the amplitude ratio can be obtained immediately by dividing the output amplitude by the input amplitude. Actually, a datum, or zero reference, line is not always available, in which case it is more convenient to take the quotient of the double amplitudes.

In Fig. 7 the output response of the component is leading the input quantity by a time t_L. The fractional lead equals the ratio of the time lead to the forcing period, but, since the forcing period is equivalent to 360°, the phase angle becomes

$$(PA)_{O[q_{in}q_{out}]} = (t_L/T_f)\ 360 \tag{46}$$

in degrees.

The technique employed in carrying out these tests consists in establishing steady-state conditions by allowing sufficient time for the transient to disappear and then in recording by oscillographic or other means both the input and output quantities. The frequency of oscillation is changed in predetermined amounts until the desired frequency spectrum is obtained. For components of a commercial automatic control, the desired frequency range is from 0 to 10 rad. per sec.

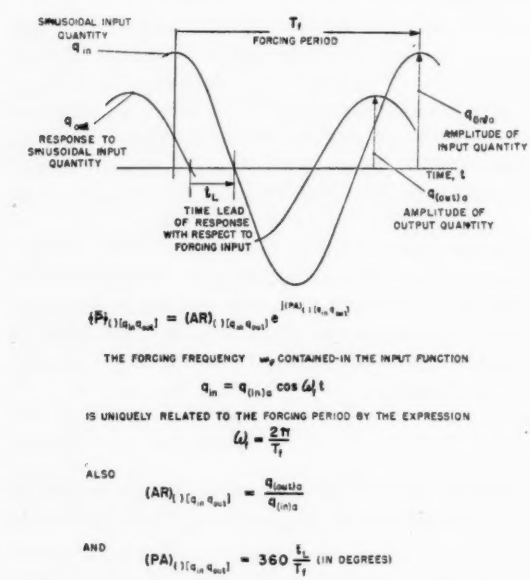

FIG. 7. Use of a sinusoidal input for the experimental determination of the vector performance operator.

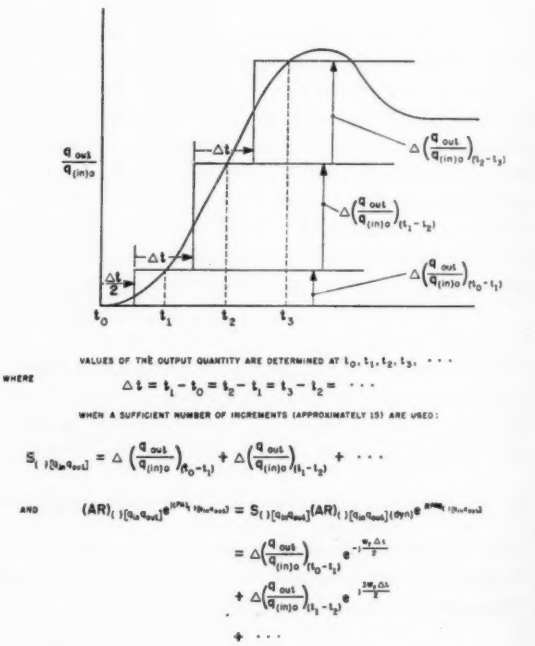
$\frac{q_{out}}{q_{(in)a}}$
Δt
$\Delta\left(\frac{q_{out}}{q_{(in)a}}\right)_{(t_2-t_3)}$
$\Delta\left(\frac{q_{out}}{q_{(in)a}}\right)_{(t_1-t_2)}$
$\Delta\left(\frac{q_{out}}{q_{(in)a}}\right)_{(t_0-t_1)}$
$\frac{\Delta t}{2}$
t_0 t_1 t_2 t_3
VALUES OF THE OUTPUT QUANTITY ARE DETERMINED AT $t_0, t_1, t_2, t_3, \cdots$
WHERE
$\Delta t = t_1 - t_0 = t_2 - t_1 = t_3 - t_2 = \cdots$
WHEN A SUFFICIENT NUMBER OF INCREMENTS (APPROXIMATELY 15) ARE USED:
$S_{(\ )[q_{in}q_{out}]} = \Delta\left(\frac{q_{out}}{q_{(in)a}}\right)_{(t_0-t_1)} + \Delta\left(\frac{q_{out}}{q_{(in)a}}\right)_{(t_1-t_2)} + \cdots$
AND
$(AR)_{(\ )[q_{in}q_{out}]} e^{j(PA)_{(\ )[q_{in}q_{out}]}} = S_{(\ )[q_{in}q_{out}]}[(AR)_{(\ )[q_{in}q_{out}]}(\text{dyn})] e^{j(PA)_{(\ )[q_{in}q_{out}]}}$
$= \Delta\left(\frac{q_{out}}{q_{(in)a}}\right)_{(t_0-t_1)} e^{-j\frac{\omega_f \Delta t}{2}}$
$+ \Delta\left(\frac{q_{out}}{q_{(in)a}}\right)_{(t_1-t_2)} e^{-j\frac{3\omega_f \Delta t}{2}}$
$+ \cdots$

FIG. 8. Diagram showing method used to obtain vector performance operator from step function data.

Military applications sometimes require response data at higher frequencies.

The sinusoidal rate-of-pitch response for a U.S. Air Force A-26 medium bomber flying at an indicated air speed of 180 m.p.h. at 10,000 ft. altitude is presented in Fig. 10. In determining the associated vector performance operators the center of gravity is located at 26 per cent of the mean aerodynamic chord. The maximum amplitude ratio occurs at a forcing frequency of 2.3 rad. per sec., which represents a forcing period of 2.7 sec. This period corresponds to the short-period oscillation of the airplane. The long-period oscillation resulting from dynamic changes in air speed is greater by one order of magnitude.

A year's work is required to obtain the level flight longitudinal and lateral performance operators by means of sinusoidal inputs when effects of air speed and center-of-gravity location are thoroughly investigated. For economic reasons, this period of time might be prohibitive. In addition, for rapidly changing flight conditions resulting from turns, climbs, or dives, the time required to establish steady-state conditions is too long for the sinusoidal method to be effective. The step input has great value for these configurations, as well as for those in level flight, for the data is then collected in seconds rather than in hours.

(c) By Experimental Application of a Step Input

The response to a step input can be presented as a transient curve departing from its initial value at the instant the step input is applied. A typical transient response is illustrated in Fig. 8. In order to obtain the vector performance operator, this curve is approximated by the series of steps indicated in the figure. For perfect matching of the actual response, infinitesimal steps are required, but for engineering purposes a choice of 15 to 20 steps gives satisfactory results. The time ordinate of the transient response, up to a point sufficiently beyond the response time to obtain the necessary accuracy, must be divided into even time increments, Δt—the number of increments depending upon the number of steps required. It is necessary to measure the change in output from the transient response during each of the time increments. These changes are denoted by the symbols

$$\Delta\left[\frac{q_{out}}{q_{(in)0}}\right]_{(t_0 - t_1)}, \qquad \Delta\left[\frac{q_{out}}{q_{(in)0}}\right]_{(t_1 - t_2)}, \text{ etc.}$$

The incremental steps can be expressed as functions of time by the use of the square wave quantity of Eq. (27). The square wave conforms to a step only for a time equal to the half period of the square wave, but no upper limit need be placed on this time duration. However, the sum of these steps is made to approximate the output response, and for this reason

$$\frac{q_{out}}{q_{(in)0}} = \Delta\left[\frac{q_{out}}{q_{(in)0}}\right]_{(t_0 - t_1)}\left\{\frac{1}{2} + \frac{1}{\pi}\sum_{\substack{n = 1, 3, \ldots \\ -1, -3, \ldots}} \frac{1}{jn} e^{jn\omega_f[t - \Delta t/2]}\right\} +$$

$$\Delta\left[\frac{q_{out}}{q_{(in)0}}\right]_{(t_1 - t_2)}\left\{\frac{1}{2} + \frac{1}{\pi}\sum_{\substack{n = 1, 3, \ldots \\ -1, -3, \ldots}} \frac{1}{jn} e^{jn\omega_f[t - 3\Delta t/2]}\right\} + \ldots \quad (47)$$

The time lead of Eq. (27) is replaced in Eq. (47) by a time delay. The time delay is selected so that most steps bracket the response curve that is to be matched. In this manner the area under the discontinuous approximating curve is kept as nearly as possible equal to the area under the actual response curve.

However, the square wave response is expressed in Eq. (31) as a summation of vectors in a form similar to that of Eq. (47). When the period of the square wave response equals the period of the incremental steps, it is possible to equate these two expressions and to solve for the vector performance operator, which becomes

$$S_{O[q_{in}q_{out}]} = \Delta[q_{out}/q_{(in)0}]_{(t_0 - t_1)} + \Delta[q_{out}/q_{(in)0}]_{(t_1 - t_2)} + \ldots \quad (48)$$

and

$$S_{O[q_{in}q_{out}]}(AR)_{O[q_{in}q_{out}](dyn)}e^{j(PA)_{O[q_{in}q_{out}]}} = \Delta\left[\frac{q_{out}}{q_{(in)0}}\right]_{(t_0 - t_1)}e^{-j\omega_f(\Delta t/2)} + \Delta\left[\frac{q_{out}}{q_{(in)0}}\right]_{(t_1 - t_2)}e^{-j\omega_f 3(\Delta t/2)} + \ldots \quad (49)$$

Eq. (48) shows that the input-output sensitivity can be determined by the direct addition of the incremental steps. However, this sum equals the ratio of the steady-state output to the input, which can be measured directly; hence, this equation serves only as an arithmetical check on the incremental values. The amplitude ratio and the phase angle can be evaluated by the vector addition indicated in Eq. (49). This addition, which can be made either graphically or algebraically, can be carried out for any forcing frequency ω_f. This forcing frequency replaces the product of the order of n and the fundamental frequency appearing in

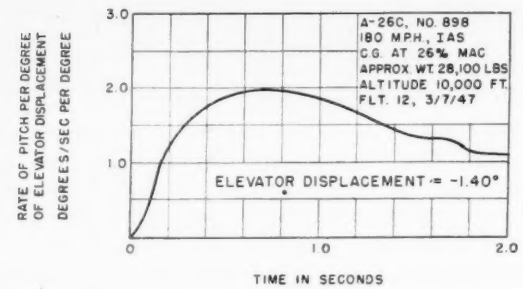

FIG. 9. Airplane rate of pitch response to elevator step displacement.

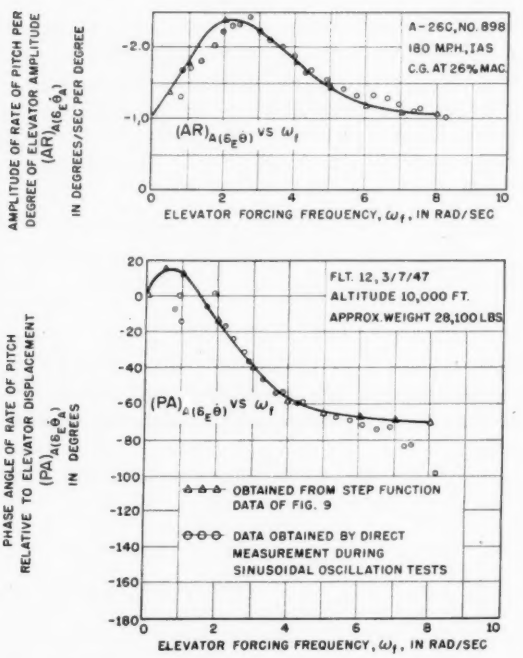
A-26C, NO. 898
180 MPH, IAS
C.G. AT 26% MAC
AMPLITUDE OF RATE OF PITCH PER DEGREE OF ELEVATOR AMPLITUDE
IN DEGREES/SEC PER DEGREE
ELEVATOR FORCING FREQUENCY, IN RAD/SEC
FLT. 12, 3/7/47
ALTITUDE 10,000 FT.
APPROX. WEIGHT 28,100 LBS.
PHASE ANGLE OF RATE OF PITCH RELATIVE TO ELEVATOR DISPLACEMENT
IN DEGREES
OBTAINED FROM STEP FUNCTION DATA OF FIG. 9
DATA OBTAINED BY DIRECT MEASUREMENT DURING SINUSOIDAL OSCILLATION TESTS
ELEVATOR FORCING FREQUENCY, IN RAD/SEC

FIG. 10. Comparison of rate of pitch vector performance operator of airplane obtained from elevator step displacement with operator obtained from sinusoidal oscillation of elevator.

Eqs. (27) and (47) because, in this case, both of these quantities are arbitrary—the only restriction being that the fundamental forcing frequency be small.

The rate-of-pitch response of the airplane to a step displacement of the elevator is shown in Fig. 9. This response is found for the same modifying quantities of altitude, air speed, and center-of-gravity position as the sinusoidal response data already presented. For this reason it is possible to compare the vector performance operator obtained by sinusoidal input displacements with that obtained by a step displacement. This comparison is demonstrated in Fig. 10, in which the circles represent individual sinusoidal measurements and the solid curve is a result of the step response. The agreement of the two sets of data is remarkably good, demonstrating the practicality of both techniques and the fact that the airplane can be considered to be a linear component.

(VI) Analysis of Multiloop Systems

Parts (I) through (V) furnish comprehensive background for an analysis of multiloop systems and suggest the basic steps to be followed in designing a specific system. These steps are summarized as follows:

(1) Specify the input and the output, and consider the various systems that might give the desired relationship between the two. Construct a functional diagram for each of the systems decided upon, and describe each of the physical quantities connecting the components contained in the systems (the components must be physically realizable—for example, circuit, motor, shaft, airplane, or instrument). Define the relationship between the input and the output of each component in terms of the vector performance operator.

(2) Express the system performance operator in terms of the component operators. This step is shown in Fig. 11 for a typical system.

(3) Determine the values of the component vector performance operators by the methods introduced in Part (V). When the components are available, base the values on experimental test. When the equipment is in the design stage or otherwise unavailable, obtain the values from computations based on mathematical reasoning.

(4) Effect a preliminary design by the use of idealized components for which the less important dynamic effects are neglected (for example, the performance operator of an idealized derivative circuit is based on the assumption that perfect differentiation occurs at all forcing frequencies). The components should be idealized to the extent that the overall system can be represented by a third or fourth order equation; then, the methods of Routh can be used to ensure positive roots

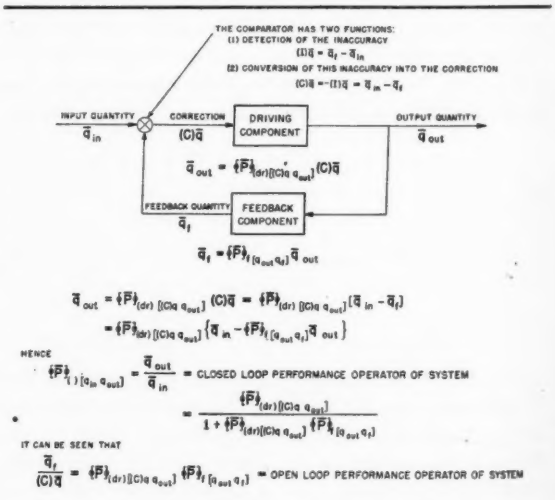

FIG. 11. Functional diagram of simple closed loop system.

and a stable system. A more complete description of the idealized performance operator is given in Appendix C.

(5) Check the stability of the system, with all possible dynamic effects included, by the use of polar plots of the vector performance operator. These plots are commonly called Nyquist diagrams. According to Nyquist criteria, a system is stable when the loci of all the open loop performance operators remain at the right of the minus unity coordinate on the complex plane and may be stable even though one of several loci passes to the left of the coordinate. The relationship between the input and the output of a typical single-loop system is shown in Fig. 11. The open-loop characteristic of the system can be obtained by measuring the variations in feedback for given correction signals, with the comparator removed. The vector performance operator governing the action of this open loop is given by the product of the operators of the two components—e.g., the driving component and the feedback component.

(6) Evaluate the closed-loop performance operator of the system by combining the component operators vectorially. Present the system performance operator as a function of forcing frequency in terms of amplitude ratio and phase angle. A further check on the dynamic response of the system can be obtained by observation of the performance operator presented in this form. For example, it can be shown that systems become unstable for which the phase angle becomes leading as the frequency approaches an infinite value. Furthermore, the degree of stability of a system can be estimated qualitatively by evaluation of the amplitude ratio. When this ratio exceeds 1.3, the stability coefficient is too low for most practical systems.

(7) Determine the square wave output of the system by introducing the closed-loop performance operator of (6) into Eq. (32). Quantitative values of the response time and the stability coefficient are then obtained from this square wave output by the method described in Part (IV). Care must be exercised when selecting the period of the square wave, for, with too short a period in comparison with the response time, steady-state conditions are not reached at the completion of each half cycle. In this case, the system does not have zero initial conditions at the start of each new cycle, and the pattern of the response is arbitrarily affected. Conversely, with too long a period, the fundamental forcing frequency is low, and an unnecessarily large number of terms is required for the Fourier series response to converge to reasonable limits.

The distortion of the square wave response involves the so-called Gibbs' phenomenon. Gibbs discovered that the summing of a Fourier series causes the graphical representation of the sum of the series to peak at points of discontinuity or at points where abrupt changes occur. The phenomenon may be observed in the square wave response by a sudden deviation from steady-state conditions just prior to the end of a half cycle. This fluctuation may be minimized by accounting for more terms in the Fourier series; however, even when the fluctuation amounts to as much as 10 per cent of the steady-state level, the remaining sections of the square wave response are practically unaffected.

More serious distortion of the square wave response occurs when the amplitude ratio is inconsistent with the phase angle. When values of the amplitude ratio are known for all frequencies, the phase angle of a physically realizable stable system is uniquely defined. There can be several reasons for a discrepancy between the amplitude ratio and the phase angle. There is the possibility of a mistake in calculation, and there is the possibility of incurring an inaccuracy when measuring the component vector performance operators during experimental tests. Finally, there is a chance that an important frequency effect, such as a resonance peak, is being neglected because the upper frequency limit of the summation is too low. This distortion, as with the Gibbs' phenomenon, gives rise to a deflection of the output response after the steady-state condition is reached but before the beginning of the next cycle.

(VII) Design of a Typical Longitudinal Control System

Aircraft control equipment must be sufficiently adaptable so that a given type unit will give satisfactory service in several different kinds of airplanes. With this provision, a manufacturer can supply a relatively economical product for both commercial and military use. However, the desired motion of the control surfaces in correcting for a divergence of the aircraft from its intended flight direction depends upon the particular airplane and the use to which it is placed. Two system adjustments are provided with the equipment: one is called the proportional control, which governs the control surface displacement for a given error signal; the other is called the derivative control, which governs the control surface displacement for a given rate of change of the signal. As a specific case, the effect is considered here of the proportional and derivative adjustments for a typical longitudinal control system that includes a Minneapolis-Honeywell elevator servo and an A-26 medium bomber.

When in cross-country flight, an airplane is usually called upon to fly for protracted periods at constant altitude. When checking his vertical flight direction the pilot utilizes such instruments as the altimeter and the rate of climb meter and must periodically retrim the airplane to account for changes in angle of attack resulting from the consumption of fuel. When in level flight, the airplane must be pitched above the horizontal by an amount equal to the angle of attack; consequently, trimming the airplane requires a setting of the pitch angle, θ_{set}. The difference between the pitch setting, θ_{set}, and the correct airplane pitch angle for the in-

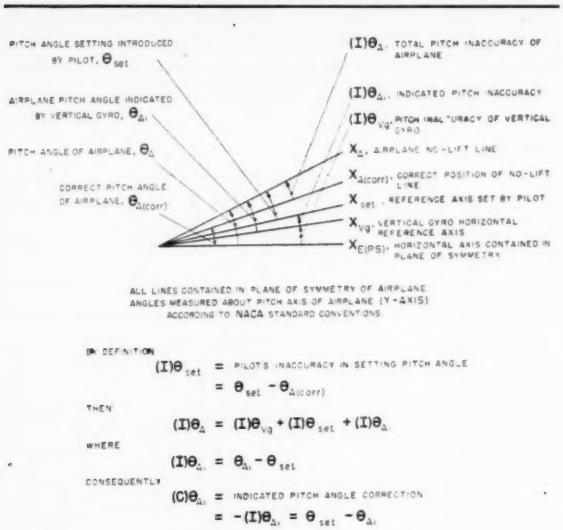
PITCH ANGLE SETTING INTRODUCED BY PILOT, θ_{set}
AIRPLANE PITCH ANGLE INDICATED BY VERTICAL GYRO, θ_{Ai}
PITCH ANGLE OF AIRPLANE, θ_A
CORRECT PITCH ANGLE OF AIRPLANE, $\theta_{A(corr)}$
$(I)\theta_A$, TOTAL PITCH INACCURACY OF AIRPLANE
$(I)\theta_{Ai}$, INDICATED PITCH INACCURACY
$(I)\theta_{VG}$, PITCH INACCURACY OF VERTICAL GYRO
X_A, AIRPLANE NO-LIFT LINE
$X_{A(corr)}$, CORRECT POSITION OF NO-LIFT LINE
X_{set}, REFERENCE AXIS SET BY PILOT
X_{VG}, VERTICAL GYRO HORIZONTAL REFERENCE AXIS
$X_{E(PS)}$, HORIZONTAL AXIS CONTAINED IN PLANE OF SYMMETRY
ALL LINES CONTAINED IN PLANE OF SYMMETRY OF AIRPLANE
ANGLES MEASURED ABOUT PITCH AXIS OF AIRPLANE (Y-AXIS) ACCORDING TO NACA STANDARD CONVENTIONS
BY DEFINITION
$(I)\theta_{set} = \theta_{set} - \theta_{A(corr)}$ = PILOT'S INACCURACY IN SETTING PITCH ANGLE
THEN
$(I)\theta_A = (I)\theta_{VG} + (I)\theta_{set} + (I)\theta_{Ai}$
WHERE
$(I)\theta_{Ai} = \theta_{Ai} - \theta_{set}$
CONSEQUENTLY
$(C)\theta_{Ai} = -(I)\theta_{Ai} = \theta_{set} - \theta_{Ai}$ = INDICATED PITCH ANGLE CORRECTION

FIG. 12. Geometrical factors involved when controlling the pitch angle of an airplane.

tended flight, $\theta_{A(corr)}$, is the pilot's setting inaccuracy $(I)\theta_{set}$—that is,

$$(I)\theta_{set} = \theta_{set} - \theta_{A(corr.)} \tag{50}$$

A vertical gyro is used to provide a horizontal reference within the aircraft, from which the pitch angle of the aircraft can be continuously measured. The vertical gyro indication of pitch angle, θ_{Ai}, is inaccurate by an angle $(I)\theta_{vg}$ when the gyro is out of plumb with the earth, in which case

$$(I)\theta_{vg} = \theta_{Ai} - \theta_A \tag{51}$$

The angle between the horizontal reference established by the vertical gyro and the horizontal reference set by the pilot is the indication of pitch inaccuracy, $(I)\theta_{Ai}$. This indication is supplied to the servo controls to initiate the required correction. The total inaccuracy in pitch, $(I)\theta_A$, is equal to the sum of the inaccuracies introduced by the pilot, the vertical gyro, and the servo control. As seen from Fig. 12,

$$\begin{aligned}(I)\theta_A &= \theta_A - \theta_{A(corr.)} \\ &= (I)\theta_{set} + (I)\theta_{vg} + (I)\theta_{Ai}\end{aligned} \tag{52}$$

The inaccuracy of the pilot setting is a random function beyond the scope of all but psychologists, and the inaccuracy of the vertical gyro is small except when the airplane maneuver involves large horizontal accelerations; therefore, for the purposes of this paper, the total inaccuracy is assumed to be equal to the indicated inaccuracy. Fig. 13 is a functional diagram of the longitudinal control system. In this diagram, the comparator, in which the vertical gyro indication is matched with the pitch angle setting, is shown as a differential. The comparator has the dual function of indicating the inaccuracy and of transforming the inaccuracy into a suitable correction signal, $(C)\theta_{Ai}$, where

$$(C)\theta_{Ai} = -(I)\theta_{Ai} = \theta_{set} - \theta_{Ai} \tag{53}$$

In the longitudinal control system the indicated pitch correction is the only input to the elevator computer. The function of the elevator computer is to provide the necessary proportional and derivative signals for stabilization and control. These signals are transmitted to the elevator servo as the elevator computer output voltage. The elevator servo consists of an appropriate power amplifier, a motor, gear train, and output shaft. A followup on the output shaft generates a voltage that is matched with the input voltage from the elevator computer. Cable wrapped around a drum fastened to the servo output shaft is connected at its ends to the elevator horns. In this manner servo shaft displacements are transferred to the elevator, which governs the pitch of the aircraft. The input to the longitudinal control system can be considered to be the pitch setting, and the output, the pitch angle, so that the system vector performance operator becomes

$$\begin{aligned}\{\bar{P}\}_{(LCS)} &= \frac{\bar{\theta}_A}{\bar{\theta}_{set}} = (AR)_{(LCS)}e^{j(PA)_{(LCS)}} \\ &= \frac{\{\bar{P}\}_c\{\bar{P}\}_s\{\bar{P}\}_r\{\bar{P}\}_{A[\delta_E\theta_A]}}{1 + \{\bar{P}\}_c\{\bar{P}\}_s\{\bar{P}\}_r\{\bar{P}\}_{A[\delta_B\theta_A]}\{\bar{P}\}_{(vg)}}\end{aligned} \tag{54}$$

With the performance operator of the complete longitudinal control system established, the next step is to determine the performance operators of the several components.

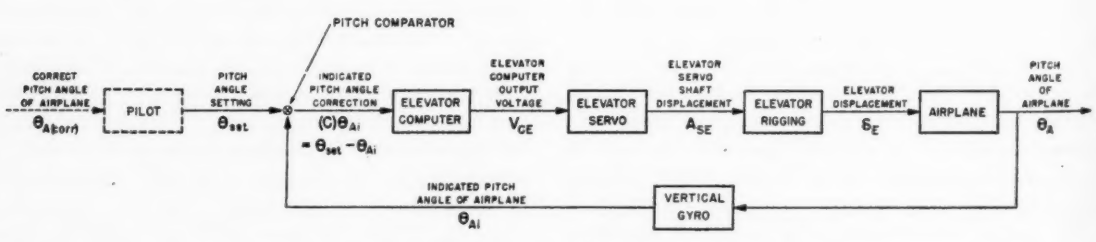

FIG. 13. Functional diagram of aircraft longitudinal control system.

(a) *Elevator Computer*

The elevator computer develops an output voltage, V_c, equal to the sum of two voltages—one proportional to the indicated pitch correction $(C)\theta_{Ai}$ and the other proportional to the rate of change of the pitch correction—so that

$$V_c = S_{cp}(C)\theta_{Ai} + S_{cd}[(C)\dot{\theta}_{Ai}] \tag{55}$$

and

$$\{\bar{P}\}_c = \bar{V}_c/(C)\bar{\theta}_{Ai} = S_{cp} + j\omega_f S_{cd}$$

$$= S_{cp}\sqrt{1 + \left(\omega_f \frac{S_{cd}}{S_{cp}}\right)^2}\, e^{j \tan^{-1}[\omega_f S_{cd}/S_{cp}]} \tag{56}$$

The elevator computer is designed to permit individual adjustment of the proportional sensitivity, S_{cp}, and the derivative sensitivity, S_{cd}. The magnitudes of these sensitivities determine the dynamic response of the longitudinal control system.

(b) *Elevator Servo*

The elevator servo selected for the longitudinal control system is part of the C-1a Minneapolis-Honeywell autopilot. The elevator servo is alternately driving and braking when introducing an angular displacement, an action called pecking. The pecking action is sufficiently fast that the unit can be considered a linear component, and its performance can be expressed as

$$\{\bar{P}\}_s = \frac{\bar{A}_s}{\bar{V}_c} = (AR)_s e^{j(PA)_s} = S_s(AR)_{s(\mathrm{dyn})} e^{j(PA)_s} \tag{57}$$

An increase in the rate of pecking throttles the response of the elevator servo and increases its effective damping. The throttling can be adjusted within limits. In Fig. 14, which shows plots of the elevator servo amplitude and phase angle as functions of the computer voltage forcing frequency, the throttling is set at a maximum. It can be seen that with maximum throttling the C-1a elevator servo acts as though it were critically damped and had a natural frequency of approximately 7 rad. per sec.

(c) *Elevator Rigging*

The elevator is coupled to the servo output shaft with a stranded steel cable, which stretches in proportion to the reactive elevator load. The source of this load can be considered to be entirely aerodynamic, since the inertia of the elevator is sufficiently small in comparison with the elasticity of the cable so that the elevator natural frequency is greater than 60 rad. per sec. The aerodynamic load, called the hinge moment, restrains the elevator motion so that its displacement, for a given servo displacement, is always less when the aircraft is in the air than when it is on the ground. Therefore,

$$\{\bar{P}\}_r = \bar{\delta}_E/\bar{A}_s = S_r \tag{58}$$

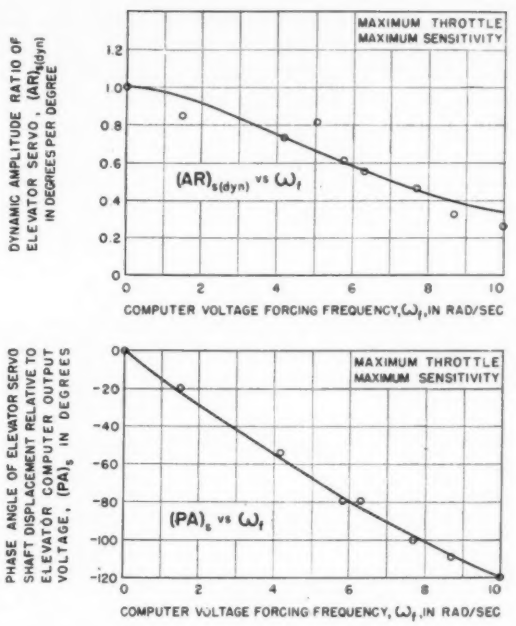
MAXIMUM THROTTLE
MAXIMUM SENSITIVITY
DYNAMIC AMPLITUDE RATIO OF ELEVATOR SERVO, $(AR)_{s(dyn)}$ IN DEGREES PER DEGREE
$(AR)_{s(dyn)}$ vs ω_f
COMPUTER VOLTAGE FORCING FREQUENCY, ω_f, IN RAD/SEC
MAXIMUM THROTTLE
MAXIMUM SENSITIVITY
PHASE ANGLE OF ELEVATOR SERVO SHAFT DISPLACEMENT RELATIVE TO ELEVATOR COMPUTER OUTPUT VOLTAGE, $(PA)_s$ IN DEGREES
$(PA)_s$ vs ω_f
COMPUTER VOLTAGE FORCING FREQUENCY, ω_f, IN RAD/SEC

FIG. 14. Vector performance operator of C-1a elevator servo manufactured by Minneapolis-Honeywell.

This equation brings out the important fact that the sensitivity of the elevator rigging, S_r, is *not* constant; it is a function not only of the rigging dimensions but also of the elevator surface area and the indicated air speed.

(d) *Airplane*

The experimental means used to determine the vector performance operator of the airplane is discussed in Part (V). The most economical timesaving method involves the measurement of the rate of pitch following a step displacement of the elevator. Note that this method cannot be used directly for pitch angle evaluation, because this quantity increases linearly with time following an elevator step input and does not reach the necessary constant steady-state value required when using the Fourier series methods of Fig. 8. However, the pitch angle is the integral of the pitch rate; therefore,

$$\{\bar{P}\}_{A[\delta_E\theta_A]} = \frac{\bar{\theta}_A}{\bar{\delta}_E} = (AR)_{A[\delta_E\theta_A]} e^{j(PA)_{A[\delta_E\theta_A]}} = \frac{\{\bar{P}\}_{A[\delta_E\dot{\theta}_A]}}{j\omega_f}$$

$$= \frac{(AR)_{A[\delta_E\dot{\theta}_A]}}{\omega_f}\, e^{j[(PA)_{A[\delta_E\dot{\theta}_A]} - (\pi/2)]} \tag{59}$$

Consequently, it can be seen by inspection

$$(AR)_{A[\delta_E\theta_A]} = (AR)_{A[\delta_E\dot{\theta}_A]}/\omega_f \tag{60}$$

and

$$(PA)_{A[\delta_E\theta_A]} = (PA)_{A[\delta_E\dot{\theta}_A]} - (\pi/2) \tag{61}$$

It is shown by Eqs. (60) and (61) that the pitch angle performance operator of the airplane can be obtained from the pitch rate operator of Fig. 10 by dividing the pitch rate amplitude ratio by the forcing frequency to obtain the pitch amplitude ratio and by increasing the pitch rate phase angle by $\pi/2$ rad. or 90° to obtain the pitch phase angle. The resulting data, originally derived from the pitch response to a step displacement of the elevator, are presented in Fig. 15.

(e) *Vertical Gyro*

The vertical gyro is essentially a long-period pendulum and is unaffected by most airplane maneuvers excepting procedure turns lasting 1 or more min. Since this discussion is concerned with effects having a much shorter period, the vertical gyro output can be assumed equal to the input, in which case

$$\{\bar{P}\}_{\bar{\theta}_{vg}} = \bar{\theta}_{At}/\bar{\theta}_A = 1 \tag{62}$$

The open-loop vector performance operator of the longitudinal control system equals the product of the vector performance operators of the computer, servo, rigging, airplane, and vertical gyro. The performance operators of these five components are expressed by Eqs. (56), (57), (58), (59), and (62), respectively, from which

$$\frac{\bar{\theta}_{At}}{(C)\bar{\theta}_{At}} = \text{open-loop vector performance operator (transfer function)}$$

$$= \{\bar{P}\}_c\{\bar{P}\}_s\{\bar{P}\}_r\{\bar{P}\}_{A[\delta_E\theta_A]}\{\bar{P}\}_{(vg)}$$

$$= \underbrace{\left\{S_{cp}S_sS_r\sqrt{1+\left(\omega_f\frac{S_{cd}}{S_{cp}}\right)^2}\,e^{j\tan^{-1}[\omega_f S_{cd}/S_{cp}]}\right\}}_{\text{to be designed}}\underbrace{\left\{(AR)_{s(\text{dyn})}(AR)_{A(\delta_E\theta_A)}e^{j[(PA)_s+(PA)_{A[\delta_E\theta_A]}]}\right\}}_{\text{previously specified}} \tag{63}$$

In Eq. (63), the parameters associated with the elevator servo performance and the airplane appear within the braces marked "previously specified." They are therefore not subject to the will of the designer. The only parameters remaining within his control appear within the alternate braces. They include the loop gain, which is equal in magnitude to the product of the computer; servo and rigging sensitivities, $S_{cp}S_sS_r$; and the ratio of the elevator computer derivative sensitivity to its proportional sensitivity, S_{cd}/S_{cp}, which has the dimension of time. The influence of these parameters can be judged by referring to the open-loop vector performance loci of the longitudinal control system contained in Fig. 16. These loci are evaluated from Eq. (63) and show that the system is stable when there is no derivative control and when there is a gain of one.* When the gain is increased to three, the locus falls on the left of the minus unity coordinate, indicating an unstable control system. With the introduction of a computer derivative signal, both loci are rotated positively about the origin, thereby increasing the stability of the system.

The longitudinal control system can be more accurately evaluated by using the relationships of Eq. (54) to compute its closed-loop vector performance operator in the form of amplitude ratio and phase angle. The results presented in Fig. 17 give an easily understandable physical representation of the frequency spectrum; in each case it can be seen that the static performance is ideal, having an amplitude ratio of unity at zero frequency. However, the dynamic performances of the four cases presented differ widely. The resonance peaks occur at a higher frequency when the gain is increased, since this increase in proportional feedback ef-

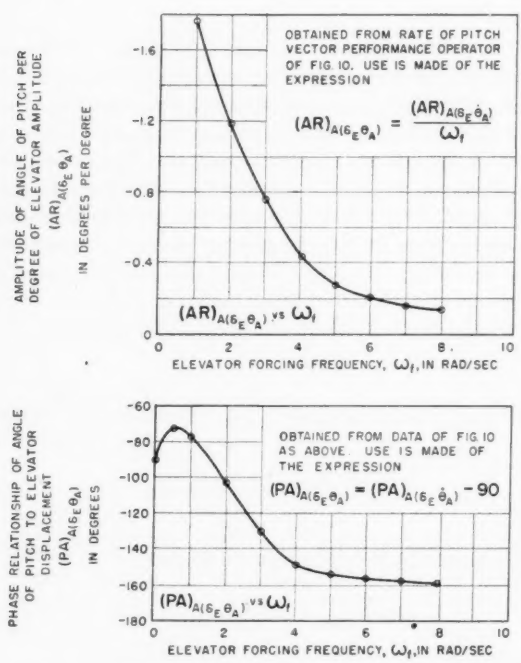

FIG. 15. Angle of pitch vector performance operator for A-26C No. 898 at 180 m.p.h., IAS, with c.g. at 26 per cent M.A.C.

* The product of the sensitivites, $S_{cp}S_sS_r$, must actually have a negative value because, by N.A.C.A. convention, a positive elevator displacement gives a negative change in pitch angle.

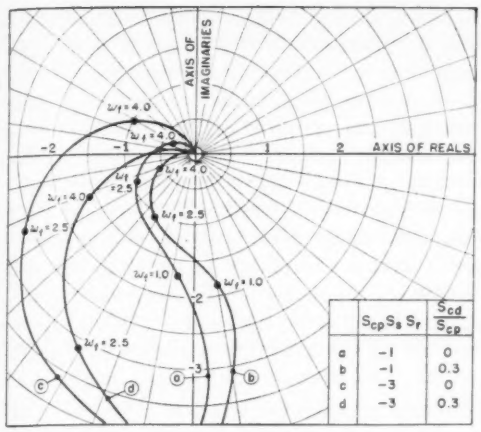

$$\text{OPEN LOOP VECTOR PERFORMANCE OPERATOR} = \{\bar{P}\}_c\{\bar{P}\}_s\{\bar{P}\}_r\{\bar{P}\}_{A[\delta_E\Theta_A]}\{\bar{P}\}_{vg}$$

$$= \left(\frac{\bar{V}_{CE}}{(C)\bar{\Theta}_{A_i}}\right)\left(\frac{\bar{A}_{SE}}{\bar{V}_{CE}}\right)\left(\frac{\bar{\delta}_E}{\bar{A}_{SE}}\right)\left(\frac{\bar{\Theta}_A}{\bar{\delta}_E}\right)\left(\frac{\bar{\Theta}_{A_i}}{\bar{\Theta}_A}\right)$$

$$= \frac{\bar{\Theta}_{A_i}}{(C)\bar{\Theta}_{A_i}}$$

$$= \left\{S_{cp}S_s S_r\sqrt{1+(\omega_f\frac{S_{cd}}{S_{cp}})}\,e^{j\tan^{-1}(\omega_f\frac{S_{cd}}{S_{cp}})}\right\}\left\{(AR)_{s(dyn)}(AR)_{A[\delta_E\Theta_A]}e^{j[(PA)_s+(PA)_{A[\delta_E\Theta_A]}]}\right\}$$

TO BE DESIGNED — PREVIOUSLY SPECIFIED

FIG. 16. Open loop vector performance loci of aircraft longitudinal control system.

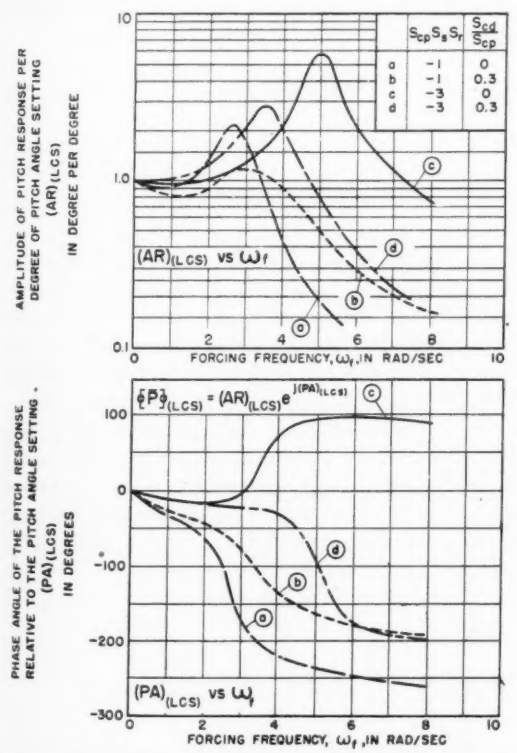
AMPLITUDE OF PITCH RESPONSE PER DEGREE OF PITCH ANGLE SETTING $(AR)_{(LCS)}$ IN DEGREE PER DEGREE
$(AR)_{(LCS)}$ vs ω_f
FORCING FREQUENCY, ω_f, IN RAD/SEC
$S_{cp}S_s S_r$ | $\frac{S_{cd}}{S_{cp}}$
a −1 0
b −1 0.3
c −3 0
d −3 0.3
$\{\bar{P}\}_{(LCS)} = (AR)_{(LCS)}e^{j(PA)_{(LCS)}}$
PHASE ANGLE OF THE PITCH RESPONSE RELATIVE TO THE PITCH ANGLE SETTING $(PA)_{(LCS)}$ IN DEGREES
$(PA)_{(LCS)}$ vs ω_f
FORCING FREQUENCY, ω_f, IN RAD/SEC

FIG. 17. Vector performance operator of aircraft longitudinal control system.

fectively stiffens the system. The increase in gain decreases the stability, as evidenced by the height of the resonance peaks and by the leading phase angle obtained at forcing frequencies greater than 3 rad. per sec. The use of derivative feedback decreases the height of the resonance peaks and thus gives evidence of a greater degree of stability.

The square wave response, shown in Fig. 18, is obtained by combining the data of Fig. 17 in the relationship of Eq. (32). Note that the response with no derivative and a gain of three has peak values that increase exponentially with time. This response does not reach equilibrium during each half cycle and, hence, fails to commence each new cycle with initial conditions equal to zero.

The response time, which is the time for the transient to decay to 5 per cent of its initial value, can be evaluated directly from the response curve; the stability coefficient can be determined by the use of Eq. (34). These results are listed in Table 1.

The system with a proportional factor of one and a derivative of 0.3 sec. clearly has the best characteristics, since the response time is the shortest and the degree of stability is the highest. It is interesting to note the appearance in this case of an exponential in addition

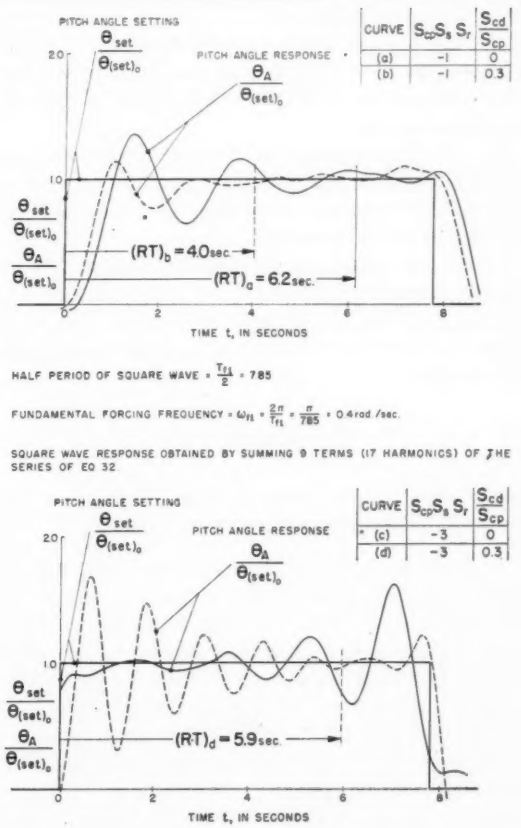
PITCH ANGLE SETTING $\frac{\Theta_{set}}{\Theta_{(set)_o}}$
PITCH ANGLE RESPONSE $\frac{\Theta_A}{\Theta_{(set)_o}}$
CURVE | $S_{cp}S_s S_r$ | $\frac{S_{cd}}{S_{cp}}$
(a) −1 0
(b) −1 0.3
$(RT)_b = 4.0$ sec.
$(RT)_a = 6.2$ sec.
TIME t, IN SECONDS
HALF PERIOD OF SQUARE WAVE = $\frac{T_{f1}}{2} = 7.85$
FUNDAMENTAL FORCING FREQUENCY = $\omega_{f1} = \frac{2\pi}{T_{f1}} = \frac{\pi}{7.85} = 0.4$ rad/sec.
SQUARE WAVE RESPONSE OBTAINED BY SUMMING 9 TERMS (17 HARMONICS) OF THE SERIES OF EQ 32
CURVE | $S_{cp}S_s S_r$ | $\frac{S_{cd}}{S_{cp}}$
(c) −3 0
(d) −3 0.3
$(RT)_d = 5.9$ sec.
TIME t, IN SECONDS

FIG. 18. Square wave response of aircraft longitudinal control system.

TABLE 1
Effect of Proportional and Derivative Control on Response Time and Stability Coefficient

Proportional Factor, $S_{ep}S_aS_r$	Derivative Factor, S_{cd}/S_{ep}	Response Time, RT, Sec.	Stability Coefficient, SC, Per Cent
−1	0	6.2	40
−1	0.3	4.0	65
−3	0	∞	−58
−3	0.3	5.9	26

to the damped sinusoid. A still further increase in derivative control or a decrease in proportional control increases the characteristic time of this exponential, thereby yielding a longer response time.

CONCLUSIONS

(1) The use of the performance operator and the square wave response presents a method of analysis of systems that have (a) an unrestricted number of degrees of freedom because the differential equations of motion do not have to be solved and (b) any number or any degree of complexity of loops.

(2) The method permits the direct use of test results, when they are available, without the need of reducing the test data to parameters defined by an assumed differential equation.

(3) The method allows each component of a system to be considered separately and the action of the loop to be obtained by a simple combination of the individual parameters.

(4) The powerful tools of the servomechanism engineer—for example, the Nyquist criterion—can be applied without recourse to arbitrary and empirical rules with regard to the transient.

(5) In the experimental determination of the performance operator of the airplane, effects such as aerodynamic lag, compressibility phenomena, and power effects are included which cannot now be computed with accuracy.

Appendix A

USE OF THE FOURIER INTEGRAL FOR DETERMINING THE STEP-FUNCTION RESPONSE

It is generally accepted that the study of the transient response of an automatically controlled system to a step function is the most effective means for its proper design and adjustment. However, the methods hitherto available have been difficult to use with all except simple systems having a limited number of degrees of freedom. The vector performance operator in a comparatively simple manner provides the steady-state sinusoidal response of any system. Hence, in studying automatic control systems, a suitable means for converting the steady-state sinusoidal response to the step-function response would be a practical tool.

The mathematical bridge between the steady-state sinusoidal response and the transient motion is the Fourier integral. Except for the most simple systems, however, its use in a formal analytical solution of transients is extremely difficult because the necessary definite integrals are not easily obtainable. Nevertheless, the existence of the Fourier integral and the Fourier transform provides the fundamental idea that any transient input motion can be expressed as a continuous function of frequencies and that the ratio of any frequency component in the input wave to the corresponding frequency component in the output wave is determined by the steady-state parameters of the system at that frequency. This idea is not new and is probably the most basic principle in electric communications theory, even though the analytical use of this principle has not been widespread because of the integration difficulties mentioned.

The developments of Parts (I) and (II) furnish a general method for establishing a step-function analysis, based on the Fourier integral. From the definition of the performance operator [Eq. (1)],

$$q_{out} = \{P\}q_{in} \tag{64}$$

By extending the reasoning of Part (IV), which carries out the operation of Eq. (64) for the square wave input function, the step-function response can be obtained by transforming the step input function into the frequency domain. The theory of the Fourier transform permits the expression of any arbitrary time function as a continuous function of frequency, as follows:

$$\bar{q}_{in} = (1/2\pi)\int_{-\infty}^{\infty} q_{in}e^{-j\omega_f t}dt \tag{65}$$

and

$$q_{in} = \int_{-\infty}^{\infty} \bar{q}_{in}e^{j\omega_f t}\,d\omega_f \tag{66}$$

In these equations, $\bar{q}_{in}$ is the Fourier transform of the input, representing the amplitude and phase of a single harmonic component entirely analogous to the complex coefficient of the Fourier series. In the latter, the Fourier coefficients are defined only for the integer values of frequency and have no definition between integers; a plot of these values against frequency would consist of ordinates erected at each integer, such plots being called step line spectra. The interval of frequency is of differential order in the Fourier transformation representation, and $\bar{q}_{in}$ can be plotted as a continuous function of ω_f.

For a step-function input, where

$$q_{in} = q_{(in)0}, \qquad t > 0$$

$$q_{in} = 0, \qquad t < 0$$

$$\bar{q}_{in} = \frac{q_{(in)0}}{2\pi}\int_{0}^{\infty} e^{-j\omega_f t}dt \quad \text{[from Eq. (66)]} \tag{67}$$

The integral of Eq. (67) is not convergent; therefore, a mathematical artifice must be employed, as follows:

$$\bar{q}_{in} = \frac{q_{(in)0}}{2\pi} \lim_{\alpha \to 0} \int_0^\infty e^{-(\alpha + j\omega_f)t} dt \qquad (68)$$

This equation is equivalent to Eq. (67). By this means the response of a system characterized by the vector performance operator $\{\bar{P}\}$ can be obtained by use of Eq. (66), as follows:

$$q_{out} = \frac{q_{(in)0}}{2\pi} \int_{\omega_f = -\infty}^{\omega_f = \infty} \{\bar{P}\} e^{j\omega_f t} d\omega_f \lim_{\alpha \to 0} \int_{t=0}^{t=\infty} e^{-(\alpha + j\omega_f)t} dt \qquad (69)$$

$$= \frac{q_{(in)0}}{2\pi} \lim_{\alpha \to 0} \int_{\omega_f = -\infty}^{\omega_f = \infty} \frac{\{\bar{P}\} e^{j\omega_f t}}{(\alpha + j\omega_f)} d\omega_f \qquad (70)$$

In general, whether the $\lim_{\alpha \to 0}$ can be taken before integration or after is dependent upon the nature of $\{\bar{P}\}$. However, in all practical cases, the limit can be taken prior to the integration of Eq. (70). Hence,

$$\frac{q_{out}}{q_{(in)0}} = \frac{1}{2\pi j} \int_{-\infty}^{\infty} \frac{\{\bar{P}\}}{\omega_f} e^{j\omega_f t} d\omega_f \qquad (71)$$

The vector performance operator $\{P\}$ has both amplitude and phase, as shown in Part (II). Hence,

$$\frac{q_{out}}{q_{(in)0}} = \frac{1}{2\pi j} \int_{-\infty}^{\infty} \frac{AR}{\omega_f} e^{j(\omega_f t + PA)} d\omega_f \qquad (72)$$

Expanding Eq. (72),

$$\frac{q_{out}}{q_{(in)0}} = \frac{1}{2\pi j} \int_{-\infty}^{\infty} \frac{AR}{\omega_f} \cos(\omega_f t + PA) d\omega_f + \frac{1}{2\pi j} \int_{-\infty}^{\infty} j \frac{AR}{\omega_f} \sin(\omega_f t + PA) d\omega_f \qquad (73)$$

The first integral on the right-hand side of Eq. (73) has a singularity point at $\omega_f = 0$ and therefore requires special treatment. Guillemin* has carried out the complex integration of a similar integral which can be applied to the first integral of Eq. (73). Using the knowledge that for all practical systems, when $\omega_f = 0$, $PA = 0$, and $AR = S$, the first integral can be evaluated as follows:

$$\frac{1}{2\pi j} \int_{-\infty}^{\infty} \frac{AR}{\omega_f} \cos(\omega_f t + PA) d\omega_f = \frac{S}{2} \qquad (74)$$

* *Communication Networks*, Vol. II, pp. 471 and 472; John Wiley and Sons, Inc., 1935.

In the second integral of Eq. (73), the j's cancel, and, because ω_f and PA are odd functions and AR is an even function, the integral can be written as follows:

$$\frac{1}{2\pi j} \int_{-\infty}^{\infty} j \frac{AR}{\omega_f} \sin(\omega_f t + PA) d\omega_f = \frac{1}{\pi} \int_0^\infty \frac{AR}{\omega_f} \sin(\omega_f t + PA) d\omega_f \qquad (75)$$

Therefore, Eq. (73) becomes

$$\frac{q_{out}}{q_{(in)0}} = \frac{S}{2} + \frac{1}{\pi} \int_0^\infty \frac{AR}{\omega_f} \sin(\omega_f t + PA) d\omega_f \qquad (76)$$

The response of a system to a step function can be evaluated by either analytical or graphical use of Eq. (76). The computational work in solving Eq. (76) appears to be rather tedious, whereas the analytical solution may be difficult, especially when the vector performance operator is obtained only in curve form.

A numerical procedure for evaluating Eq. (76) can be obtained by changing the integration to a summation. As in most numerical schemes, the infinitesimal value of $d\omega_f$ is replaced by a small but finite value $\Delta\omega_f$. Thus

$$\frac{1}{\pi} \int_0^\infty \frac{AR}{\omega_f} \sin(\omega_f t + PA) d\omega_f = \frac{1}{\pi} \sum_{n=1}^{n=\infty} \frac{AR}{\omega_{fn}} \sin(\omega_{fn} t + PA) \Delta\omega_f$$

Let

$$\Delta\omega_f = 2\omega_{f1}, \qquad \omega_{fn} = n\omega_{f1}$$

where ω_{f1} is a reference frequency. Then

$$\frac{1}{\pi} \int_0^\infty \frac{AR}{\omega_f} \sin(\omega_f t + PA) d\omega_f = \frac{2}{\pi} \sum_{n=1,3,5\ldots}^{\infty} \frac{AR}{n} \sin(n\omega_{f1} t + PA) \qquad (77)$$

or, finally, the response of a system to a step function can be approximated by

$$\frac{q_{out}}{q_{(in)0}} = \frac{S}{2} + \frac{2}{\pi} \sum_{n=1,3,5\ldots}^{\infty} \frac{AR}{n} \sin(n\omega_{f1} t + PA) \qquad (78)$$

Eq. (78) is precisely the same as that derived in Part (IV) for the response of a system to a square wave. The ω_{f1} thus takes on a physical meaning— it is the angular velocity of the basic harmonic of the square wave. This result might have been anticipated, in that the Fourier integral is the limit of the Fourier series as the fundamental frequency ω_{f1} is reduced to an infinitesimal.

Appendix B

Techniques for Summation of Fourier Series

The performance of an automatically controlled aircraft when subjected to input disturbances is important because these disturbances (mathematically, step functions) are repeatedly applied to the aircraft in the form of gusts, pilot trim adjustments, and small excitations generated within the automatic equipment because of its minor imperfections. A system similar to an airplane has two fundamental properties that govern its response to a step function—namely, its degree of stability and its speed of response. These properties can be specified quantitatively in terms of the stability coefficient and the response time parameters defined in Part (IV). In designing a system, values of the stability coefficient and the response time should be obtained, so that the system can be compared with other systems constructed for the same task.

It is shown in Part (IV), and confirmed in Appendix A, that these parameters can be determined from the response of a system to a square wave input of sufficiently long period. Furthermore, the square wave response can be related to the vector performance operator by use of the equation

$$\frac{q_{out}}{q_{(in)0}} = \frac{S_{0[q_{in}q_{out}]}}{2} + \frac{2S_{0[q_{in}q_{out}]}}{\pi} \sum_{n=1,3,5..} \frac{(AR)_{0[q_{in}q_{out}](dyn)}}{n} \sin\left[n\omega_{fl}t + (PA)_{0[q_{in}q_{out}]}\right] \tag{79}$$

The success of this approach hinges on the convenience of the method used to effect the summation of the Fourier series of Eq. (79).

In one method of summation, values for t are substituted into Eq. (79), using sufficient terms for the desired accuracy. The summation performed in this manner can be arranged in a tabular form suitable for computation by calculating machine operators. This method is tedious, but can be carried out to any degree of accuracy; consequently, it is occasionally used to check results obtained by other techniques.

The square wave response can be obtained more rapidly by using graphical methods for summing the Fourier series. One possible graphical scheme, described by Bromberg,* involves the use of "transient analysis charts." In any graphical scheme each sinusoidal term is represented as a vector quantity in the complex plane with magnitude

$$\frac{2S_{0[q_{in}q_{out}]}(AR)_{0[q_{in}q_{out}](dyn)}}{\pi n}$$

and with angle displacement with respect to the axis of reals

$$[n\omega_{fl}t + (PA)_{0[q_{in}q_{out}]}]$$

The position of each vector can be quickly plotted for the desired times by means of the transient analysis chart or, when this is not available, by means of compasses and protractor. However, the imaginary parts of the vectors are equal to the sine functions of Eq. (79); therefore, by means of a T-square and dividers, the vectors can be projected onto the axis of imaginaries and the indicated summation can be effected.

The square wave response can be determined most conveniently by means of an electromechanical synthesizer, one of which has been constructed by the Instrumentation Laboratory, M.I.T. In this device each harmonic is represented by a synchro as shown in Fig. 19. The synchro rotor is driven by a gear train so constructed that the speed ratio of any synchro with respect to the speed of the fundamental synchro equals the particular harmonic number. Nine synchros are available in the synthesizer, which makes it possible to take into account the 17 odd harmonics. The angular position of each synchro housing can be set to give the proper phase for the particular harmonic, and the output from each synchro can be attenuated by means of a potentiometer to give the proper magnitude. The resulting output voltages are transmitted to Consolidated Engineering Corporation recording equipment, where the signals are amplified, rectified, and summed. This summation is impressed on a galvanometer in order to obtain a curve of the square wave response on oscillograph paper.

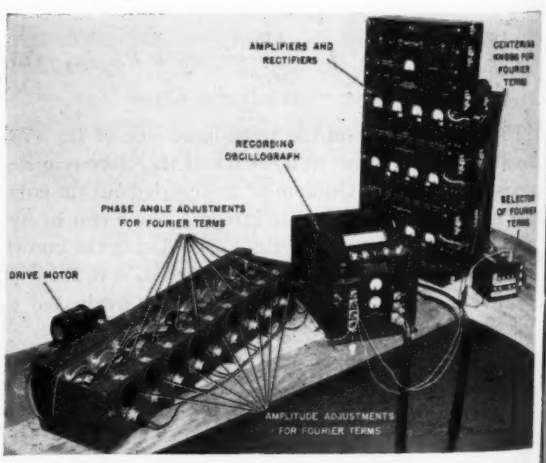

Fig. 19. Square wave synthesizer with associated recording equipment.

* Bromberg, B. G., *Graphical Application of Fourier Series to Automatic Tracking Systems*, Thesis submitted for Sc.D., M.I.T. 1947.

Appendix C

The Ideal Performance Operator

When analyzing compound systems, it is necessary in some cases and expedient in others to idealize certain of the components included in the system. In a dynamic analysis the effect of Coulomb friction and electrical hash on mechanical and electrical components is uncertain and is usually neglected. This idealization is necessary and justified because, for all practical and usable components, these effects are minimized by careful design. Derivative and proportional circuits are provided in the elevator computer described in Part (VII) to stabilize and stiffen the longitudinal control system. Most derivative circuits provide exact differentiation of their inputs over only a limited frequency band. On the basis of the analysis of Part (VII), the electronic engineer can be supplied with frequency specifications for the design of the elevator computer that will justify the assumption of perfect differentiation.

It is sometimes necessary to idealize components to an extent known not to be realizable in actual practice in order to simplify the performance equations of the system for a preliminary analysis, as mentioned in (4) of Part (VI). The simplification of the performance equations should at least permit generalized conditions for stability to be established by the methods of Routh and, if possible, should permit a complete solution of the performance equations. When a component is knowingly idealized for these purposes, an additional subscript is affixed to the performance symbols, in which case Eq. (14) becomes

$$\{\bar{P}\}_{O[q_{in}q_{out}](ideal)} = (AR)_{O[q_{in}q_{out}](ideal)} e^{j(PA)_{O[q_{in}q_{out}](ideal)}} \quad (80)$$

For the simplified analysis to be significant, the difference between the actual performance operator and the idealized performance operator must be relatively small; consequently, when including the effects neglected in the idealization, it is convenient to express this difference as the alteration of the idealized performance operator necessary to obtain the actual performance operator. Changes in amplitude can be represented by a performance ratio, PR, and changes in phase angle can be represented as a deviation, D, or

$$(PR)_{O[(AR)_{[q_{in}q_{out}]}]} = \frac{(AR)_{O[q_{in}q_{out}]}}{(AR)_{O[q_{in}q_{out}](ideal)}} \quad (81)$$

and

$$(D)(PA)_{O[q_{in}q} = (PA)_{O[q_{in}q_{out}]} - (PA)_{O[q_{in}q_{out}](ideal)} \quad (82)$$

Eqs. (81) and (82) permit the vector performance operator of a component to be written in the form

$$\{\bar{P}\}_{O[q_{in}q_{out}]} = \{\bar{P}\}_{O[q_{in}q_{out}](ideal)} (PR)_{O[(AR)_{[q_{in}q_{out}]}]} e^{j(D)(PA)_{O[q_{in}q_{out}]}} \quad (83)$$

In this manner the actual vector performance operator is related to the ideal vector performance operator, and it becomes a simple matter to include effects originally neglected in the analysis.

Bibliography

Routh, E. J., *An Elementary Treatise on The Dynamics of Rigid Bodies;* London, 1877.

Eagle, A., *Fourier's Theorem and Harmonic Analysis;* New York, 1925.

Nyquist, A., *Regeneration Theory,* Bell System Technical Journal, Vol. XI, No. 1, January, 1932.

Hazen, H. L., *Theory of Servomechanisms,* Journal Franklin Institute, Vol. 218, No. 3, September, 1934.

Guillemin, E. A., *Communication Networks,* Vols. I and II; John Wiley and Sons, Inc., New York, 1935.

Titchmarsh, C., *Introduction to The Theory of Fourier Integrals;* Oxford, 1937.

Brown, G. S., *Behavior and Design of Servomechanisms,* N.D.R.C. (Sec. D-2), 1940.

Draper, C. S., and Bentley, G. P., *Design Factors Controlling the Dynamic Performance of Instruments,* A.S.M.E. Transactions, July, 1940.

Hall, A. C., *The Analysis and Synthesis of Linear Servomechanisms;* Cambridge, Mass., 1943.

Durand, W. F., (Editor) *Aerodynamic Theory,* Vol. V; 1943.

Gardner, Murray F., and Barnes, John L., *Transients in Linear Systems,* Vol. I; John Wiley and Sons, Inc., 1945.

Bode, H. W., *Network Analysis and Feedback Amplifier Design;* New York, 1945.

James, H. M., Nichols, N. B., and Phillips, Ralph S., *Theory of Servomechanisms,* McGraw-Hill Book Company, Inc., New York, 1947.

Lauer, Henri, Lesnick, Robert, and Matson, Leslie F., *Servomechanism Fundamentals,* McGraw-Hill Book Company, Inc., New York, 1947.

Ahrendt, William R., and Taplin, John F., *Automatic Regulation,* Vol. I; August, 1947.

Seamans, R. C., Muzzey, C. L., Whitaker, H. P., *Determination of the Performance Operators of Army Attack Bomber,* A-26C No. 898, Tracking Control Progress Report No. 4, 1947.

Bromberg, B. G., *The Graphical Application of Fourier Series to Automatic Tracking Systems,* Thesis for Sc.D., M.I.T., 1947.

Rea, J. B., *Automatic Tracking Control of Aircraft,* Thesis for Sc.D., M.I.T., 1947.

Milliken, William F., Jr., *Progress in Dynamic Stability and Control Research,* Journal of the Aeronautical Sciences, Vol. 14, No. 9, p. 493, September, 1947.

Seamans, R. C., Wilkins, F. P., and Brainerd, H. B., *Application of Minneapolis-Honeywell Type C-1a Servopilot Components to Automatic Tracking Systems,* Tracking Control Progress Report No. 3, 1947.

Aerothermodynamic Design of Turbines for Aircraft Power Plants

JOHN E. TALBERT AND J. C. SMITH
Wright Aeronautical Corporation

SUMMARY

The great increase in activity in the aircraft gas-turbine field in recent years has focused attention on problems associated with the attainment of very high efficiency of the various turbine components. The expansion or turbine component has had its share of attention from many research and development engineers. Since design work is progressing at such a rapid rate, it is felt that it would be helpful for all concerned to pause at various points in the progress to summarize present knowledge, evaluate the progress thus far obtained, and enumerate the problems still confronting us. In this paper, the authors have tried to present their views of such a summary.

INTRODUCTION

ALTHOUGH THE AIRCRAFT GAS TURBINE is an outgrowth of the stationary gas turbine and steam turbine, it has peculiarities that make it a different and more sensitive animal. It differs from stationary turbine power plants mainly by the fact that extremely high cycle efficiencies must be obtained with a much lighter weight power plant than the stationary turbine types. This requirement has a pronounced effect upon the expansion unit of the turbine, because it means that the same amount of work must be accomplished with a fewer number of stages. For example, a two-stage aircraft turbine may operate with a pressure ratio of 5 to 1 or more, while a stationary turbine operating with the same pressure ratio may use eight or more stages. These fewer stages, must therefore, work a lot harder, which means that velocities or Mach Numbers, turning angles, tip speeds, and stresses must be much greater. Tip speeds of the order of 1,300 ft. per sec. are used as compared to 700 to 800 ft. per sec. for a stationary gas turbine. Velocities slightly over sonic in the first stator and near sonic in the remaining nozzles are required. Axial leaving velocities are usually above 600 ft. per sec. for the aircraft turbine, whereas they are usually below this figure for the stationary power plant. Rotor turning angles of the order of 135° are sometimes used in aircraft turbines, whereas those of stationary turbines are generally nearer 100°.

Blades are usually of the reaction type rather than the impulse type, such as generally used in a stationary turbine.

Received March 8, 1948. Based on a paper titled "Aero-Thermodynamic Aspects of Aircraft Turbine Expansion Unit Design," which was presented at the National Aircraft Propulsion Meeting, I.A.S., Cleveland, March 28, 1947.

The higher tip speeds, stresses, and lightweight construction usually require greater radial clearances than those obtained in a stationary power plant. This tends to increase leakage losses. The requirement for extremely high work per stage is usually so much greater compared to the tip speed allowed that the U/C is lower than that obtained in stationary turbine practice, and this means that the relative Mach Numbers entering the rotor blades are considerably higher. With such high Mach Numbers and the greater turning angles required, the design of the blade shape and passage for high efficiency is much more difficult.

The greater work per stage or fewer stages to do the same work means that the blade heights tend to increase at a faster rate than those for a stationary turbine, which introduces problems associated with flow over a rapid divergence of the inner and outer contours of the annulus. In order to keep this divergence from being too extreme, a tendency in aircraft turbine practice is to increase the axial velocity from the first to the last stage. Thus, the axial velocity leaving the last stage tends to be higher than it would be in a stationary turbine. These factors tend to make the last rotor blade of the aircraft gas turbine shorter than the blade for a comparable job in the stationary turbine, but, because it operates at a higher tip speed and does more work, the inlet temperature to it is greater. Therefore centrifugal, vibration, and bending stresses can be more critical.

Another characteristic peculiar to the aircraft gas turbine which makes it more difficult to design is the fact that it must be efficient under much more varied operating conditions than the stationary turbine. For instance, even at constant r.p.m. the aircraft turbine must operate under a great number of different altitudes and air-speed flight conditions. These changes in temperature, pressure, air speed, etc., result in a considerable variation in pressure ratio across the expansion unit at substantially the same engine r.p.m. Thus, a wide variation in Mach Number and in angle of attack on the blade is encountered, particularly when the number of stages has been held to a minimum.

As newer and better high-temperature materials are developed, it becomes possible to improve the gas-turbine cycle efficiency by increased combustion chamber outlet temperature. This tends to require air- or liquid-cooled rotor blades, which introduce compromises in blade shape and construction. The requirement for

low weight dictates short chord length of blades, which introduces Reynolds Number problems as well as difficulties in design of blade shapes.

All these differences peculiar to the aircraft turbine mean that knowledge gained from stationary turbine practice is only the beginning and that a great many problems remain to be solved in order to develop an aircraft turbine to its highest efficiency.

Design Procedure

(I) *Design Conditions and Assumptions*

Before beginning the design of the turbine expansion component, the following factors must be known: turbine expansion unit inlet temperature and pressure, weight flow, discharge static pressure, desired shaft output and turbine efficiency, maximum permissible wheel speed and maximum diameter, and r.p.m. range. From this preliminary information the designer can then determine the general dimensions and characteristics of the machine.

The number of stages should be kept as small as possible because of weight considerations but should not be so small as to affect markedly the efficiency. Pressure ratios per stage as high as 3:1 and 4:1 are now used without seriously lowering efficiency.

(II) *Velocity Diagram*

Having decided upon the number of turbine stages, the percentage of work done by each stage must be selected. In general, the first stages are designed for a greater amount of work than the later stages for the following reasons:

(a) Higher temperatures in the first stages permit higher velocities (more work) without exceeding Mach Number limitations.

(b) Aircraft turbines operate under widely varying pressure ratios. Since the incidence angles and Mach Numbers of the later stages are more affected by overall pressure ratio changes than the initial stages, the less work done in the later stages, the less will be the effect on overall power output under changed conditions.

(c) Work done in any stage is, in the final analysis, a function or rotor turning angle, and this angle should be kept smaller in the last stage to provide a low leaving velocity in a direction as close to axial as possible.

Because of these factors, the Mach Number for each nozzle is made less than that for the preceding nozzle.

In the design of most machines, the assumption is made that total energy of the fluid is constant, root to tip. With this assumption, several designs with respect to basic rotational airflow may be used, among which are:

(a) Free vortex, in which tangential components of absolute velocity vary inversely with radius from root to tip and axial velocity is constant at all radii.

(b) Constant mass flow per unit area at all points from root to tip (ρV_{axial} = constant). In this type of diagram the maximum Mach Numbers may be reduced for the same work.

(c) Solid rotation in which tangential components of absolute velocity vary directly as the radius from root to tip. In this type of diagram the axial velocity varies greatly from root to tip.

With the exception of the free vortex type, the calculation of a velocity diagram involves considerable trial and error, since the axial velocity is not constant root to tip. A radial pressure gradient is necessary in all types of diagram to balance the centrifugal forces arising from the absolute whirl velocities. For equal work root to tip, the velocity vectors at one radius, coupled with the centrifugal pressure gradient, determine the density and absolute velocity at any other radius. Since the absolute whirl component at any radius depends on the centrifugal pressure gradient, the axial velocity at any radius may be determined. All these velocities at both stator and rotor exit must be balanced so that the stage work root to tip is equal. Free vortex, though not necessarily the most efficient type of design, permits simple geometrical determination of all velocities at any radius, having established a particular velocity at a particular radius. The free vortex type of design has, therefore, been chosen as a basis for discussing design procedure.

Having decided upon the type of design, the vector diagram angles and velocities are calculated as follows:

(a) The approximate first stator nozzle area and blade height are determined by means of a conventional nozzle formula using the given weight flow, inlet pressure and temperature conditions, pressure ratio across the nozzle, and a stator exit nozzle angle. Maximum diameter ratios of the order of 0.85 are now in use. From the approximate first stator blade height, root and tip design radii that will be within the physical blade height dimensions are next selected.

(b) Since high pressure drop through the first stator is desirable for previously mentioned reasons, a stator root velocity close to sonic is assumed. The use of highly supersonic velocity, over 1.2 Mach Number, is undesirable, since a purely convergent nozzle is inefficient above this Mach Number and a convergent-divergent nozzle above this Mach Number has too critical performance under variations in operating conditions.

In order to determine Mach Number, the static enthalpy, H_{2s}, must of course be known and is determined from equation

$$H_{2s} = H_1 - (V^2/2gJ)$$

where H_1 is the stator entering total enthalpy, B.t.u. per lb., and V is the actual stator discharge velocity, ft. per sec. The value of H_{2s} thus calculated is valid for *any nozzle efficiency*, since any energy not converted into velocity must, from the energy conservation law, still exist in the form of heat (temperature). Having H_{2s}, the static temperature T_{2s} may be ascertained from tables,

such as *Thermodynamic Properties of Air* by Keenan and Kaye.

The discharge pressure required for generation of the desired velocity is a function of the nozzle efficiency and may be determined as follows:

$$H_{2TH} = H_1 - (V^2/2gJE)$$

where H_{2TH} is the theoretical discharge enthalpy and E is the assumed nozzle efficiency, which, for careful design, is close to 92 per cent. The pressure corresponding to this theoretical enthalpy is then determined from air tables or, more laboriously, by application of the adiabatic gas law.

(c) The work in each stage per pound of fluid is directly proportional to $U\Delta U$ where

U = rotor speed in ft. per sec at any diameter
ΔU = algebraic difference of tangential components of the rotor absolute entering and leaving velocities at the diameter in question

The sum of U and $\Delta U (U + \Delta U)$ forms the base of the velocity diagram at any diameter. (See velocity diagram of Fig. 1.) This base is also equal to the sum of the tangential component of the stator leaving velocity and the tangential component of the rotor relative leaving velocity. In the design calculations these two tangential velocity components are so proportioned that the rule of decreasing Mach Number for successive nozzles is maintained. At the same time, the axial velocity of the rotor is maintained equal to, or slightly greater than, the axial velocity in the stator. These factors determine the axial velocities in the stator and rotor and the angles leaving the stator and rotor and should not be allowed to result in a rotor relative inlet Mach Number greater than 0.70.

(d) The tip diagram is determined from the root diagram for a free vortex machine by use of the fact that axial velocity root to tip is a constant and $V_w r$ = constant, where

V_w = whirl or tangential component of absolute velocity
r = radius

(e) The static enthalpy and specific volume leaving the stator were found in (b) above. The static enthalpy and specific volume entering the rotor are the same as that leaving the stator, since the process of moving onto the wheel has not changed them.

(f) The static enthalpy leaving the rotor is determined from the fact that the difference in static enthalpy from entering to leaving conditions is equal to the energy difference represented by the squares of the relative velocities. As before, the static temperature is determined on an adiabatic basis directly from the static enthalpy and air tables, while the pressure is dependent upon the nozzle efficiency.

(g) Knowing the specific volume and *axial* velocity at root and tip sections and the weight flow required,

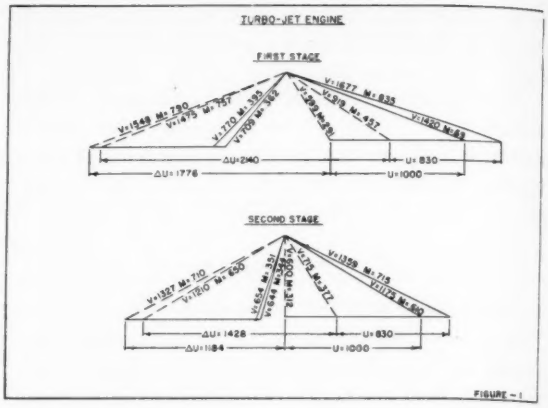

the *annular* area and blade height required at the stator and rotor exit is calculated by means of the continuity equation $W/A = V/\bar{v}$ (weight flow per unit area equals ratio of velocity to specific volume). In the same manner, using the same specific volumes but the *relative* exit velocities, the nozzle *throat* area required is calculated.

(h) The same process is followed in successive stages with velocities leaving the nozzles being assumed on the basis of decreasing Mach Number in each successive nozzle. Also the axial velocities are allowed to increase in order to keep the increase in blade height as small as possible.

(i) In the last stage of the machine an attempt is made to proportion the stator and rotor enthalpy drops so that the absolute discharge velocity is as nearly axial as possible, since the whirl component of this velocity is considered useless even in a jet machine.

(j) Fig. 1 shows the vector diagram of a free vortex-type turbine such as might be used to supply compressor power for a turbojet machine. For those interested, detailed calculations for this machine appear in the Appendix. It will be seen that the discharge velocity of the machine is not axial. The design, however, is based upon sea-level conditions, and the increase in overall pressure ratio resulting from operation at specified altitude is such that this velocity shifts to a nearly axial position.

(III) *Blade Profile Shape*

Having determined the required blade angles, root and tip, for both stator and rotor, the profile shapes that will most efficiently operate at these angles must be developed. As mentioned before, because of requirements that dictate high turning angles and Mach Number limits for stator and rotor exit and rotor inlet velocities most blades are of the reaction rather than the impulse type. Therefore, the remarks to follow apply more specifically to the reaction type blade.

The chord length of the blade must be sufficient to provide a Reynolds Number greater than 100,000 based

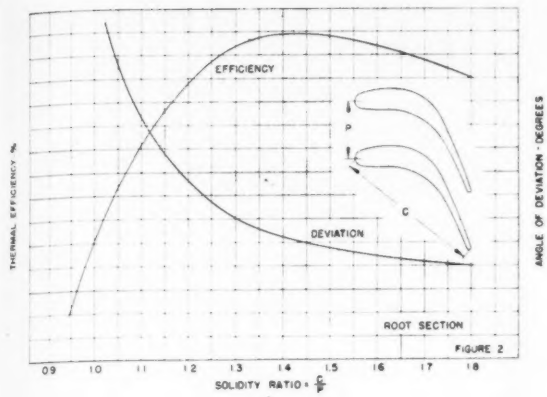

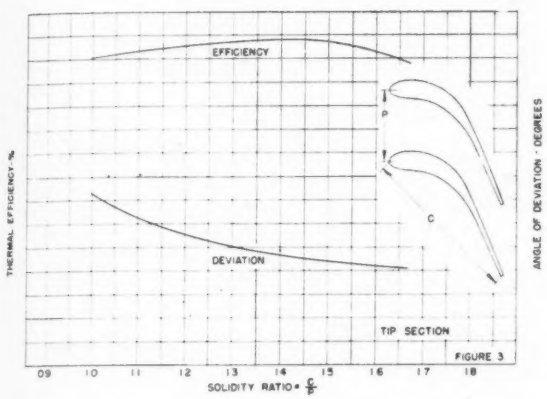

on fluid conditions at the blade passage exit. In addition, high turning-angle blades require correspondingly high chord lengths in order to provide a sufficiently generous radius of curvature for the channel walls. The so-called radius ratio of the curvature should be maintained so that the local Mach Number over the convex surface of the blade does not exceed the Mach Number at the blade passage exit, in order to prevent local diffusion or adverse pressure gradient, with losses and possibly separation.

The mean velocity in the channel should be constant or steadily increasing in order to avoid the possibility of diffusion in the passage. It is sometimes preferable to allow the air to diffuse ahead of the airfoil. This may be accomplished by a change in blade shape and use of a positive angle of incidence.

The solidity or chord pitch ratio has an optimum value, which appears to be a function of turning angle and chord length and, in general, lies between 1.2 and 1.7. Figs. 2 and 3 show the effect of solidity on efficiency and deviation for some typical turbine blades. Deviation is the angle by which the airflow leaving the blade does not follow the physical exit angle of the blade. These curves were obtained from the Wright Aeronautical stationary cascade test rig shown in Figs. 4 and 5. With this rig it is possible to obtain sonic velocities in the nozzles. To check the information obtained from this rig, tests are run on a rotating rig such as shown in Fig. 6. The stand incorporates a combustion chamber for supplying hot gas and steam ejectors to simulate altitude exhaust.

Trailing-edge thickness should not exceed 4 per cent of the blade pitch. Thick trailing edges result in high wake losses, which, in addition to reducing nozzle efficiency, may change the effective gas discharge angle.

The leading-edge contour should, in general, be elliptical. The theory that a blunt nose, though less sensitive to incidence angle changes, gives a lower peak efficiency has been fairly well established for isolated airfoils operated at low Mach Numbers. Tests of airfoils in cascade indicate that, for a given airfoil, there is an optimum nose shape, determinable by trial and error, which will provide both high peak efficiency and broad incidence angle range.

Slightly negative incidence angles appear to give better efficiency than zero or slightly positive angles. Considerable care must be used in the evaluation of incidence angle effects, since, if incidence angle is changed with no change in blade shape, air turning angle is also changed. Thus, a change in efficiency, though credited to an incidence angle effect, may in reality result from the accompanying change in air turning angle.

Stress and vibration factors influence the blade shape design especially for the rotor. For a given blade area at the tip section, the area at the root is sometimes dictated by the stresses due to centrifugal force. So also the center of gravity of the root section must be in nearly a radial line with the center of gravity of the tip section.

The permissible twist of the blade, root to tip, is dependent upon the twist forces and the stress they produce at various sections of the blade. In highly cambered blades, the choice of incidence angle is influenced considerably by the allowable twist.

(*IV*) *Miscellaneous Design Factors*

Radial clearances should be as low as possible, particularly at the outer diameter where fluid density is highest and where area per unit of clearance width is greatest. This clearance is at present held below 0.020 in. per in. of blade height. Axial clearance is not believed to be important and is usually held within the range of $^1/_4$ to $^1/_2$ in.

The shape of the inner and outer contours of the annulus should be such that a smooth and gradual increase of annular area is provided in order to ensure against breakaway and excessive boundary-layer thickness. Desired contour shape is obtained by minor adjustments of the individual nozzle Mach Numbers.

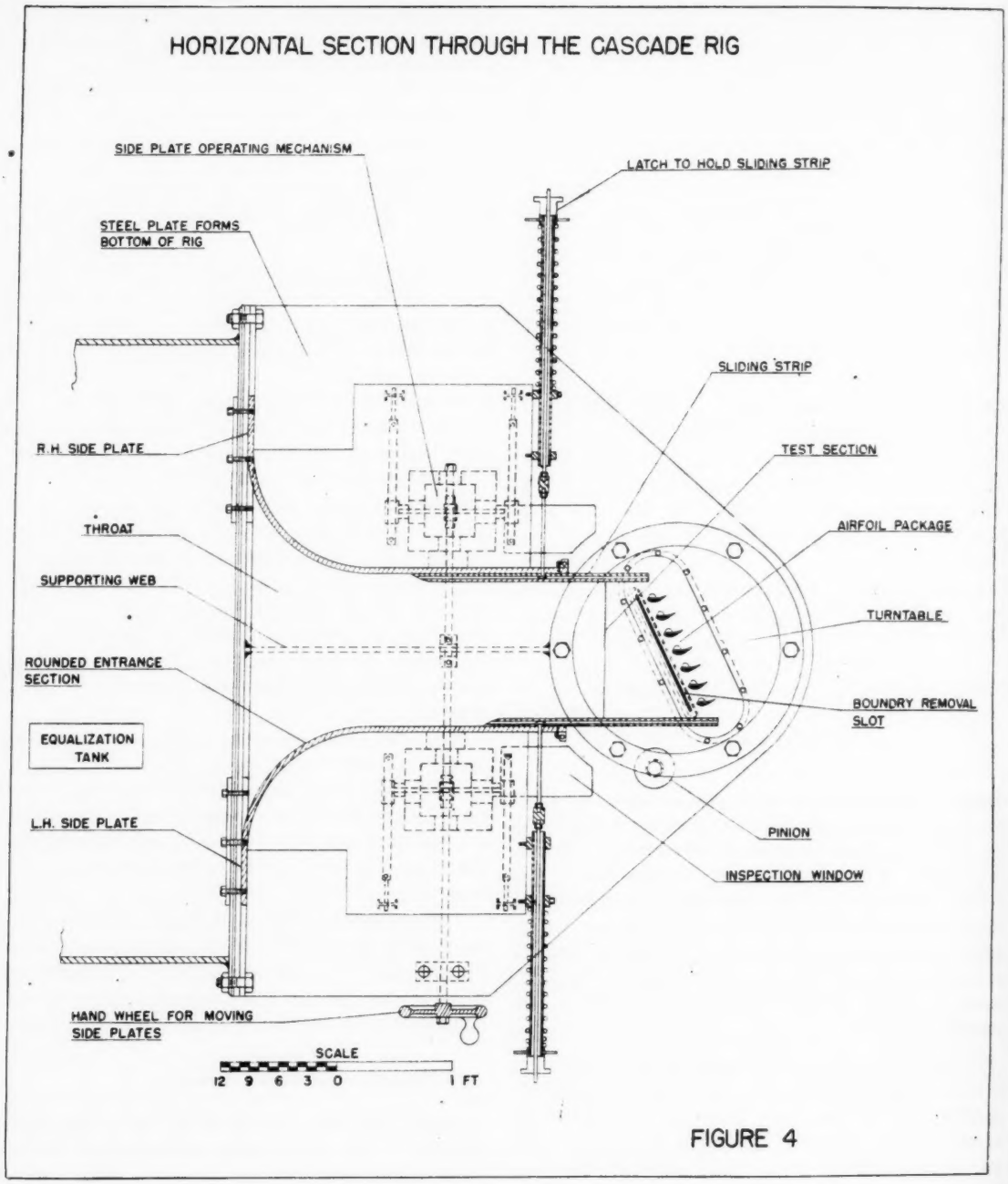

FIGURE 4

The turbine machine is designed for a particular altitude but must, in addition, perform satisfactorily at other altitudes. If turbine inlet conditions and exhaust pressure at any altitude are known, a valid performance calculation is possible. Unfortunately, the only method of obtaining such a calculation is the involved and laborious one of cut and try. Briefly, a weight flow is assumed, and the velocity in each successive nozzle is then determined by trial and error to satisfy the continuity equation $W/A = V/\bar{v}$. If the correct weight flow has been assumed, the velocities in the individual nozzles will have adjusted themselves to give the required discharge pressure at the last nozzle. If the required discharge pressure does not result from the calculation, a new weight flow involving new velocities must be assumed and the entire calculation repeated.

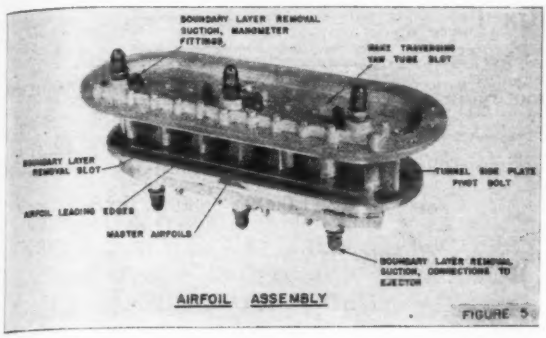
BOUNDARY LAYER REMOVAL SUCTION, MANOMETER FITTINGS
WAKE TRAVERSING TAW TUBE SLOT
BOUNDARY LAYER REMOVAL SLOT
TUNNEL SIDE PLATE PIVOT BOLT
AIRFOIL LEADING EDGES
MASTER AIRFOILS
BOUNDARY LAYER REMOVAL SUCTION, CONNECTIONS TO EJECTOR
AIRFOIL ASSEMBLY
FIGURE 5

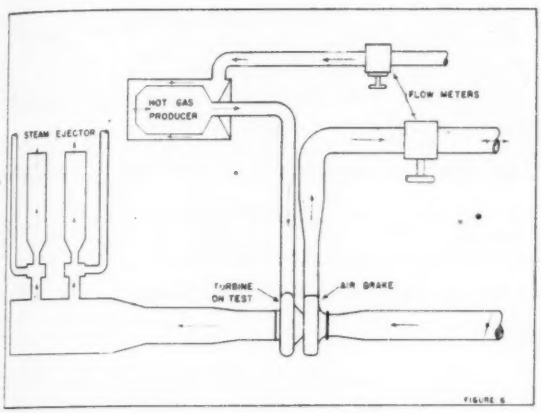

Unsolved Problems

A close study of the above design procedure indicates that there are many assumptions and "guesstimates" that still need to be accurately evaluated. One of the first of these problems is the analysis of the action of the boundary layer at the inside diameter (I.D.) and outside diameter (O.D.) of the blade annulus, as well as the action of the boundary layer on the blade itself. Its effect on the velocity vectors must be considerable and may mean that we do not obtain the velocity vector diagram that we calculate. When this effect is more completely evaluated, it may be possible to improve efficiency by revising the vector diagram to take account of it. For example, if the boundary layer at the I.D. of the stator blades reduces the weight flow of air through the sections near it, it must tend to increase weight flow and velocities at other sections. The question of how far up the blade this can influence the vector diagram is, as yet, unanswered.

The problem of obtaining high efficiency at high turning angles is a paramount one. Calculations indicate that wall-friction and trailing-edge wake losses may, with careful design, be kept reasonably low, and, thus, if a blade shape can be drawn which prevents breakaway and local shock, it would seem reasonable to expect to obtain high efficiencies with high turning angles.

In the selection of blade chord length and shape we encounter the problem of Reynolds Number or turbulence. In the case of the isolated airfoil as in an aircraft wing, the turbulence is stated as a Reynolds Number that is a function of chord length and free-stream velocity ahead of the airfoil. In the turbine case, we encounter a series of airfoils in cascade having a much greater velocity difference, entering to leaving, and a much more curved airfoil. In the design of such blades we are interested in obtaining a turbulence that will give us a low drag coefficient that will not vary appreciably under a great number of operating conditions.

The question of optimum incidence angle in a cascade of turbine blades is still unsettled. This angle is, of course, tied in closely with turning angle, blade shape, and passage area. For instance, a change of shape in more than the first 10 per cent of the chord of the blade in order to obtain a more negative angle of incidence may bring about a divergence in the passage area.

We encounter the problem of selecting the optimum leaving velocity from the blade for a given relative inlet velocity or Mach Number. In other words, is it better to accelerate more and increase the favorable pressure gradient at the expense of the possible increase in drag due to the increase in friction at the higher velocities? A corollary to this is the question of how much of the loss in a blade is due to the turning or the work done and how much is due to inlet velocity.

When designing a blade and passage we are faced with the problem of deviation of the air from the actual blade angles especially at the exit. We need to know more about the flow pattern that dictates this deviation, but, still further, we must apply corrections such as overturning of the blade for this deviation in order to be sure to get the work done. However, overturning actually reduces the physical throat area, and, if throat Mach Numbers are already close to one, a reduction in weight flow will be involved unless the blade height is increased. This blade height change means a lower axial velocity after the blade and thus affects our velocity diagram.

More must be learned of blade vibration and damping resulting from aerodynamic forces, because the vibration stress adds to the centrifugal stresses and helps dictate the relation of blade thickness at the root compared with that at the tip section. This, in turn, prescribes a relation of the blade shape at the root to the blade shape at the tip. Solutions are desired to stress problems involving the allowable relative twist of the blade root to tip, since such twist helps govern the angle of incidence of the blade at the root for a given angle of incidence at the tip.

Appendix I

HYPOTHETICAL 4,000-LB. THRUST TURBOJET ENGINE. DETAILED CALCULATIONS FOR VECTOR DIAGRAM VELOCITIES AND NOZZLE AREAS

Initial conditions, sea-level operation, 4,000-lb. thrust turbojet engine:

Airplane speed	= 0 mph. (take-off conditions)
Turbine inlet temperature	= 1,500°F.
Turbine inlet pressure (total)	= 179.3 in. Hg
Turbine weight flow	= 70 lbs. per sec.
Turbine r.p.m.	= 7,800
Assumed nozzle efficiency	= 92 per cent
Required turbine output	= 11,720 hp.
Maximum allowable turbine diameter	= 32 in.

Nomenclature

V	= velocity, ft. per sec.
T	= temperature, °R.
H	= actual enthalpy, B.t.u. per lb.
H'	= theoretical enthalpy, B.t.u. per lb.
ΔH	= actual enthalpy change, B.t.u. per lb.
$\Delta H'$	= theoretical enthalpy change, B.t.u. per lb.
$\bar{v}$	= specific volume, cu.ft. per lb.
P	= pressure, in. of mercury absolute
PR	= relative pressure, as used in Keenan and Kaye's *Thermodynamic Properties of Air*
W	= weight flow, lbs. per sec.
A	= area, sq.ft.
a	= area, sq.in.
U	= rotor speed, ft. per sec.
ΔU	= vector sum of tangential components of rotor entering and leaving velocities

Determination of Root and Tip Design Radii

Choose a rotor tip speed of 1,000 ft. per sec. Then, tip radius

$$R_{tip} = \frac{U}{2\pi}\left(\frac{60}{\text{r.p.m.}}\right) = \frac{1{,}000}{2\pi}\left(\frac{60}{7{,}800}\right) = 1.222 \text{ ft.} = 14.70 \text{ in.}$$

Assuming critical flow conditions at first stator nozzle throat, determine required area from standard nozzle flow formula:

$$a = \frac{W\sqrt{T_{inlet}}}{P_{inlet}}(3.82) = \frac{(70)\sqrt{1{,}960}}{179.3}(3.82) = 66 \text{ sq.in.}$$

Assume an average nozzle angle of 18°. Then

$$\text{annular area} = \frac{\text{throat area}}{\sin 18°} = \frac{66}{0.3090} = 213.5 \text{ sq.in.}$$

$$\text{root radius} = \sqrt{R_{tip}^2 - \frac{A}{\pi}} = \sqrt{14.7^2 - \frac{213.5}{\pi}} = 12.21 \text{ in.}$$

$$U_{root} = \frac{12.21}{14.7}(1{,}000) = 830 \text{ ft. per sec.}$$

From the formula

$$U\Delta U = HP(550g)/W$$

determine the quantity $U\Delta U$. Thus,

$$U\Delta U, \text{ total root} = \frac{11{,}720 \times 550 \times 32.17}{70} = 2{,}960{,}000$$

Assume a work distribution of 60 per cent first stage and 40 per cent second stage. Then,

$$U\Delta U \text{ first stage, root} = 0.60 \times 2{,}960{,}000 = 1{,}776{,}000$$

$$\therefore \Delta U_{tip} = 1{,}776{,}000/1{,}000 = 1{,}776$$

Assuming equal work root and tip,

$$\Delta U_{root} = 1{,}776{,}000/830 = 2{,}140$$

Then,

$$U_{root} + \Delta U_{root} = 830 + 2{,}140 = 2{,}970$$

The total base length of the vector diagram, which is always equal to $U + \Delta U$, is thus determined for the first stage.

In order to provide for decreasing Mach Number through the machine, the diagram base is so divided that the right-hand side, which is actually the tangential component of stator discharge velocity, is slightly greater than the left-hand side. A right-hand side length equal to 54 per cent of the total base length is ordinarily used. Thus,

$$V_{1\,root\,tan} = 0.54 \times 2{,}970 = 1{,}601 \text{ ft. per sec.}$$

Try $V_{axial} = 500$ ft. per sec. Then,

$$\tan \alpha_{root} = 500/1{,}601 = 0.312, \qquad \alpha_{root} = 17.3°$$

Since 18° was chosen for an approximate average nozzle angle and since root angle is always smaller than average angle, the values of 500 ft. per sec. and 17.3° α_{root} are satisfactory. Then,

$$V_{1\,root} = \sqrt{1601^2 + 500^2} = 1{,}677 \text{ ft. per sec.}$$

Having determined the first stator root absolute velocity and the axial and tangential components thereof, the remaining vector diagram calculations are set down in tabular form.

Turbine Entrance Conditions

Turbine entering enthalpy = H_3 = 398.47 root and tip; corresponding relative pressure, PR_3 = 332.2

(from air tables and the given inlet temperature of 1,500°F.).

Diagram Velocities and Enthalpy Drops

(A) First Stage. Root—First Stator:

V_1 = 1,677 ft. per sec. (as determined previously, $M_n = 0.835$)
$\Delta H = (1{,}677/223.7)^2 = 56.17$
$\Delta H' = 56.17/0.92 = 61.10$ B.t.u. per lb.
$H_4 = 398.47 - 56.17 = 342.30$ ($T_4 = 1{,}755$°R., $PR_4 = 213.60$)
$H_4' = 398.47 - 61.1 = 337.37$ ($PR_4' = 204.99$)
$P_4 = (204.99/332.2)179.3 = 110.8$ in. Hg
$\bar{v}_4 = 0.755(1{,}755/110.8) = 11.98$ cu.ft. per lb.
$V_1 \text{rel} = \sqrt{(1{,}601 - 830)^2 + 500^2} = 919$

Root—First Rotor:

$V_{\text{axial}} = 550$ ft. per sec.
$V_2 \text{ rel tan} = U + \Delta U - V_1 \text{ abs tan} = 2{,}970 - 1{,}601 = 1{,}369$
$V_2 \text{ rel} = \sqrt{1{,}369^2 + 550^2} = 1{,}475$ ft. per sec.
$\Delta H = (1{,}475/223.7)^2 = 43.5$
$H_5 = 342.3 + (919/223.7)^2 - 43.5 = 359.13 - 43.5 = 315.63$
$T_5 = 1{,}656$°R. ($PR_5 = 169.98$)
$\Delta H' = 43.5/0.92 = 47.3$
$H_5' = 359.13 - 47.3 = 311.83$ ($PR_5' = 164.40$)
$P_5 = (164.4/213.6)\ 110.8 = 85.3$ in. Hg
$\bar{v}_5 = 0.755\ (1{,}656/85.3) = 14.68$ cu.ft. per lb.
$V_2 \text{ abs} = \sqrt{(1{,}369 - 830)^2 + 550^2} = 770$

Tip—First Stator:

$$V_1 \tan = \frac{R_{\text{root}}}{R_{\text{tip}}}\ (V_1)\ \tan_{\text{root}} = \left(\frac{12.21}{14.71}\right) 1{,}601 = 1{,}329$$

$V_1 = \sqrt{1{,}329^2 + 500^2} = 1{,}420$ ft. per sec.
$\Delta H = (1{,}420/223.7)^2 = 40.30$
$H_4 = 398.47 - 40.3 = 358.17$ ($T_4 = 1{,}813$, $PR_4 = 243.25$)
$\Delta H' = 40.3/0.92 = 43.8$
$H_4' = 398.47 - 43.8 = 354.67$ ($PR_4' = 236.45$)
$P_4 = (236.45/332.2)\ 179.3 = 127.7$ in. Hg
$\bar{v}_4 = 0.755\ (1{,}813/127.7) = 10.74$ cu.ft. per lb.
$V_1 \text{ rel} = \sqrt{(1{,}329 - 1{,}000)^2 + 500^2} = 599$

Tip—First Rotor:

$V_{\text{axial}} \text{ tip} = V_{\text{axial}} \text{ root} = 550$ ft. per sec.
$V_2 \text{ rel tan} = U + \Delta U - V_1 \text{ abs tan} = 1{,}000 + 1{,}776 - 1{,}329 = 1{,}447$
$V_2 \text{ rel} = \sqrt{1{,}447^2 + 550^2} = 1{,}548$ ft. per sec.
$\Delta H = (1{,}548/223.7)^2 = 47.9$
$H_5 = 358.17 + (599/223.7)^2 - 47.9 = 365.34 - 47.9 = 317.44$
$T_5 = 1{,}663$°R. ($PR_5 = 172.72$)
$\Delta H' = 47.9/0.92 = 52.0$
$H_5' = 365.34 - 52.0 = 313.34$ ($PR_5' = 166.62$)
$P_5 = (166.62/243.25)\ 127.7 = 87.4$
$\bar{v}_5 = 0.755\ (1{,}663/87.4) = 14.38$ cu.ft. per lb.
$V_2 \text{ abs} = \sqrt{(1{,}447 - 1{,}000)^2 + 550^2} = 709$

(B) Second Stage. Root—Second Stator:

$U\Delta U = 2{,}960{,}000 - 1{,}776{,}000 = 1{,}184{,}000$
$\Delta U = 1{,}184{,}000/830 = 1{,}428$
$U + \Delta U = 830 + 1{,}428 = 2{,}258$
right-hand side $= 0.54 \times 2{,}258 = 1{,}219$
$V_{\text{axial}} = 600$ ft. per sec.
$V_1 = \sqrt{1{,}219^2 + 600^2} = 1{,}359$
$\Delta H = (1{,}359/223.7)^2 = 36.9$
$\Delta H' = 36.9/0.92 = 40.1$
$H_6 = 315.63 + (777/223.7)^2 - 36.9 = 327.68 - 36.9 = 290.78$
$T_6 = 1{,}564$°R. ($PR_6 = 135.75$)
$H_6' = 327.68 - 40.1 = 287.58$ ($PR_6' = 131.70$)
$P_6 = (131.70/169.98)85.3 = 66.0$
$\bar{v}_6 = 0.755(1564/66.0) = 17.9$
$V_1 \text{ rel} = \sqrt{(1{,}219 - 830)^2 + 600^2} = 715$

Root—Second Rotor:

$V_{\text{axial}} = 620$ ft. per sec.
$V_2 \text{ rel tan} = 2{,}258 - 1{,}219 = 1{,}039$
$V_2 \text{ rel} = \sqrt{1{,}039^2 + 620^2} = 1{,}210$
$\Delta H = 1{,}207/223.7 = 29.1$
$H_7 = 290.78 + (715/223.7)^2 - 29.1 = 301.01 - 29.1 = 271.91$
$T_7 = 1{,}493$°R. ($PR_7 = 113.40$)
$\Delta H' = 29.1/0.92 = 31.7$
$H_7' = 301.01 - 31.7 = 269.31$ ($PR_7' = 110.50$)
$P_7 = (110.50/135.75)66.0 = 53.8$
$\bar{v}_7 = 0.755(1{,}493/53.8) = 21.00$ cu.ft. per lb.
$V_2 \text{ abs.} = \sqrt{(1{,}039 - 830)^2 + 620^2} = 654$

Tip—Second Stator:

$V_1 \tan = (12.21/14.71)\ 1{,}219 = 1{,}010$
$V_1 = \sqrt{1{,}010^2 + 600^2} = 1{,}175$
$\Delta H = (1{,}175/223.7)^2 = 27.55$
$H_6 = 317.44 + (709/223.7)^2 - 27.55 = 327.51 - 27.55 = 299.96$
$T_6 = 1{,}598$°R. ($PR_6 = 147.75$)
$\Delta H' = 27.55/0.92 = 29.9$
$H_6' = 327.51 - 29.9 = 297.61$ ($PR_6' = 144.60$)
$P_6 = (144.60/172.72)87.4 = 73.1$

$\bar{v}_6 = 0.755\ (1{,}598/73.1) = 16.5$

V_1 rel $= \sqrt{(1{,}010 - 1{,}000)^2 + 600^2} = 600.1$

Tip—Second Rotor:

$V_{axial} = 620$

V_2 rel tan $= U + \Delta U - V_1$ abs tan $= 1{,}000 + (1{,}184{,}000/1{,}000) - 1010 = 1{,}174$

V_2 rel $= \sqrt{1{,}174^2 + 620^2} = 1{,}327$

$\Delta H = (1{,}327/223.7)^2 = 35.2$

$H_7 = 299.96 + (600.1/223.7)^2 - 35.2 = 307.15 - 35.2 = 271.95$

$T_7 = 1{,}493°\text{R.}\ (PR_7 = 113.40)$

$\Delta H' = 35.2/0.92 = 38.3$

$H_7' = 307.15 - 38.3 = 268.85\ (PR_7' = 110.01)$

$P_7 = (110.01/147.75)\ 73.1 = 54.5$

$\bar{v}_7 = 0.755(1{,}493/54.5) = 20.7$ cu.ft. per lb.

V_2 abs $= \sqrt{(1{,}174 - 1{,}000)^2 + 620^2} = 644$

Overall Efficiency. Root:

actual overall pressure ratio $= 179.3/53.8 = 3.33$

PR_7' overall $= PR_3/3.33 = 332.2/3.33 = 99.8$

H'_7 overall $= 259.13$

$\Delta H'$ overall $= H_3 - H_7'$ overall $= 398.47 - 259.13 = 139.34$

$U\Delta U = 2{,}960{,}000$

$$E = \frac{2U\Delta U/2gJ}{\Delta H' - (V_{LV}/223.7)^2} = \frac{118.30}{139.34 - (654/223.7)^2} = 118.3/130.79 = 0.91$$

Tip:

actual overall pressure ratio $= 179.3/54.9 = 3.261$

PR_7' overall $= PR_3/3.261 = 332.2/3.261 = 101.8$

H_7' overall $= 261.0$

$\Delta H'$ overall $= H_3 - H_7'$ overall $= 398.47 - 261.0 = 137.47$

$U\Delta U = 2{,}960{,}000$

$$E = \frac{2U\Delta U/2gJ}{\Delta H' - (V_{LV}/223.7)^2} = \frac{118.3}{137.47 - (644/223.7)^2} = 118.3/129.8 = 0.915$$

Calculation of Annular Area

To calculate the annular area required to pass the design weight flow, the basic continuity equation is used. This is: $Q = AV$, $W\bar{v} = AV$, or $W/A = V/\bar{v}$.

In averaging the W/A for the entire nozzle, the values for the two sections considered are weighted in direct proportion to the magnitude of the radii at which the sections are located. This is done because of a fixed annular height; the area of an annulus increases directly with the radius. Thus,

$$\left(\frac{W}{A}\right)_{average} = \frac{(V_R/\bar{v}_R)R_R + (V_T/v_t)R_t}{R_R + R_t}$$

$$A = \frac{W(R_R + R_t)}{(V_R/\bar{v}_R)R_R + V_t/v_t)R_t}$$

For first stator:

$$a \text{ annular} = \frac{70(12.21 + 14.7) \times 144}{(500/11.98)12.21 + (500/10.74)14.7} = 227.0 \text{ sq.in.}$$

For first rotor:

$$a \text{ annular} = \frac{70(12.21 + 14.7) \times 144}{(550/14.68)12.21 + (550/14.38)14.7} = 265.9 \text{ sq. in.}$$

For second stator:

$$a \text{ annular} = \frac{70(12.21 + 14.7) \times 144}{(600/17.9)12.21 + (600/16.5)14.7} = 287.0 \text{ sq.in.}$$

For second rotor:

$$a \text{ annular} = \frac{70(12.21 + 14.7) \times 144}{(620/21.0)12.21 + (620/20.7)14.7} = 338.0 \text{ sq.in.}$$

Having established the required annular areas, the blade heights required are easily determined. Blade entrance and exit angles are obtained from the vector diagram, using proper correction factors for deviation of air flow from the physical angles. The amount of correction depends upon the characteristics of the particular blade shape involved.

The Aerodynamic Forces on an Oscillating Flap at Supersonic Speeds

JOHN W. MILES*

University of California at Los Angeles

SUMMARY

Using the general results developed in an earlier paper, the complex flutter coefficients A_{bh} (hinge moment due to plunging), $A_{b\alpha}$ (hinge moment due to pitching), $A_{c\beta}$ (lift due to flapping), $A_{a\beta}$ (pitching moment coefficient due to flapping), and $A_{e\beta}$ (hinge moment coefficient due to flapping) are found. All of these coefficients are expressed in terms of the previously known coefficients $A_{a\alpha}$, A_{ah}, $A_{c\alpha}$, and A_{ch}. Numerical results are given in the form of curves for $M = 1.2$, 1.4, 1.6, and 2.0, the real and imaginary parts of the coefficients being plotted vs. k for a range of $k = 0$ to 1.4. In the case of $A_{a\beta}$, $A_{b\beta}$, and $A_{c\beta}$, the results are applicable to any flap, while the numerical results for $A_{b\alpha}$ and A_{bh} are given for a 50 per cent chord flap.

NOTATION

- a_s = amplitude of sth degree of freedom
- b = semichord of airfoil
- c = fraction of semichord of the flap hinge aft of the mid-chord
- h = plunging motion
- j = $(-1)^{1/2}$ = imaginary unit
- k = $(\omega b/U)$ = reduced frequency
- k' = $[(1 + c)/2]k$
- p = pressure (gage)
- t = time
- x, z = airfoil coordinates
- A_{rs} = dimensionless flutter coefficient giving force in rth degree of freedom due to motion in sth degree of freedom
- $G(v)$ = Green's function; cf. Eq. (10)
- J_0 = Bessel function, first kind, zero order
- L = lift
- M = Mach Number; also mid-chord stalling moment
- U = free-stream velocity
- α = angle of attack
- β = $(M^2 - 1)^{1/2}$ in. Eqs. (4), (5), (6), (7), (10); otherwise denotes flap deflection
- ω = angular frequency of harmonic motion

INTRODUCTION

IN AN EARLIER PAPER[1] the Green's function giving the pressure on an airfoil in a supersonic stream due to an arbitrary harmonic velocity distribution was derived. The result was utilized to find the lift and mid-chord pitching moment due to plunging and pitching motions and, later,[2] to find the response of an airfoil entering a sharp edged gust or to a sudden change in angle of attack or flap deflection. The present paper will extend the results to include the forces on an oscillating flap, because of both its own motion and the motions of the airfoil as a whole. The notation and assumptions, namely, small perturbations, the specification of the velocity at the mean location of the airfoil, and two-dimensional flow are the same as in reference 1.

Received October 12, 1947.

* Assistant Professor of Engineering, Department of Engineering.

VELOCITY DISTRIBUTIONS

The motions of the airfoil due to plunging (h) and pitching (α) about the mid-chord are defined by Eqs. (17) and (18) of reference 1; to these a third motion, elevon flapping (β), will be added. The displacements in these three modes of motion are described by

$$z_h(x, t) = a_h b e^{j\omega t} \tag{1}$$

$$z_\alpha(x, t) = -a_\alpha b x e^{j\omega t} \tag{2}$$

$$z_\beta(x, t) = -a_\beta b(x - c)e^{j\omega t}, \quad x > c \tag{3}$$

$$= 0, \quad x < c$$

The positive displacements in these modes are illustrated in Fig. 1.

FLUTTER COEFFICIENTS

The lift, mid-chord stalling moment, and hinge moment (positive when acting to increase β) due to the motion $z_s(t)$ are given by

$$L_s(t) = \left(\frac{\pi\rho b^3\omega^2}{\beta}\right) a_s e^{j\omega t} A_{cs} = -2\int_{-1}^{1} p_s(x, t)dx \tag{4}$$

$$M_s(t) = \left(\frac{\pi\rho b^4\omega^2}{\beta}\right) a_s e^{j\omega t} A_{as} = 2\int_{-1}^{1} x p_s(x, t)dx \tag{5}$$

$$N_s(t) = \left(\frac{\pi\rho b^4\omega^2}{\beta}\right) a_s e^{j\omega t} A_{bs} = 2\int_{c}^{1} (x - c) p_s(x, t)dx \tag{6}$$

and are nondimensionally described by the flutter coefficients A_{rs}.

In deriving the flutter derivatives it is convenient to express the pressure distribution in the form

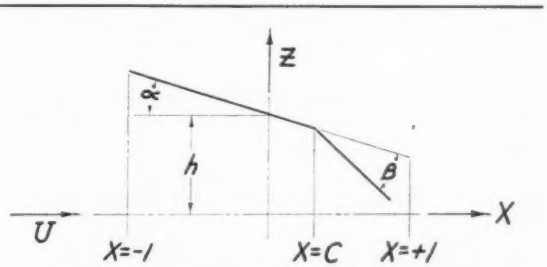

FIG. 1. Flat plate airfoil with flap

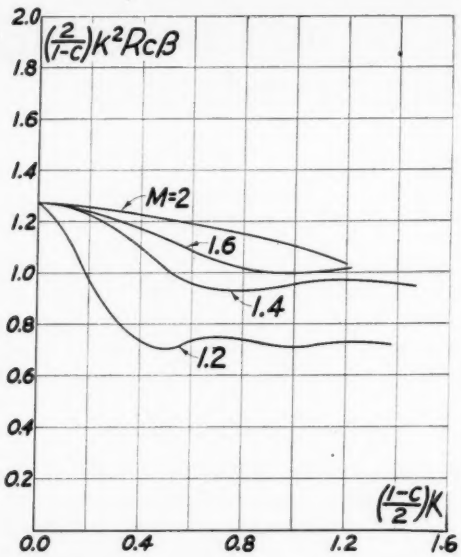

FIG. 2. $[2/(1 - c)]k^2R_{c\beta}$ vs. $[(1 - c)/2]k$.

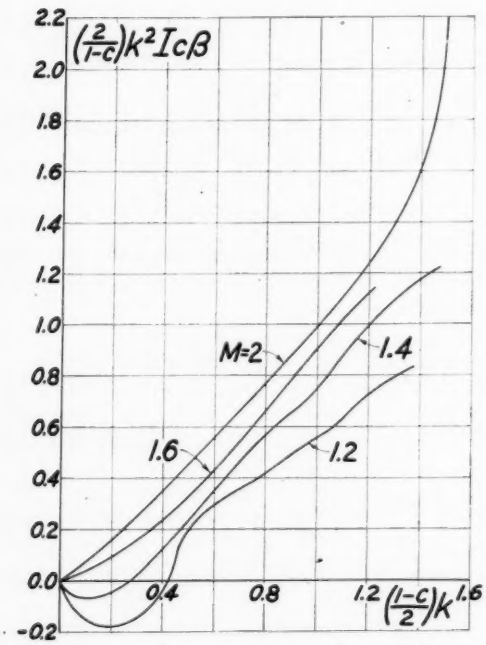

FIG. 3. $[2/(1 - c)k^2I_{c\beta}$ vs. $[(1 - c)/2]k$.

$$p_s(x, t) = \left(\frac{j\omega\rho U}{\beta}\right) a_s e^{j\omega t} \bar{p}_s[k(x + 1)] \qquad (7)$$

where $\bar{p}_s$ is a nondimensional distribution in the variable $k(x + 1)$. From Eqs. (12), (20), and (21) of reference 1 it is found that

$$\bar{p}_h(ku) = G(ku) + j\int_0^{ku} G(v)dv \qquad (8)$$

$$\bar{p}_a(ku) = \left(1 + \frac{j}{k}\right)\bar{p}_h(ku) - \frac{1}{k}\int_0^{ku} p_h(v)dv \qquad (9)$$

$$G(v) = e^{-j(M/\beta)^2 v} J_0[(M/\beta^2)v] \qquad (10)$$

where $(x + 1)$ has been replaced by u.

Introducing Eq. (7) in Eqs. (4)–(6), the flutter coefficients may be rewritten

$$A_{cs}(k, M) = -\frac{2j}{\pi k}\int_0^2 \bar{p}_s(ku)du \qquad (11)$$

$$A_{as}(k, M) = \frac{2j}{\pi k}\int_0^2 (u - 1)\bar{p}_s(ku)du \qquad (12)$$

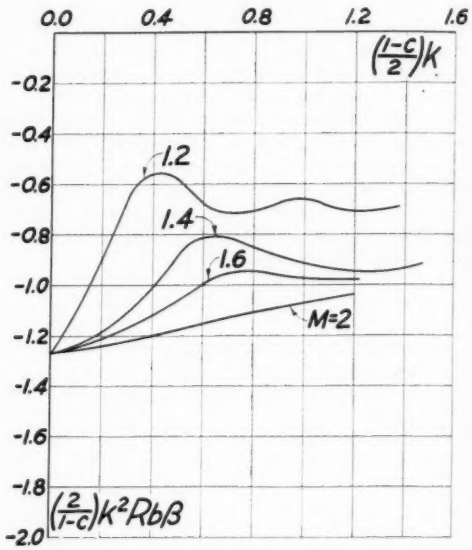

FIG. 4. $[2/(1 - c)]^2R_{b\beta}$ vs. $[(1 - c)/2]k$.

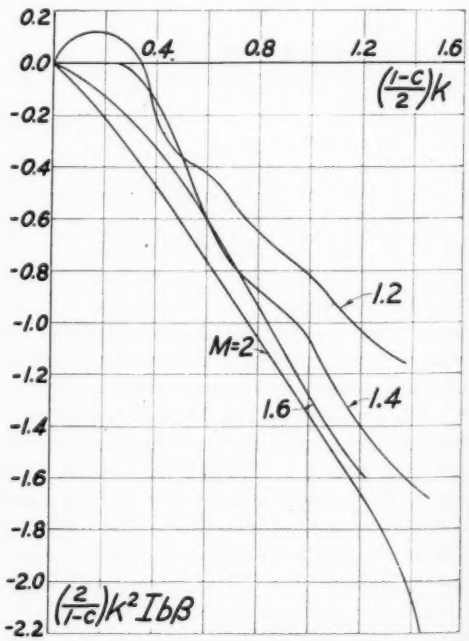

FIG. 5. $[2/(1 - c)]^2I_{b\beta}$ vs $[(1 - c)/2]k$.

$$A_{bs}(k, M, c) = \frac{2j}{\pi k}\int_{(1+c)}^{2}(u - 1 - c)\bar{p}_s(ku)du \quad (13)$$

The last coefficient may be rewritten

$$A_{bs}(k, M, c) = A_{as}(k, M) + cA_{cs}(k, M) + A'_{bs}(k, M, c) \quad (14)$$

$$A'_{bs}(k, M, c) = \left(\frac{1+c}{2}\right)^3\left(\frac{2j}{\pi k'}\right)\int_{1}^{2}(2 - w)\bar{p}_s(k'w)dw \quad (15)$$

$$k' = [(1 + c)/2]k \quad (16)$$

where the change of variable $w = [2/(1 + c)]u$ has been introduced in the integral of Eq. (15).

In the case where $s = h$, it may be observed from Eqs. (8) and (9) that $\bar{p}_h$ is a function of the single variable kv for any k (but for fixed M), whereas $\bar{p}_\alpha$ is a function of both ku and k. Thus, letting $s = h$ in Eqs. (11), (12), and (15), it follows directly that

$$A'_{bh}(k, M, c) = -\left(\frac{1+c}{2}\right)^3\left[A_{ah}\left(\frac{1+c}{2}k, M\right) + A_{ch}\left(\frac{1+c}{2}k, M\right)\right] \quad (17)$$

To evaluate $A'_{b\alpha}$, Eq. (9) may be substituted in Eq. (15) to obtain

$$A'_{b\alpha}(k, M, c) = \left(1 + \frac{j}{k}\right)A'_{bh}(k, M, c) + \left(\frac{1+c}{2}\right)^4\left(\frac{2j}{\pi k'}\right)\left(\frac{1}{k'}\right)\int_{1}^{2}(w - 2)dw\int_{0}^{k'w}\bar{p}_h(v)dv \quad (18)$$

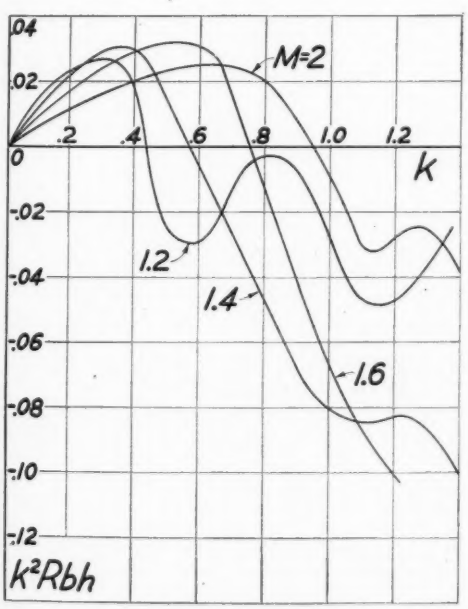

FIG. 6. k^2R_{bh} vs. k, $c = 0$.

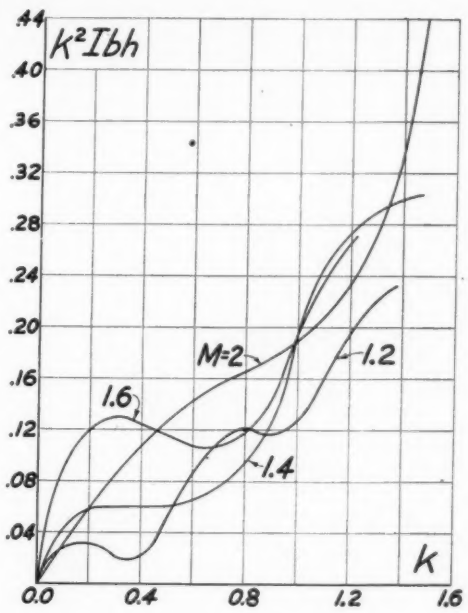

FIG. 7. k^2I_{bh} vs. k, $c = 0$.

Now from Eqs. (9), (11), and (12), it is found that

$$A_{a\alpha}(k, M) + A_{c\alpha}(k, M) = \left(1 + \frac{j}{k}\right)[A_{ah}(k, M) + A_{ch}(k, M)] - \left(\frac{2j}{\pi k}\right)\left(\frac{1}{k}\right)\int_{1}^{2}(u - 2)du\int_{0}^{ku}\bar{p}_h(v)dv \quad (19)$$

Comparing Eqs. (17), (18), and (19) yields the result:

$$A'_{b\alpha}(k, M, c) = \left(\frac{1-c}{2}\right)A'_{bh}(k, M, c) - \left(\frac{1+c}{2}\right)^4 \times \left[A_{a\alpha}\left(\frac{1+c}{2}k, M\right) + A_{c\alpha}\left(\frac{1+c}{2}k, M\right)\right] \quad (20)$$

Substituting Eqs. (18) and (20) in Eq. (14) yields the desired coefficients:

$$A_{bh}(k, M, c) = A_{ah}(k, M) + cA_{ch}(k, M) - \left(\frac{1+c}{2}\right)^3\left[A_{ah}\left(\frac{1+c}{2}k, M\right) + A_{ch}\left(\frac{1+c}{2}k, M\right)\right] \quad (21)$$

$$A_{b\alpha}(k, M, c) = A_{a\alpha}(k, M) + cA_{c\alpha}(k, M) - \left(\frac{1-c}{2}\right)\left(\frac{1+c}{2}\right)^3\left[A_{ah}\left(\frac{1+c}{2}k, M\right) + A_{ch}\left(\frac{1+c}{2}k, M\right)\right] - \left(\frac{1+c}{2}\right)^4 \times \left[A_{a\alpha}\left(\frac{1+c}{2}k, M\right) + A_{c\alpha}\left(\frac{1+c}{2}k, M\right)\right] \quad (22)$$

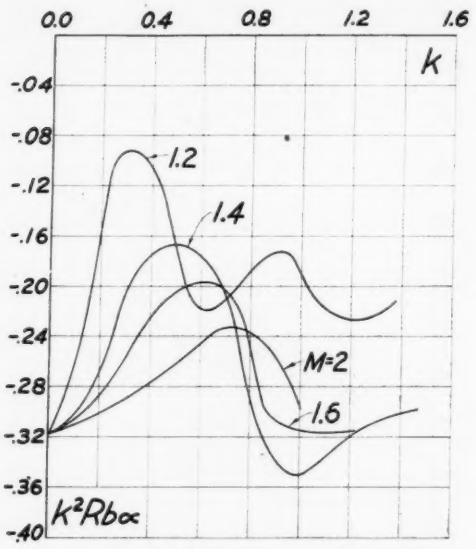

FIG. 8. $k^2R_{b\alpha}$ vs. k, $c = 0$.

FORCE AND MOMENT DUE TO OSCILLATING FLAP

In computing the forces due to the motion of an oscillating flap, as described by Eq. (3), it may be concluded immediately (since the flow is supersonic) that the pressure distribution due to the motion vanishes except over the flap itself. It follows that the forces due to an oscillating flap are analogous to those due to an oscillating (in pitch) airfoil of chord $[(1 - c)/2]2b$, differing only in the fact that the rotation of the flap and the desired hinge moment are about the leading edge, whereas these quantities were computed with respect to the mid-chord in the case of the pitching airfoil. It therefore follows directly that

$$\left(\frac{2}{1-c}\right)^3 A_{c\beta}(k, M, c) = A_{c\alpha}\left(\frac{1-c}{2}k, M\right) - A_{ch}\left(\frac{1-c}{2}k, M\right) \quad (23)$$

$$\left(\frac{2}{1-c}\right)^4 A_{b\beta}(k, M, c) = A_{a\alpha}\left(\frac{1-c}{2}k, M\right) - A_{ah}\left(\frac{1-c}{2}k, M\right) - \left(\frac{2}{1-c}\right)^3 A_{c\beta}(k, M, c) \quad (24)$$

where the factor of $[(1 - c)/2]^3$ enters in Eq. (23) because b^3 enters the nondimensionalizing coefficient in Eq. (4), where $[(1 - c)/2]^4$ enters in Eq. (24) because of b^4 in Eq. (5), and where $[(1 - c)/2]k$ is used because k is defined in terms of b.

The remaining coefficient $A_{a\beta}$, giving the pitching moment due to flapping, is given by

$$A_{a\beta}(k, M, c) = A_{b\beta}(k, M, c) - cA_{c\beta}(k, M, c) \quad (25)$$

as may be seen from Eqs. (11)–(13).

NUMERICAL RESULTS

The coefficients A_{rs} are conveniently broken into their real and imaginary parts, viz:

$$A_{rs} = R_{rs} + jI_{rs} \quad (26)$$

Using the results of reference 1, the real and imaginary parts of the above flutter coefficients are plotted in Figs. 2–9. The coefficients $R_{b\beta}$, $I_{b\beta}$, $R_{c\beta}$, and $I_{c\beta}$ are plotted so that the results are valid for all values of c, while those for the remaining coefficients are plotted only for $c = 0$, corresponding to a 50 per cent chord flap. The results for other values of c are easily obtained from the results of references 1 or 3 and from Eqs. (21), (22), and (25) above, the last being particularly simple.

REFERENCES

[1] Miles, John W., *The Aerodynamic Forces on an Oscillating Airfoil at Supersonic Speeds*, Journal of the Aeronautical Sciences, Vol. 14, No. 6, pp. 351–358, June, 1947.

[2] Miles, John W., *Transient Loading of Airfoils at Supersonic Speeds*, Journal of the Aeronautical Sciences (to be printed).

[3] Garrick, I. E., and Rubinow, S. I., *Flutter and Oscillating Air-Force Calculations for an Airfoil in a Two-Dimensional Supersonic Flow*, N.A.C.A. T.N. No. 1158, October, 1946.

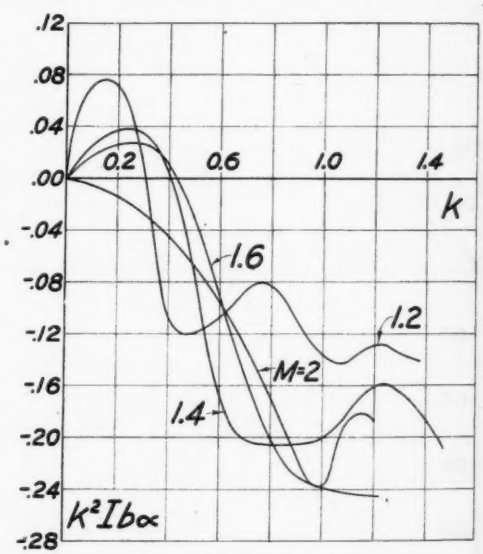

FIG. 9. $k^2I_{b\alpha}$ vs. k, $c = 0$.

MA
desire
conse
allow
chang
is, the
Typo
wish
mailin
flat.
protec
Scienc
script
Editor
the pa

TIT
initial
of the
quent
makes
partic
service
of the
placed
paper
title sl

SUM
beginn
quate
ment
cases c
scienti
especia
printed
possibl
and sh
length

SUBI
at freq
simplif

MAT
little te
tice.
may be
or proc
ceded f

REFE
footnot
end of
(for bo
Vol. 1,
[1] Englu
Results
Proc. I
Please

SUGGESTIONS *for* CONTRIBUTORS

to the Publications of the

INSTITUTE *of the* AERONAUTICAL SCIENCES

The Institute of the Aeronautical Sciences invites both members and nonmembers from any country to submit papers for publication in the JOURNAL OF THE AERONAUTICAL SCIENCES and the AERONAUTICAL ENGINEERING REVIEW. The Institute, following the practice of other societies, does not pay for contributions.

The following directions for the preparation of papers, if followed by authors, will save correspondence, avoid the return of papers for changes, minimize the work of preparation for the printer, and save the expense due to the charges made for "author's corrections."

MANUSCRIPTS: The original typewritten copy of the paper is desired, double or triple spaced on one side of white paper sheets, consecutively numbered. There should be wide margins to allow for the marking of directions to the printer. Correcting, changing, or adding to papers after they are in type is costly. It is, therefore, imperative that papers submitted be in final form. Typographical errors may be corrected on proofs, but if authors wish to add material, they may do so at their own expense. In mailing, drawings may be rolled, but manuscripts should be sent flat. Send by first class mail (register, if you wish, for your own protection) to the Editorial Office, Institute of the Aeronautical Sciences, 2 East 64th Street, New York 21, N.Y. All manuscripts will be examined by the Editorial Committee and by the Editor. Authors will be advised as promptly as possible whether the paper is acceptable for publication.

TITLES: The title of the paper should be brief. The name and initials of the author should be written as he prefers. The use of the full name of an author is advocated because of the frequent duplication of initials and surnames which sometimes makes it difficult to establish the identity of the author. This is particularly important for large annual indexing and abstracting services. All titles and degrees or honors are omitted. The name of the organization with which the author is associated should be placed after his name on a separate line. The date on which the paper is received will be inserted by the Editor. The author's title should be indicated in a footnote.

SUMMARIES OR ABSTRACTS: An abstract to be printed at the beginning should accompany each article. It should be adequate as an *index* and as a *summary*. It should contain a statement of major conclusions reached, since summaries in many cases constitute the only source of information used in compiling scientific reference indexes. Abstracts printed in other journals, especially foreign, in most cases, consist of summaries from printed papers. The summary should explain as adequately as possible the major conclusions to a nonspecialist in the subject and should contain from 100 to 300 words, depending on the length of the paper.

SUBHEADINGS: Subheadings should be inserted by the author at frequent intervals. The work of editorial preparation will be simplified by the author providing many subheadings.

MATTER USUALLY DELETED: Photographs or illustrations of little technical interest and not showing advances in general practice. Too detailed tabular matter (general results of such tables may be included in the text). Lengthy descriptions of materials or processes or of preliminary experiments or theories that preceded final results; salient features only are of interest.

REFERENCES AND FOOTNOTES: References should appear as footnotes only, numbered consecutively, grouped together at the end of the manuscript. The arrangement should be as follows: (for books)—[1] Durand, W. F., *Aerodynamic Theory*, 1st Ed., Vol. 1, p. 23; Julius Springer, Berlin, 1934. (For magazines)—[1] Englund, C. R., Crawford, A. B., and Mumford, W. W., *Some Results of a Study of Ultra-Short-Wave Transmission Phenomenon*, Proc. I. R. E., Vol. 20, No. 12, pp. 481 and 482, March, 1933. Please give author, title, edition, volume, page, publisher, and date of publication as indicated. Omission of one required fact causes much extra editorial work and possible inaccuracies.

ILLUSTRATIONS: Illustrations should accompany manuscripts and each should always be referred to in the text, by number. Drawings or graphs should not be larger than 12 × 16 inches, and must be made with jet black India Ink on white paper or tracing cloth, the latter being preferred. *Do not use typewriter for lettering.* The smallest lettering on 8 × 10 inch figures should be no less than 1/4 inch high. Cross-section paper (white with black lines) may be used, but should not have more than 4 lines per inch. If finer ruled paper is used, the major division lines should be drawn in with black ink, omitting the finer divisions. In the case of finely ruled paper, only blue-lined paper can be accepted. *Tracing paper and blueprints* are not acceptable. Lettering and all markings must be large enough to be readable after reduction. Mail rolled or flat, never fold. Drawings that cannot be reproduced (including pencil drawings) will be returned to the author for redrawing, thus delaying publication of the paper. Photographs should be distinct and show clear black and white contrasts. They must be on glossy white paper. Avoid round and oval photographs.

CAPTIONS AND LEGENDS: Legends or captions must accompany each drawing or photograph submitted. If written on the drawing or photograph, they should be placed below and well outside the part to be reproduced. Each table should have a caption such as Table 1, Table 2, Table 3, etc. Captions should be complete in themselves so as to make the data intelligible to the reader without reference to the text. A duplicate list of captions for figures should be included as the last page of the manuscript. Use "Fig. 1" (not Figure 1), Figs. 3 and 4, etc., in both the text and the numbering of illustrations. In the text, "Eq. (1)," or "Eqs. (1) and (2)" are preferable to "Equation (1)." In captions and legends, except for "Fig." and "Eq.," and in table headings, write all words in full; do not abbreviate.

MATHEMATICAL WORK: Only the simplest formulas should be typewritten, all others should be carefully written in pen and ink, the writing to be large enough so that ample room is provided to mark mathematical matter for the printer. A considerable space for marking should be allowed above and below all equations. All complicated equations should be repeated on separate sheets with plenty of space left for marking. The solidus should be used for simple fractions appearing within the text. Make all expressions clear to the typesetter. Greek letters used in formulas should be clearly designated by name on the margin of the manuscript. All symbols should be clearly written and carefully checked. The difference between capital and lowercase letters should be clearly distinguished and care taken to avoid confusion between zero (0) and the letter (o), between the numeral (one) and the letter (ell) and the prime (′), between alpha and a, kappa and k, u and mu, v and nu, n and eta. All subscripts and exponents should be clearly marked and dots and bars over letters or mathematical expressions should be avoided. Avoid complicated exponents and subscripts. When it is necessary to repeat a complicated expression, it should be represented by some convenient symbol.

NOMENCLATURE AND ABBREVIATIONS: Standard abbreviations should be used, and it should be noted that most abbreviations are lower case such as m.p.h., b.m.e.p., i.hp., b.hp., hp., . . . etc.

INSTITUTE *of the* AERONAUTICAL SCIENCES

1932–1948

Since its incorporation in October, 1932, as a scientific membership society to advance the art and science of aeronautics, the Institute of the Aeronautical Sciences, in over fifteen years of service to aviation, has become the representative technical society for the aviation industry and profession. It is the only organization in the United States which brings together all of the sciences and branches of engineering and technology which are applied to aeronautics.

Publications

Papers presented at meetings or submitted to the Editorial Board are published in the JOURNAL OF THE AERONAUTICAL SCIENCES or the AERONAUTICAL ENGINEERING REVIEW. The JOURNAL prints in each issue several full-length scientific papers on new research and developments in various fields applied to aviation. The REVIEW keeps members and subscribers up to date on aeronautical news and literature through reviews of new books and periodical articles, government publications and trade literature and publishes papers on applied engineering and aircraft production.

The AERONAUTICAL ENGINEERING CATALOG, published yearly, is a guide to sources and specifications of materials, parts, and accessories used in the design and production of aircraft, aircraft engines, and parts.

Research Facilities

Through the Aeronautical Archives of the Institute, members have for their use the most complete aeronautical library and reference research facilities maintained by any technical society. At the New York building of the Institute, The W. A. M. Burden Library of books, reports and periodicals, the Aeronautical Index of subject files, biographic files and bibliography, and the historical and art collections in the Archives are available for study. The Pacific Aeronautical Library at 6715 Hollywood Boulevard, Los Angeles, maintains a reference collection and reading room for members and loans books to company libraries in the area. Through The Paul Kollsman Lending Library, aeronautical books are lent by mail without charge to members anywhere in the continental United States. In addition to a complete collection of standard aeronautical reference works, the Kollsman Lending Library has available for loan new aviation books as they are reviewed in the AERONAUTICAL ENGINEERING REVIEW.

Membership

In addition to membership in professional societies representing their particular fields, specialists applying their knowledge and experience to aeronautics find membership in the Institute of great value in the contacts made with others engaged in aeronautical work and in the broad coverage of all aeronautical problems furnished through its meetings and publications. All applications for membership are carefully reviewed by the Membership Committee, which recommends the grade of membership for which the applicant is found eligible. There are advanced grades of membership—Fellow and Honorary Fellow—to which members may be elected as their experience warrants. Thus, a member receives due recognition—more valuable because it is given by his colleagues—for his contributions to the progress of aeronautics. New applicants may be elected by the Membership Committee to the grade of Associate Fellow if they have been engaged for not less than ten years in the practice of the aeronautical sciences and shall have been in responsible charge of important scientific or engineering work, or shall have otherwise made outstanding contributions to the aeronautical sciences; to the grade of MEMBER if they have been engaged in professional work for at least eight years and have acquired a recognized standing in engineering, design, or other special work applied to aeronautics; to the grade of Associate Member if they have acquired a recognized standing in an administrative capacity in the aviation industry; to the grade of Technical Member if they are recent engineering school graduates or are engaged in technical aeronautical work. Student Members are admitted by application through Student Branches organized at their schools. Aeronautical companies, as well as individuals, are affiliated with, and participate in, the support of the Institute through Corporate Membership.

Dues

An entrance fee of $10 is required of all new members who apply for admission to a grade of membership to be specified by the Membership Committee (Corporate Members, Foreign Members, and Student Members being excepted).

Annual membership dues include a subscription to the AERONAUTICAL ENGINEERING REVIEW. Dues for the various grades of membership are as follows: Fellows—$16.50; Associate Fellows—$16.50; MEMBERS—$13.50; Associate Members—$13.50; Technical Members—(26 years of age and over) $13.50, (under 26) $6.50.

The regular subscription price for the JOURNAL OF THE AERONAUTICAL SCIENCES and the AERONAUTICAL ENGINEERING REVIEW is $12 and $3.00 per year, respectively. Members may subscribe to the JOURNAL at $4.00 per year.

Those who are engaged in aeronautical work or who have an interest in any technical phase of aviation will find the services of the Institute to be a necessary aid in keeping abreast of developments in these times of such rapid progress. An application form and further information about membership can be obtained from an Institute member or by writing to the Secretary.

INSTITUTE OF THE AERONAUTICAL SCIENCES, INC.

2 EAST 64TH STREET

NEW YORK 21, N.Y.